2010

An anatomical investigation of higher visual structures in the pigeon (Columba livia)

Tadd B. Patton
University of South Florida

An Anatomical Investigation Of Higher Visual Structures In The Pigeon (*Columba livia*)

by

Tadd B. Patton

A dissertation submitted in partial fulfillment
of the requirements for the degree of
Doctor of Philosophy
Department of Psychology
College of Arts and Sciences
University of South Florida

Major Professor: Toru Shimizu, Ph.D.
Michael Brannick, Ph.D.
Michael Coovert, Ph.D.
Cheryl Kirstein, Ph.D.
Thomas Sanocki, Ph.D.

Date of Approval:
June 2, 2010

Keywords: telencephalon, lateralization, birds, rotundus, zenk

Dedication

This work is dedicated to the people in my life who understood how important it was for me to finish what I started. Completing this dissertation represents more than achieving a certain credential; it shows that with perseverance, the sky is the limit. I dedicate this dissertation to those who, like me, believe in doing something to the best of their ability and not settling for anything less. I owe a tremendous debt of gratitude to a very special person in my life, Sophie. She never stopped believing in me even when my self-confidence wavered, as I often did. Thank you, Sophie. This one's for you.

Acknowledgments

I would like to thank the following students for helping me with various aspects of this project: Jeremy Brenner, Amanda Bunton, Frank Fishburn, Asef Mahmud, David Nicholson, and Justine Vandenbosche. Their relentless desire to assist me with this seemingly never ending project will always be greatly appreciated.

I would also like to thank Dr. Byeong Cha from the Lisa Muma Weitz Advanced Microscopy & Cell Imaging Core Laboratory in USF's College of Medicine for allowing me to use his microscope. Dr. Cha was generous with his time and resources, both of which greatly facilitated the completion of this project.

I would be remiss if I did not acknowledge the very patient and accommodating Dissertation committee members: Dr. Michael Brannick, Dr. Michael Coovert, Dr. Cheryl Kirstein, and Dr. Thomas Sanocki. I have no doubt that each of them has eagerly awaited the completion of my graduate work.

Last, but not least, I would like to thank my Major advisor and mentor, Dr. Toru Shimizu. Without his patient and thoughtful guidance, none of this would have been possible and I would not be the person I am today.

Table of Contents

List of Figures

List of Tables

An Anatomical Investigation of Higher Visual Structures in the Pigeon (*Columba livia*)

Tadd B. Patton

Abstract

Early visual processing in the avian brain has been studied extensively, the retina and midbrain in particular. However, a clear understanding of the higher visual centers in the forebrain (the telencephalon and thalamus) remains poor. Two structures located within the avian visual telencephalon, the entopallium (E) and the lateral portion of the intermediate nidopallium (NIL), merit extensive investigation based on their critical role in visual processing. The goal of the current study was to further clarify the anatomical characteristics of E and NIL. Visual information that reaches these telencephalic structures is mostly from the contralateral retina. Thus, blocking visual input on one side affects the opposite hemisphere, but leaves the hemisphere on the same side largely unaffected. This unique property of the avian visual system was used in order to emphasize neurochemical expression in the higher visual structures. After blocking visual input to one hemisphere either by monocular occlusion or unilateral lesion of the nucleus rotundus we examined the expression of specific neuroanatomical markers; namely cytochrome oxidase (CO) and the calcium binding protein, parvalbumin (PV) in E and ZENK protein expression in NIL. . Our results showed there were significantly more PV-ir cell bodies in the inner region of E compared to the outer region. In terms of PV-ir neuropil, regional differences within E were significant. In particular, the ventrolateral E tended to have a higher density of PV-ir neuropil than other regions except the most

ventromedial area which was also high in PV-ir. Differential CO staining patterns were observed as well. However, unlike PV-ir neuropil the ventro-intermedial area showed a low level of CO staining compared to the other areas. Finally, there was a significant reduction of ZENK-ir cell bodies on NIL in the experimental hemisphere compared to control side. Based on this differential expression of ZENK, it was possible for the first time to visualize the location of NIL. The findings presented here are discussed in terms of their relevance to the identification of the size and extent of NIL and the heterogeneous nature of E.

Introduction

Birds have superb visual abilities that are on par and sometimes better than those of highly visual primates (Hodos, 1993; Frost & Sun, 1997; Shimizu, Patton, & Szafranski, 2008). Birds use these abilities to locate food sources, find a potential mate, remain vigilant against predators, and avoid obstacles during flight. Such well-developed vision makes the avian brain an excellent model for investigating the underlying mechanisms which drive these abilities and for the comparative analysis of complex visual systems in general. The goal of this investigation was to clarify the anatomical characteristics of two important visual structures in the avian cerebrum (telencephalon).

There are numerous anatomical and physiological studies that have investigated the early stages of visual processing in birds, the retina and structures within the midbrain in particular. In contrast, a clear understanding of the higher visual centers in the forebrain (the telencephalon and thalamus) remains unclear. Two structures located within the avian visual telencephalon, the entopallium (E) and the lateral portion of the intermediate nidopallium (NIL), merit extensive investigation based on their critical role in visual processing. The current study focused on anatomical properties of these two structures.

This investigation had three main objectives: 1) to clarify the anatomical and physiological subgroups of E, 2) to anatomically define the higher visual structure, NIL, and 3) to determine the degree to which neural activity in E and NIL are dependent on visual information. Each of these specific aims was investigated through the examination

of neural activity detected by the expression of various neurochemicals (i.e., a mitochondrial enzyme, a calcium-binding protein, and an immediate-early gene).

This set of experiments was one of the first systematic anatomical studies to employ lesion and occlusion techniques to directly analyze the higher visual structures, E and NIL. Furthermore, the results reported here are important because they provide information that can be used to examine the similarities and differences of the visual systems between phylogenetically remote animal classes, birds and mammals. Furthermore, based on such comparisons with the mammalian system, the findings in the current study can be used to understand the general and specific neural principles for visual processing.

General Background

Visuo-cognitive abilities of birds.

The remarkable visual and cognitive abilities of pigeons have been demonstrated both in the laboratory and field. Using operant conditioning techniques, researchers have shown that birds can be trained to categorize a variety of visual stimuli. Pigeons (*Columba livia*) have been trained to respond differently to the presence or absence of photographic images of humans (Herrnstein & Loveland, 1964), trees, bodies of water, a particular person (Herrnstein, Loveland, & Cable, 1976), and different styles of painting (Watanabe, Sakamoto, & Masumi, 1995; see Huber, 2001 for review). Based on these studies, some authors argue that pigeons can form "concepts" of these objects through discrimination training (Lubow, 1974; Cook, Cavoto, & Cavoto, 1995; Watanabe, Lea, & Dittrich, 1993).

Several bird species also have remarkable visual memory ability. For example, it is well known that food-caching birds, such as the Western Scrub-jay (*Aphelocoma californica*), will harvest food and store it in different locations when food is abundant and then return to these caches at a later time as food becomes scarce (Sherry, Krebs, & Cowie, 1981; Shettleworth, 1983; Sherry, 1984; Shettleworth & Krebs, 1986). One particularly impressive example comes from the behavior of the Clark's nutcracker (*Nucifraga columbiana*). In the late summer and early fall, these birds will store over 30,000 seeds in various locations and recover the majority of them later in the winter (Vander Wall & Balda, 1977). Discrimination studies in laboratories have shown that even non-food storing birds, such as pigeons, also have extraordinary visual memories (Vaughan & Greene, 1984; Cook, Levision, Gillet, & Blaisdell, 2005). In the study by Cook et al. (2005), pigeons were trained to remember large numbers of photographs, each of which were randomly selected to be associated with the choice stimulus on the left or right side. The results showed that pigeons can memorize between 800 and 1,200 picture-response associations.

It is clear why food-storing birds have such remarkable memory capacity as this ability is crucial to their survival. But, why do pigeons and other birds have such remarkable visuo-cognitive abilities? In addition to the foraging purpose for food-storing birds, one possible important reason for these abilities is that birds use them to survive in a highly developed social world. Birds must be able to quickly tell the difference between predator and prey, as well as locate a potential mate. Success at each of these behaviors requires the ability to recognize which animals are members of their own species and which are not. As described above, many discrimination studies use operant conditioning

techniques to investigate how pigeons process complex natural objects, including social stimuli. However, because these operant procedures essentially require birds to discriminate such stimuli for access to a food reward, it is possible that the birds discriminate the stimuli using strategies that are very different from those they may use in their natural setting. Under the operant conditioning paradigm, birds may be able to discriminate photographs of conspecifics based on small details (Brown & Dooling, 1992, 1993). But again, one cannot conclude that birds use such details to discriminate individuals in the real world. An instructive alternative to the operant conditioning paradigm is to measure a subject's natural responses to ecologically relevant stimuli.

A previous investigation conducted in our laboratory (Shimizu, 1998) showed that male pigeons exhibit courtship behavior in response to video playbacks of a female pigeon. In particular, male pigeons reacted with strong courtship display even when the body of the female was covered, as long as the head remained visible. In contrast, only weak courtship responses were observed when the head of the video pigeon was covered, so that only the female body was visible. This study (Shimizu, 1998) suggested the overwhelming significance of the head in conspecific detection and mate selection in birds just as in humans. Based on this finding, Patton, Szafranski, and Shimizu (2010) examined the significance of different facial features, such as the beak and eyes, by analyzing the preference of male pigeon subjects between images of females whose facial features were digitally manipulated. The results showed that the beak is important since males preferred females with an abnormally large beak. In contrast, the presence or lack of the eyes had less of an effect on their preference. This finding is interesting since humans and other primates tend to innately pay specific attention to eyes in the face

(Farroni, Massaccesi, Menon, & Johnson, 2006). Moreover, the spatial rearrangement of these facial features did not affect preference, suggesting that the configural relationship of the features is not essential. This is also different from the human data that indicate we are sensitive to the spatial arrangement of the facial features (Gauthier & Logothetis, 2000). These results suggest that although the face and facial features are important to birds and humans, the salience of the facial features and thus the meaning of these features are fundamentally different between them. These perceptual differences between birds and mammals are likely a result of the differences in the underlying neural mechanisms associated with such complex visual behavior.

The current study was an extension of this previous research on avian visual cognition to study the underlying neural mechanism for visual processing of complex stimuli. Unlike the case of human and non-human primates, it is unclear exactly which higher avian brain structures are involved in these sophisticated visuo-cognitive functions. Two specific visual structures, E and NIL, were the focus of this study.

Two major ascending visual pathways.

In all amniotes (reptiles, mammals, and birds), visual information is sent to the telencephalon along two ascending pathways: the tectofugal pathway and the thalamofugal pathway (Butler & Hodos, 1996; Shimizu & Bowers, 1999). The E and NIL are two primary telencephalic structures associated with the tectofugal pathway, which is the major route for visual processing in birds. Based on connection patterns, the avian tectofugal pathway has been compared to the retino-colliculo-pulvinar-cortical system in mammals, whereas the thalamofugal pathway is comparable to the mammalian retino-

geniculo-cortical pathway (Shimizu & Karten, 1993). In birds, the majority (over 90%) of the retinal fibers are sent to the optic tectum (TeO) (the tectofugal pathway) rather than directly to the thalamic center of the thalamofugal pathway. This pattern is in contrast to that of highly visual mammals, such as primates, in which the retino-geniculo-cortical pathway is often a prominent pathway (Shimizu & Bowers, 1999). In the avian tectofugal pathway, the TeO, the avian equivalent of the mammalian superior colliculus (Güntürkün, 2000; Shimizu, 2001), is a large structure which protrudes laterally between the cerebellum and the cerebrum. The TeO is highly laminated, with the superficial layers receiving retinotopically-organized input and the deeper layers giving rise to ascending efferents. The TeO projects bilaterally and non-topographically to the largest thalamic structure, the nucleus rotundus (Rt), the avian equivalent of the mammalian pulvinar (Shimizu & Karten, 1991). Multiple subdivisions have been identified within Rt (i.e., anterior, central, and posterior Rt) based on analysis of cytoarchitecture, neurochemicals, and connections (Benowitz & Karten, 1976; Nixdorf & Bischof, 1982; Karten, Cox, & Mpdozis, 1997; Hellmann & Güntürkün, 1999; Laverghetta & Shimizu, 2003). Visual information from Rt is further sent to a large nuclear mass in the telencephalon, E, which in turn projects to multiple telencephalic structures, including NIL (see Figure 1).

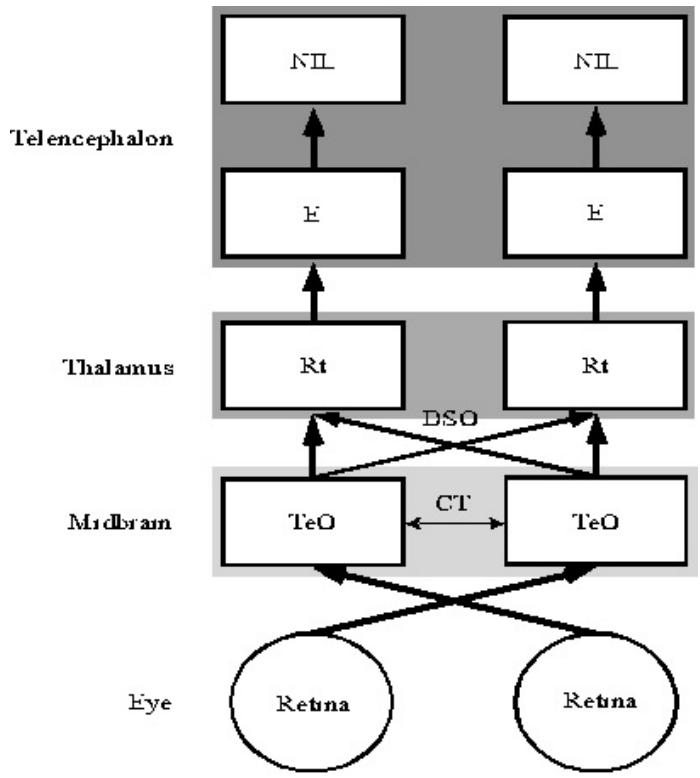

Figure 1. Schematic view of the tectofugal pathway of the pigeon. Information from each eye is sent to the midbrain of the opposite hemisphere. In the midbrain is the optic tectum (TeO). TeO from each hemisphere is connected by tectal commissure (CT). Information from TeO is sent to the thalamus bilaterally via the supraoptic decussation (DSO). From Rt, visual information is sent ipsilaterally to the primary telencephalic target, E. From E, information is sent to several higher visual structures such as the lateral portion of the intermediate nidopallium (NIL).

Functions of early visual processing.

Investigations of the response properties of individual neurons (electrophysiology) and lesion studies have shown that neurons in the tectofugal pathway are sensitive and/or selective to different aspects of visual stimuli, such as motion, direction, luminance, and color (Engelage & Bischof, 1993). Many TeO neurons respond preferentially to certain aspects of moving stimuli. For example, some TeO neurons show responses to objects moving out of phase with the background and tend to be inhibited when the stimulus object is moving with the background, suggesting that these cells play

a role in figure-ground segregation or the discrimination of motion of an object as opposed to self-induced optical motion (Frost & Nakayama, 1983). In general, neurons in Rt have similar response characteristics to TeO cells. However, Rt is not a homogenous structure, but is composed of multiple subdivisions along the rostral-caudal axis. The anterior Rt has neurons that are sensitive to changes in luminance and color (Granda & Yazulla, 1971; Maxwell & Granda, 1979; Wang, Jiang, & Frost, 1993). Neurons in the central and posterior Rt are sensitive to features of motion such as, changes in stimulus size, direction, and velocity (Revzin, 1979). Some neurons in the posterior Rt are sensitive to approaching stimuli, suggesting that they act as collision detectors (Wang & Frost, 1992).

Destruction, by way of lesions, to structures within the tectofugal pathway results in critical deficits in intensity, color, pattern, acuity, and movement discrimination (Hodos, 1993). Severe and often irreversible deficits in a variety of visual discrimination tasks, such as stimulus intensity, pattern, and location discriminations result when TeO is damaged (Jarvis, 1974). Similar deficits can be seen when lesions are made in Rt. Rotundal lesions cause significant deficits in discrimination of intensity difference thresholds (Hodos & Bonbright, 1974), visual acuity thresholds (Macko & Hodos, 1984), and size threshold differences (Kertzman & Hodos, 1988). In contrast to the tectofugal pathway, the functional significance of the thalamofugal pathway remains elusive. However, there is some evidence that this pathway is important for processing the binocular portion of the visual field, especially for frontal-eyed birds such as most raptors when they are in the process of capturing prey (Davies & Green, 1990). In studies of lateral-eyed birds, such as pigeons, lesions to the thalamofugal pathway cause little to no

discrimination deficits (Watanabe, 1992; Güntürkün, Miceli, & Watanabe, 1993). Specifically, virtually no deficits have been found in visual acuity or brightness intensity thresholds after lesions of the thalamic structure, nucleus opticus principalis thalami (OPT complex) (Macko & Hodos, 1984) or the telencephalic target, Wulst (Pasternak & Hodos, 1977; Hodos, Macko, & Bessette, 1984).

These findings suggest that the tecotofugal pathway plays a crucial role in processing visual information that is essential to higher cognition compared to the thalamofugal pathway. Despite extensive studies in the lower visual structures of the tectofugal pathway (TeO and Rt), the structure and function of higher visual structures are not as well understood as the early visual stations. The first specific aim will be to examine the subgroups of the primary visual telencephalic structure, E.

Background for Specific Aim One

Functional significance of E.

The primary telencephalic visual structure in the tectofugal pathway is E. Studies have shown that lesions to E cause similar deficits in visual discrimination tasks as seen after lesions to Rt. Bilateral lesions of E cause significant deficits in discrimination of intensity difference thresholds (Hodos, Weiss, & Bessette, 1988), visual acuity thresholds (Hodos, Macko, & Bessette, 1984), size threshold differences (Hodos, Weiss, & Bessette, 1986), as well as intensity, color, and pattern discrimination (Bessette & Hodos, 1989). Hodos et al. (1988) demonstrated that lesions to E caused a severe decline (50% to 83% of the preoperative performance) in pigeons' ability to discriminate differences in

luminous intensity. These results indicate that E, similar to lower stations of the tectofugal pathway, processes multiple aspects of the visual stimulus in parallel.

However, it may also be involved with processing higher, more complex aspects of visual stimuli, such as object class or membership (Watanabe, 1992, 1996). Watanabe (1992) trained pigeons to discriminate between two bird species (pigeon vs. quail) and individual birds within a species (pigeon vs. pigeon). After successful training, bilateral lesions were applied to E and the birds were tested again on both tasks. The results showed that when E has been destroyed, birds can still perform the species discrimination task, but not the individual discrimination task. This finding suggests that object classifications such as species membership is at least in part controlled by E.

Heterogeneity of E.

For many years, E was considered to be an anatomically homogenous structure based on cytoarchitecture and neurochemistry. Specifically, early anatomical studies showed that E was composed of a "core" region (E) and an outer "belt" or "shell" region (Ep) based on connections (Ritchie & Cohen, 1977; Watanabe, Ito & Ikushima, 1985). Furthermore, projections from Rt extend directly to E, not Ep (Karten & Hodos, 1970). There is now evidence from electrophysiological, hodological, and lesion studies indicating that E is composed of multiple subgroups in a similar fashion to Rt.

Anterior-posterior organization of E.

As described above, Rt is organized in a parallel fashion in terms of cytoarchitecture, response characteristics, and connections. That is, processing of distinct

visual features takes place in the anterior, central, and posterior portions of Rt. This parallel organization appears to be extended to E because the projection from Rt to E is topographically organized along the anterior – posterior axis (i.e., the anterior, central, and posterior E receives inputs from anterior, central, and posterior Rt, respectively) (Benowitz & Karten, 1976; Nixdorf & Bischof, 1982; Laverghetta & Shimizu, 2003). This projection pattern has not been easily recognized in the past, partly due to the fact that brain sections used in many previous studies were made based on standard bird brain atlases that are significantly rotated in the anterior direction (Laverghetta & Shimizu, 2003) (see Figure 2).

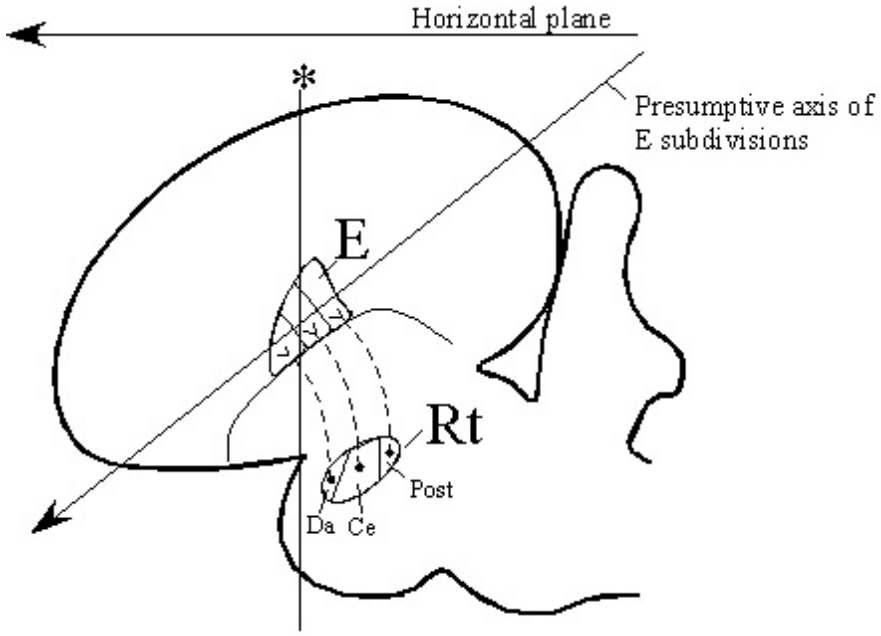

Figure 2. Schematic view of pigeon brain (sagittal view). Schematic shows rotundal (Rt) projections to the core region of E. The projections from the anterior portion of Rt (Da) project to the anterior portion of E, whereas neurons in the central portion of Rt (Ce) and the posterior region of Rt (Post) project to the central and posterior regions of E, respectively. The top horizontal line represents the horizontal plane. The vertical line in the middle of the figure (*) represents the transverse plane typically used for cutting the pigeon brain. Note that the presumptive axis of E subdivisions is not parallel to the horizontal plane. Instead, E subdivisions appear to be arranged along an axis rotated in the anterior direction. This figure was taken from Laverghetta and Shimizu (2003).

Early electrophysiological studies have shown that many neurons in E respond to motion stimuli. In particular, many of the cells within E fire preferentially when an object in the receptive field moves in an upward/downward or fore/aft fashion (Revzin, 1970; Kimberly, Holden, & Bamborough, 1971). A more recent study showed that a group of cells in the caudal portion of E respond to looming stimuli similar to the cells that have been identified in Rt (Xiao, Li, & Wang, 2006). This finding suggests that looming sensitive cells in Rt send their information directly to the looming sensitive cells in E, which lends further support to the notion that information from Rt is transferred in an orderly and parallel manner to E.

The majority of previous lesion studies destroyed the entire E and there were no clear data showing functional segregation among possible subdivisions. However, a study conducted by Nguyen et al., (2004) showed that cells in E can be functionally grouped along the rostral-caudal axis. In their study, pigeons that received lesions to the anterior portion of E performed poorly on spatial pattern discrimination tasks, but showed no deficits on motion discrimination tasks. In contrast, pigeons which received lesions restricted to the caudal portion of E showed deficits in visual motion discrimination, but showed little or no deficits on the spatial pattern discrimination. The double dissociation found in this study suggests that visual information in the avian brain may be processed in at least two major parallel streams, similar to that which has been demonstrated in primates (DeYoe & Van Essen, 1988; Goodale & Milner, 1992).

Internal-external organization of E.

Various anatomical staining techniques have been used to visualize the physical characteristics of E, including its size, shape, and subgroups (Hellmann, Waldmann, & Güntürkün, 1995; Krützfeldt & Wild, 2004; Krützfeldt & Wild, 2005). Hellmann et al. (1995) used cytochrome oxidase (CO), a metabolic activity marker which can be used to identify highly active groups of neurons, to examine the neural activity within E. The results showed that in terms of cellular activity, E is not homogenous. High levels of CO activity were found, the medial, central and ventrolateral areas, while CO activity in the centroventral and dorsolateral areas were weak. These CO parcellations in the intact E strongly suggest that multiple cellular subdivisions exist here and perhaps these cells perform different visual functions.

Krützfeldt and Wild (2005) used tract tracing methods to visualize Rt efferents and, histochemical methods to examine the calcium-binding protein (CaBP) parvalbumin (PV) and CO activity. There were three main findings in this study which have important implications regarding the accurate definition of the core and shell region of E. Specifically, the results showed that 1) E can be accurately defined by the overlap of the pattern of CO activity and the rotundal efferents, 2) Ep receives few rotundal efferents, but sends most of its efferents to other areas of the ipsilateral hemisphere, including NIL, and 3) based on the pattern of PV-immunoreactivity, the core region of E can be divided into two separate regions, an internal division (Ei) and an external division (Ex) (see Figure 3A).

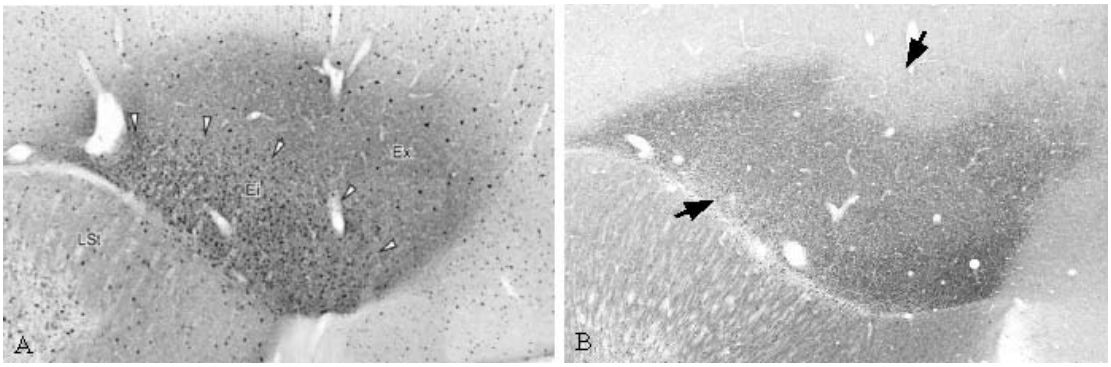

Figure 3. Microphotographs showing PV and CO activity in E. A. Microphotograph showing two divisions of E, an internal division (Ei) where a great number of PV-ir cells are located and an external division (Ex) which consists of fewer PV-ir cells. This photograph was taken from Krützfeldt and Wild (2005). B. Microphotograph showing CO expression in similar location of E. Regions of weak staining can be seen in the centroventral and dorsolateral areas (arrows). Both microphotographs are of transverse sections through the right hemisphere E.

However, the definition of E based on PV immunoreactivity is not congruent with the shape and size of this structure as defined by CO immunoreactivity (see Figure 3B). Due to the importance of E for visual processing, it is necessary to clarify the anatomical boundaries of this structure. To date, there has been no comprehensive investigation to "map" the organization of E, combining these data described above.

Background for Specific Aim Two

Definition of NIL.

In addition to E, several studies have analyzed the relationship between the development of other forebrain regions and various cognitive abilities (Timmermans, Lefebvre, Boire, & Basu, 2000; Jarvis et al., 2005). There are specific areas within the forebrain called the mesopallium and nidopallium, the size of which varies among different types of birds. Sophisticated behaviors which require cognitive flexibility or

"innovativeness" such as, using novel food foraging strategies or tool use seem to be dependent on these brain regions. Birds that possess a large mesopallium and nidopallium tend to exhibit "innovative" behaviors compared to birds with relatively small forebrains (Timmermans et al., 2000). The NIL is one specific region within the nidopallium. However, there is currently very little information regarding the anatomical and functional characteristics of NIL. In the next section, I discuss what is currently known about the higher visual system of birds.

The NIL is the main target of projections from E. When Husband and Shimizu (1999) injected anterograde tract tracers into E, the majority of the efferents projecting from E terminated in Ep and Ep2 (an additional cell layer located immediately dorsal to Ep). Most projections from Ep terminated in Ep2, which in turn, sent projections to diverse regions of the telencephalon, including the fronto-lateral portion of the nidopallium (NFL), area temporo-parieto-occipitalis (TPO), and NIL.

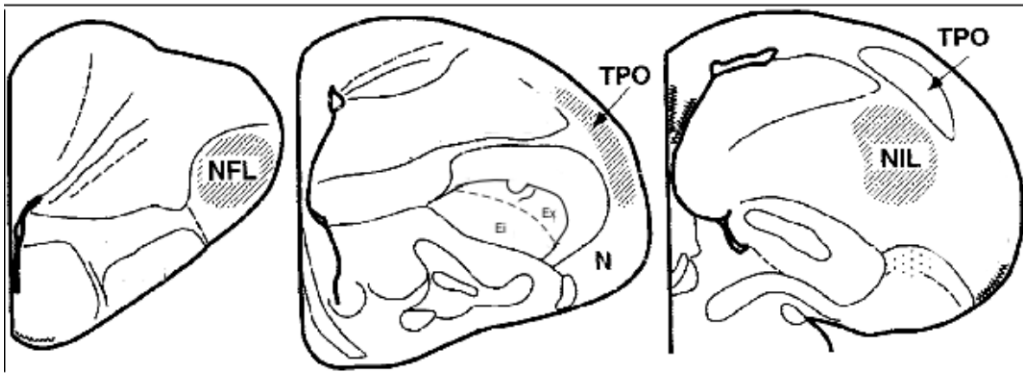

Figure 4. Schematic showing the spatial relationship between E and NIL. This figure was taken from Husband & Shimizu (1999).

NIL is thought to be located intermediately in the anterior-posterior axis and adjacent laterally to TPO and dorsally to the mesopallium. NIL is only a part of the

nidopallium, which includes several hodologically and functionally distinct subdivisions. However, the cytoarchitecture of the nidoplallium is rather homogeneous in general and it is difficult to differentiate among these subdivisions based solely on cell types. In particular, the size and extent of NIL with the anterior, posterior, medial, and ventral neighboring nidopallium are ambiguous and have not been examined systematically.

NIL connections are reminiscent of NCM.

Currently, there has been no report of a physiological investigation of NIL. One possible hint to the function of this structure comes from its connectional similarities to auditory telencephalic structures, specifically, the caudomedial neostriatum (NCM). Note that NIL receives efferents from the primary visual area E (Husband & Shimizu, 1999). In a similar fashion, the NCM receives input from a primary (L2) and secondary (L3) auditory areas (Vates, Broome, Mello, & Nottebohm, 1996). In the songbird, NCM is involved in the processing of new songs and the formation of song-related memories. Studies have also shown that, in this brain region, certain immediate early genes (IEGs) are induced in response to complex auditory stimuli (Mello, Vicario, & Clayton, 1992; Mello & Clayton, 1995; Nastiuk, Mello, George, & Clayton, 1994). It has been suggested by some researchers (Husband & Shimizu, 1999) that NIL serves a similar function in the visual system. That is, perhaps NIL is involved with the formation of visual memories.

In the above referenced songbird studies, the expression of an IEG known as *zenk* was examined. *Zenk* induction and the expression of its protein product, ZENK, have been associated with the formation of long-term memories and it has been used as a neuroanatomical marker for cellular activation in direct response to specific stimuli.

Furthermore, *zenk* expression has been used for mapping brain regions associated with the perception of species-specific song stimuli in the songbird (Mello et al., 1992). In that study, adult canaries and zebra finches were presented with audio playbacks of their conspecific or heterospecific song and then the distribution pattern of *zenk* was analyzed. The results showed that *zenk* expression in the song learning regions of the brain was much higher when the subject bird listened to a playback of a conspecific song than for a heterospecific song, suggesting that neurons in these regions were selectively responding to biologically and socially relevant stimuli. In the current study, ZENK expression was examined in NIL after presentation of species-specific visual stimuli.

Background for Specific Aim Three

Neuromarkers used to identify visual structures.

Several neuromarkers (some of which have been discussed already) have been used to delineate visual structures that are cytoarchitectonically difficult to define. Among them, three different classes of neuronal markers have proven to be particularly useful: 1) the CaBP, PV, 2) CO, and 3) the IEG, *zenk*. These neuromarkers reflect directly and indirectly the cellular changes associated with neural activity, and they have been used extensively for studies of the avian neural system.

Parvalbumin (PV).

One class of neuromarkers are calcium-binding proteins (CaBPs), which are a large class of proteins that have been studied extensively for their roles in neuronal regulatory processes (Baimbridge, Miller, & Parkes, 1982) as well as their potential role

in neuronal plasticity and development (Celio & Heizmann, 1981; Celio, 1990). In avian literature, a specific family of CaBPs, known as the EF-Hand family, includes parvalbumin (PV), calbindin D-28k (CB), and calretinin (CR). These CaBPs have been a major focus of studies because they are abundant in the avian forebrain (Braun, Scheich, Schachner, & Heizmann, 1985a; Braun, Scheich, Schachner, & Heizmann, 1985b; Braun, Scheich, Braun, Rogers & Heizmann, 1991). Although the precise function of many of these CaBPs remains elusive, PV is of particular interest in that it may play a role in neuronal plasticity because of its association with developing neurons. A transient presence of PV-ir has been observed in some of the structures associated with auditory filial imprinting in birds, suggesting that this protein is in some way involved in neural plasticity necessary for long-term imprinting behavior (Braun et al., 1991). Similarly, PV-containing neurons are found in the higher visual structures in birds (Krützfeldt & Wild, 2004, 2005; Husband & Shimizu, 1999). Often, a reduction of PV expression is observed in a particular brain region after destruction of its afferents, suggesting that the expression of PV is dependant on this afferent information (Tigges & Tigges, 1991, 1993). Such effects have been observed in the avian telencephalon after lesions in Rt (unpublished observation).

Cytochrome oxidase (CO).

Neural activity can also be determined by examining the expression of the enzyme, CO. Like all eukaryote cells, neurons rely on cellular respiration to convert oxygen into energy. Cells that make up vital organs, such as the brain depend heavily on the process of oxidative energy to survive. Specifically, a biochemical reaction called the

electron transport chain takes place within the mitochondria of the cell. This biochemical process of respiration produces the energy source adenosine triphosphate (ATP), which is used for several cellular processes including the sodium-potassium pump, fast axonal transport, and the synthesis of some neurotransmitters (Wong-Riley, 1989). The enzyme CO is a byproduct of the respiration process. Therefore, when activity is required of the neuron, more ATP is produced, which in turn, causes more CO to accumulate inside of the cell. Neurons containing high concentrations of CO relative to other neurons are considered to be more active. Histochemical procedures have been used to visualize the expression of CO, particularly as a reliable marker for long-term cellular activity (Wong-Riley, 1989).

Several studies have shown that the expression pattern of CO can be used to identify subregions of avian brain structures, which may be difficult to differentiate cytoarchitectonically (Hellmann, Waldmann, & Güntürkün, 1995; Krützfeldt & Wild, 2004; Krützfeldt & Wild, 2005). As mentioned earlier, CO expression revealed anatomical subdivisions of E (Hellmann et al., 1995; Krützfeldt & Wild, 2005). These studies show that CO is a neuromarker that can be very useful in physiological studies aimed at clarifying poorly understood brain structures

ZENK.

The IEGs, such as *zenk*, *c-jun*, and *c-fos*, are among the first class of genes to be regulated following neuronal activation (Goelet, Castelucci, Schacher, & Kandel, 1986; Morgan & Curran, 1989; Sheng & Greenberg, 1990; Tischmeyer & Grimm, 1999; Clayton, 2000). Many proteins encoded by IEGs are important because they act as

transcriptional regulators that activate late response genes thought to be involved in long-term cellular changes associated with learning and memory (Chaudhuri, 1997; Tischmeyer & Grimm, 1999). ZENK (an acronym for *zif*-268, *egr*-1, NGFI-A, and Krox 24) is the protein product of the IEG, *zenk.* Activation patterns of this particular IEG have been studied extensively in the avian brain, including the analysis of the song control system in songbirds (Mello et al., 1992; Jarvis, Mello, & Nottebohm, 1995; Mello & Ribeiro, 1998), sexual behavior in quail and starlings (Ball & Balthazart, 2001; Can, Domjan, & Delville, 2007), sexual imprinting in finches (Lieshoff, Grosse-Ophoff, & Bischof, 2004; Huchzermeyer, Husemann, Lieshoff, & Bischof, 2006), and homing behavior in pigeons (Shimizu et al., 2004). Moreover, IEGs, such as *zenk* can be induced by a variety of different stimuli. In addition, they can be used as endogenous markers of neuronal activity and, consequently, to map functional activity within the vertebrate brain (Chaudhuri, 1997; Herdegen and Leah, 1998; Tischmeyer and Grimm, 1999). Immunohistochemistry for ZENK was used in this study to identify differential brain activity in response to a biologically and socially relevant visual stimulus.

Although these neurochemicals are useful markers to define higher visual structures, E and NIL, it is also important to understand whether or not the normal expression of the neurochemicals is dependent on a truly visual signal *per se*. It was hypothesized that if the expression of these markers is indeed associated with the neuronal activity of the regions, they will be extremely valuable to understand the functional significance of these structures. However, it is also possible that these chemical markers are not correlated to neural activity in the regions. No systematic studies on this issue had previously been carried out. A major obstacle to conduct such

studies is that they would require tissue samples of different brains, each of which would be placed in a different condition. While processing tissues from different brains, there are subtle, but inevitable, differences in parameters of histological procedures (e.g., tissue thickness, incubation duration, and temperature), which make it difficult to determine whether the differences are truly due to the experimental condition.

The avian brain provides the researcher with an excellent opportunity to avoid this problem and to compare the control and the experimental condition in a single brain. In birds, retinal fibers from one eye project almost completely to the contralateral hemisphere (Shimizu & Karten, 1991, 1993). In addition, unlike placental mammals, birds do not have a massive interhemispheric commissure, the corpus callosum. With exception of a few small commissures and decussations, information from one visual field is processed in the opposite hemisphere. Because of this neural design, it is rather easy to block the visual input from one eye reaching E and NIL.

Despite previous research, the exact function of the interhemispheric connections is not clear. Nevertheless, they are discussed briefly here. The left and right TeO are connected by two commissures, the tectal commissure (CT) and the posterior commissures (CP), which are located adjacently (Ehrlich & Saleh, 1982). Although the exact function of CT is not clear, results from electrophysiology studies indicate that this commissure plays an inhibitory role. The other commissure is the supraoptic decussation (DSO). The deeper layers of TeO send bilateral projections to the thalamic structure, Rt. The contralateral projection ascends to Rt through the DSO.

Rationale

As described above, the anatomy of higher visual structures had not been investigated sufficiently until now although they must play essential roles in visual and cognitive abilities. There is only scarce information about the organization and subdivisions of E (Specific Aim 1), the anatomical border and organization of NIL (Specific Aim 2), and the significance of visual signal to E and NIL (Specific Aim 3). The present study capitalized on the unique organization of visual projections of birds, in which there is no corpus callosum and virtually complete decussation of retinal fibers at the optic chiasm. This preparation created a unique opportunity to examine each hemisphere separately by administering a different treatment in each visual route to the left and right hemispheres. These treatments included lesions in Rt and occlusion of eyes, which interrupted the visual signal to higher visual areas (E and NIL) at the level of the thalamus and retina, respectively. By carrying out these treatments unilaterally, E and NIL in only one hemisphere were affected by the procedures, whereas the other hemisphere was used as control. This enabled me to evaluate the effect of the procedures in one hemisphere compared to the other hemisphere within the same brain.

For Specific Aim 1, detailed analyses of differential patterns of CO and PV were used to clarify the physical characteristics (shape and extent) of the subregions in E. The information provided here served as the first step towards mapping this very important region for visual processing. A detailed atlas of anatomical subdivisions within E can be used for highly specific lesions which, in turn, will allow investigators to more clearly define the functional divisions within this structure.

For Specific Aim 2, the expression pattern of ZENK immunoreactivity was examined in the nidopallium in order to provide a clear anatomical definition of NIL based on neural activity. The information will be important for future studies of this elusive, but functionally important structure, such as physiological recording of NIL neurons and the understanding of the role of NIL in visual and cognitive functions.

For Specific Aim 3, the expression of CO, PV, and ZENK was compared between the two hemispheres after occlusion or lesion was made unilaterally. The results clarified the significance of neural signal for chemical expression in higher visual areas. The information was essential to confirm whether or not these neural markers are dependent on visual signal per se. It was hypothesized that if the visual signal had significant effects, E and NIL could be distinguished from the surrounding regions.

Method

Subjects

In total, twelve adult white Carneaux pigeons (*Columba livia*) obtained from Palmetto Pigeon Plant, South Carolina were used in this study. The sex of each bird was determined behaviorally before experimentation by observing their behavioral responses to a live conspecific, and was verified post-mortem by visual inspection of the reproductive organs. All birds were housed individually in cages, separated by opaque partitions to restrict visual and physical interaction with other birds throughout the entire duration of the study. The vivarium was maintained on a constant 12h light: 12 h dark cycle. The birds had free access to water and a balanced diet of mixed grains and were weighed weekly to ensure their health and maintenance of a stable weight. All procedures outlined in this study were conducted in accordance with the NIH guidelines and approved by the University of South Florida Institutional Animal Care and Use Committee.

Unilateral Lesions

The subjects were divided into two groups: Lesion and Occlusion groups (n = 6 each). Pigeons in the Lesion group received a unilateral electrolytic lesion to destroy the thalamic structure, Rt. For the lesion surgery, pigeons were deeply anesthetized with ketamine (40mg/kg of body weight, i.m. Aveco Co., Inc., Fort Dodge, IA) and xylazine (10 mg/kg of body weight, i.m. Lloyd Laboratories., Shenandoah, IA), and were then

placed in a stereotaxic apparatus (David Kopf Instruments, Tujunga, CA). All lesions were administered through an insulated electrode attached to a D.C. Constant Current Lesion Maker (Grass model # D.C. LM5A, Quincy, MA) at a current of 1mA for 20 seconds. The location of lesion target was specified according to coordinates in the stereotaxic atlas of the pigeon brain (A: 6.10, L: 3.00, and V: 5.50; Karten & Hodos, 1967). Lesion electrodes were made by coating insect pins with epoxy (EPOXYLITE Corp., Irvine, CA) and then exposing the tip (0.5 mm). The side of lesion (left or right) was counterbalanced among subjects. After surgery, the pigeon was returned to its cage for recovery and monitored daily for seven days.

Monocular Occlusions

One eye of each subject in the Occlusion group was blocked by applying a small opaque cap made of polyvinyl chloride (1.5 cm internal diameter, 2 mm thickness) around the outside of one pigeon eye using a non-toxic surgical tissue adhesive (3M Vetbond). The open end was covered with opaque tape (black electrical tape) to keep light from entering. After the eye-cap was applied, the subject was returned to its cage and monitored daily for seven days to make sure this occlusion procedure did not cause any undue stress and that the eye-cap remained in place.

Exposure to Live Stimulus

Following a seven-day period of post-lesion recovery for the Lesion group or eye-cap application for the Occlusion group, all subjects were sacrificed immediately after they were exposed to a live conspecific stimulus. The purpose of the exposure to

conspecifics was to maximize the ZENK expression in the telencephalon (Mello & Ribeiro, 1998; Patton, Husband, & Shimizu, 2009). The subject was first placed in a testing apparatus (90 X 90 X 90 cm) in complete darkness for approximately 12 hours (overnight). After the period of darkness, an overhead light was turned on and a live pigeon (male) was be placed in front of the subject for 1.5 hours. Although the subject and the live conspecific stimulus did not have physical contact, the separation by a clear Plexiglas window permitted visual, auditory, and olfactory interaction. A wire-mesh cover on the top of the chamber was used to prevent flight and escape, but in no other way inhibited the birds' behavior. The subject was sacrificed following the end of the stimulus exposure session. The timeframe of 1.5 hours of live stimulus exposure was to allow for peak expression of ZENK (Mello & Ribeiro, 1998).

Perfusions

Pigeons were deeply anesthetized via ketamine (at least 40mg/kg of body weight, i.m.) and xylazine (at least 10 mg/kg of body weight, i.m.) and then perfused transcardially with a 0.9% saline solution followed by 4% ice-cold paraformaldehyde in phosphate buffer (0.1 M PB, pH 7.4). Brains were post fixed for 12 hours at 4° C, followed by immersion in a 30% sucrose solution for 24 hours at 4° C. Brains were then frozen in dry ice and cut in 40μm transverse sections on a sliding microtome. Sections were washed three times at 10 min. each in PB in preparation for further histological processing.

Parvalbumin and ZENK Immunohistochemistry

For visualization of parvalbumin (PV) and ZENK, the appropriate antibodies against them were used in the primary incubation. For PV, the primary antibody was a monoclonal mouse anti-PV (dilution 1:10000; Sigma, St. Louis, MO). For ZENK, the antibody was a polyclonal rabbit anti-Egr-1 (dilution 1:10000; Santa Cruz Biotechnology, Santa Cruz, CA). The tissue sections were incubated in the respective antibody solution along with PB with 0.3% Triton X-100 at 4˚C for 12 hours. The tissues were then washed in PB (3 x 10 min.) followed by 1 hour of incubation in biotinylated secondary antibodies (anti-mouse for PV, and anti-rabbit for ZENK, both 1:200, Vector Laboratories, Burlingame, CA) and 0.3% Triton X-100 in PB for 1 hour at room temperature. The tissues were washed again in PB (3 x 10 m). Antibody binding was visualized with an avidin-biotin reagent (1:200 dilution of the Vectastain ABC Elite kit, Vector Laboratories) followed by incubation in a 0.025% solution of 3,3´-diaminobenzidine (DAB, Polysciences, Warrington, PA) and hydrogen peroxide. Once stained, tissue sections were mounted onto glass slides and coverslipped.

Cytochrome Oxidase Histology

Tissues were incubated in a centrifuge tube containing 4.5 mL 0.1M PB, 0.0025g DAB, 0.0025 g cytochrome C (equine heart, Sigma C7752), and 0.2 g sucrose at 37˚C, in the dark, for 2 hours. Following staining, tissues were washed in PB (3 x 10 min.) at room temperature, mounted onto glass slides, and coverslipped.

Additional Histology

Adjacent tissue sections from each brain were also stained with cresyl violet to show major cell groups and fiber tracts for precisely locating anatomical boundaries of the relevant structures.

Parvalbumin and Cytochrome Oxidase Image Capturing and Analysis

All tissues stained for PV and CO were examined and photographed using a macroscope (Wild Makroskop) or a microscope (Nikon Microphot FX). The digital images were acquired using a NIKON CCD camera (DXM 1200) or SPOT Insight QE camera (Diagnostic Instruments, Sterling Heights, MI) which can be mounted on each of these scopes. The images were then loaded to Adobe Photoshop software as black and white positive images (Adobe Systems Inc., Mountain View, CA) using a Dell Optiplex PC. Brightness and contrast were adjusted for the final images. No additional filtering or manipulation of the images was performed.

The distribution of PV-ir cell bodies, PV-ir neuropil, and CO staining in E was mapped by using quantitative analysis at specific tissue sections through the anterior-posterior extent of E were selected. Specifically, E was examined at atlas sections A10.50, A10.00, A9.50, and A9.00 according to the pigeon stereotaxic brain atlas by Karten and Hodos (1967). Within each tissue section of E, two square target regions each 250 X 250 µm (0.0625 mm^2) were designated to measure the number of PV-ir cell bodies in the inner region and the outer region of E. Figure 5 shows the location of the inner and outer target regions.

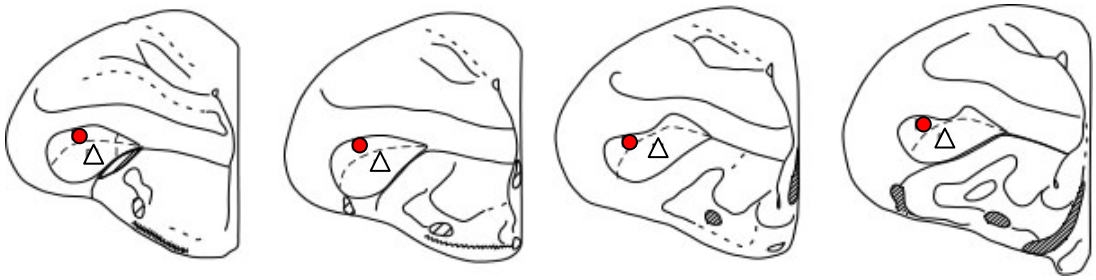

Figure 5. Schematics showing the inner (triangles) and outer (circles) target regions of E where the number of PV-ir cells were counted. The anterior coordinates of the sections shown in the figure from the left are: A10.50, 10.00, 9.50, and 9.00.

The density analysis of PV-ir neuropil and CO staining was conducted as follows. Microphotographic images taken at constant illumination were converted to grayscale using Photoshop (CS3), and then the optical density values were acquired for each target region via NIH ImageJ (v. 1.41). All analyses were conducted blind to the treatment condition and hemisphere. The total density values from each subject were then used to calculate summary statistics and perform subsequent statistical tests. Similar to the procedure used to count PV-ir cell bodies, target regions were designated within each tissue section of E. However, instead of two regions, six square target regions each 250 X 250 µm (0.0625 mm^2) were designated to measure the density of PV-ir neuropil and CO staining in E. Figure 6 shows the location of the six regions. Processed sections from all brains were under constant illumination and digitally recorded using a CCD camera (Nikon DXM1200) mounted on a macroscope (Wild M420). Using ImageJ (v. 1.41, Abramoff, Magelhaes, & Ram, 2004), the six target regions of E were delineated and calibrated according to a Kodak step tablet (Rasband, 1997-2009). The relative density measurements were compared to examine the regional differences within E. The protocol for this density analysis can be found in Appendix A.

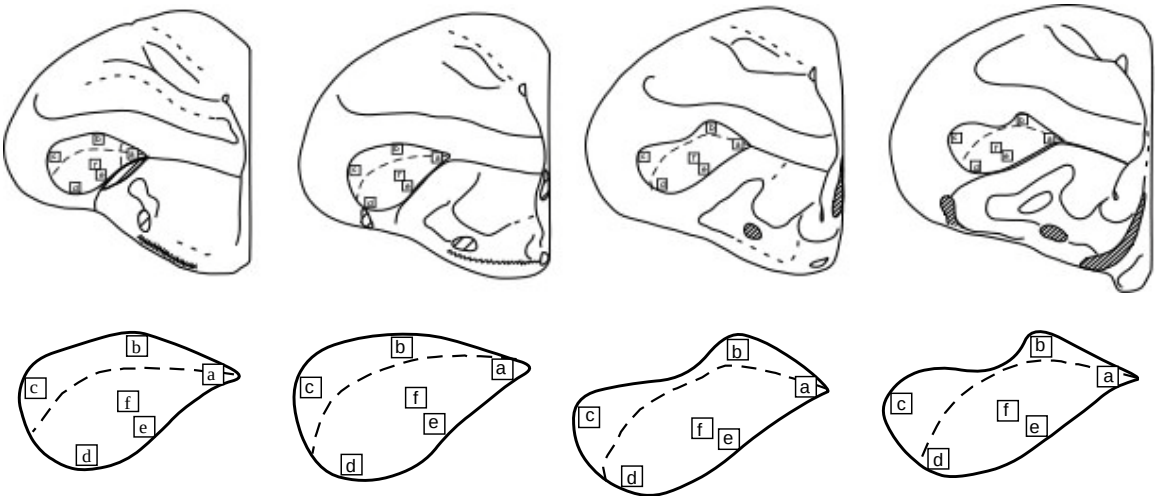

Figure 6. Schematics showing the six target regions within E where the density of PV-ir neuropil and CO staining was measured in lower magnification (top) and higher magnification (bottom). The anterior coordinates of the sections shown in the figure from the left are: A10.50, 10.00, 9.50, and 9.00.

The PV-ir cell bodies were counted as follows. A signal was counted as a cell if staining within the neurons revealed a complete soma perimeter, and it was clearly differentiated from background. Any potential bias was eliminated by the blind counting procedure. Each neuron was marked with a paint spot using CANVAS (v.11.0, Deneba Systems) graphic software and the spots were counted with ImageJ software. The total cell counts from each subject were then used to calculate summary statistics and perform subsequent statistical tests.

ZENK Image Capturing and Analysis

For all tissues stained for ZENK, low-power microphotographs were taken of the entire forebrain in the left and right hemisphere simultaneously using a motorized Nikon TE 2000U inverted microscope to capture ZENK-ir patterns across both hemispheres simultaneously. Based on the images, the presumptive borders of NIL were identified

visually by comparing the quantity of ZENK-ir cells in the left and right hemispheres. This procedure was based on the assumptions that 1) NIL is relatively homogeneous in terms of ZENK expression and that 2) the level of ZENK expression in NIL was significantly reduced by lesions in the ipsilateral Rt and by occlusions of the contralateral eyes. Because the exact size and shape of NIL was not known in advance, it was necessary to be conservative in assuming which group of ZENK-ir cells belonged to NIL. To do this, NIL was tentatively defined to be located dorsolateral to the caudal end of E, and ventromedial to the tractus arcopallium dorsalis (DA). Figure 7 is an illustration, which shows the location of the putative NIL.

For quantitative analysis, the central portion of NIL was suggested to be at A7.00 and A6.00 (Husband & Shimizu, 1999), in each of which a square target region of 750 X 750 μm (0.5625 mm^2) was used to count the number of ZENK-ir cells. Figure 7 shows schematic drawings illustrating the areas for quantitative analysis of the ZENK expression.

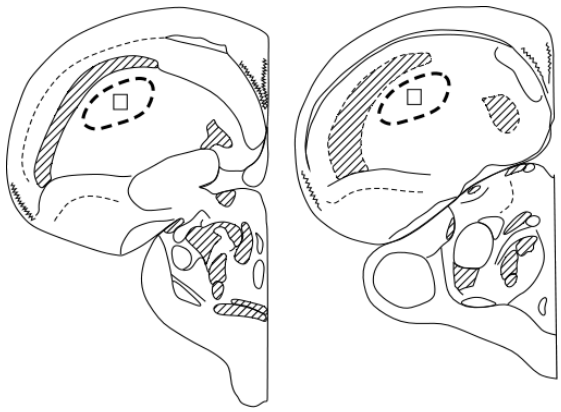

Figure 7. Schematic showing two transverse sections of the avian brain where NIL is thought to be located. The dotted line shows the region thought to be NIL and the square target region shows where ZENK-ir cells were counted. The elongated hatched region dorsolateral to the putative NIL is the tractus arcopallium dorsalis (DA). The locations (anterior-posterior coordinates) shown in the figure from the left are: A7.00 and 6.00.

The number of ZENK-ir neurons was counted using the following method. When ZENK proteins are stained, the chromatin remains in the nucleus of the neuron and not in the dendrites or axons. Therefore, ZENK protein expression is morphologically highly similar from cell to cell; ZENK-ir cells can be differentiated from artifact staining and counted quickly. Using existing optical analysis functions in ImageJ, Mahmud (2008) developed a new image analysis technique. This new method of analysis called, *A New Digital Imaging Protocol for Signal Detection and Distribution Analysis in Histological Samples*, uses a *Find Maxima* function to identify and label ZENK-ir cells as localized spikes of chromatic value on an image. Thus, the function works by recognizing any pixel with a high chromatic value relative to its neighboring pixels. Specifically, the *Find Maxima* function was used to detect signals based on spikes of chromatic values present in the tissue sample. The concept is logical, since signals are traditionally localized dark spots against a lighter background, which is the exact definition of Maxima according to ImageJ. In addition, since the function only looks at local color values, it is not subject to overall optical inconsistencies such as uneven staining, lighting or weak signal strength. For instance, staining patterns often clump up near the edges of samples masking signals in a generally dark color that visual and even threshold-based analysis can not analyze. The threshold function actually views the entire region as one dark signal due to its relative darkness in comparison with the rest of the slide instead of a region of multiple signals.

Once the *Find Maxima* function was executed, the image was reproduced with only the maxima highlighted. Then, a function known as *Dilation* was used on this reproduced image, which simulated a form of signal extraction. The concept is based on

the fact that once the maxima are dilated, the signals have a finite black area. Therefore, the more signals that are present in any given space, the more area is colored black in those squares. Once the squares are averaged, darker squares can be correlated with higher signal count. The protocol is included in Appendix B.

Lesion Reconstructions

Rotundal lesion reconstruction was carried out on a series of standard plates derived from the atlas of the pigeon brain of Karten and Hodos (1967). Gliosis and necrosis in the diencephalon was recorded. The extent of each lesion was determined from measurements of reconstructions made with camera and graphics software (CANVAS. v.11.0).

Statistical Analyses

For Specific Aim One, cell count data were statistically analyzed using 4-way (treatment x hemisphere x region of E x location) mixed analysis of variance (ANOVA), where the hemisphere (control versus experimental), region of E (inner versus outer), and location (anterior-posterior coordinates) were repeated (within subject) measures and treatment (lesion versus occlusion) was an independent variable (see Figure 5). Similar tests were conducted for analysis of PV-ir neuropil and CO staining intensity where the hemisphere (control versus experimental), region within E (six different target regions of E), and location (anterior-posterior coordinates) were repeated (within subject) measures and treatment (lesion versus occlusion) was an independent variable (see Figure 6)

For Specific Aim Two, the differences in the mean number of ZENK-ir cells in NIL were analyzed by conducting a 2 x 2 factorial mixed model ANOVA where hemisphere (control versus experimental) was a repeated (within subject) measure and treatment (lesion versus occlusion) was an independent variable. The statistical designs conducted for the first two specific aims also addressed the questions of Specific Aim Three. For each of these statistical analyses, Significant 3-way ANOVAs (alpha = 0.05) were followed up with Fishers LSD (protected t) tests.

Results

In the present study, the brain tissues from the same animals were processed and analyzed for, not only one specific Aim, but sometimes for other Aims as well. In order to avoid presenting redundant data, the results section is organized by presenting the lesion reconstruction data (Specific Aims 1, 2, and 3), followed by data from PV-immunohistocehmistry (Specific Aims 1 and 3), CO-histochemistry (Specific Aims 1 and 3), and ZENK-immunohistochemistry (Specific Aims 2 and 3).

Lesion Reconstructions

Overall, six pigeons received a unilateral lesion to the thalamic nucleus, Rt (PG236, PG239, PG234, PG259, PG254, and PG47). In each of the lesion cases, Rt was either mostly or completely destroyed in one hemisphere. In some cases the lesion site was large enough to include neighboring structures, such as n. triangularis (T). Below is a brief description of each lesion case starting from the smallest lesions to the most extensive lesions.

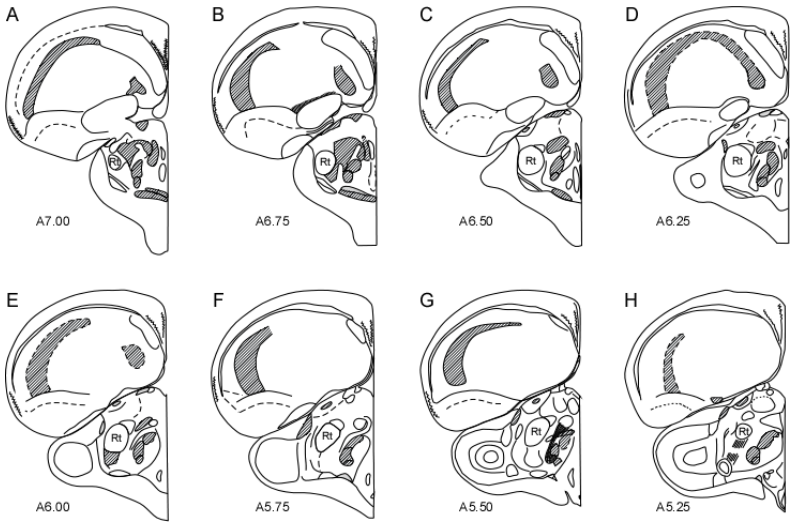

Figure 8. Schematics showing the location of the nucleus rotundus (Rt). Only the left hemisphere of each anterior-posterior coordinate is shown here.

Individual lesion reconstruction cases.

Figure 9 illustrates the degree of lesion damage for subject PG236. Overall, the lesion was relatively small, extending just from anterior coordinate 7.00 through 6.50. The lesion was mainly localized in the anterior portion of Rt leaving intact a large portion of the posterior sections (Figure 9 D-H).

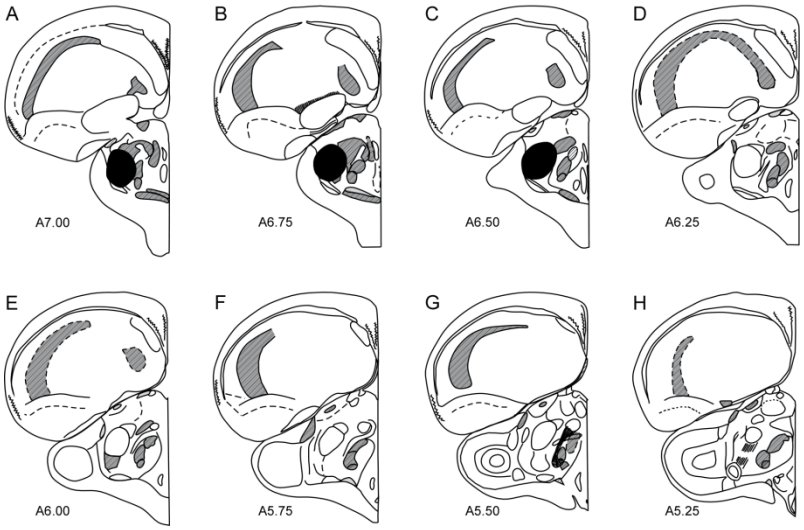

Figure 9. Rt damage reconstruction for subject PG236. Ablated or damaged tissue in the Rt is indicated by solid black areas.

Figure 10 illustrates the degree of lesion damage for subject PG239. The damage overall was moderate, extending from A7.00 through A6.25. The lesions were seen in the rostral portion of Rt, but left all of the caudal sections intact (Figure 10 E-H). Damage to other structures was restricted to some moderate damage in the adjacent T (Figure 10 C-D).

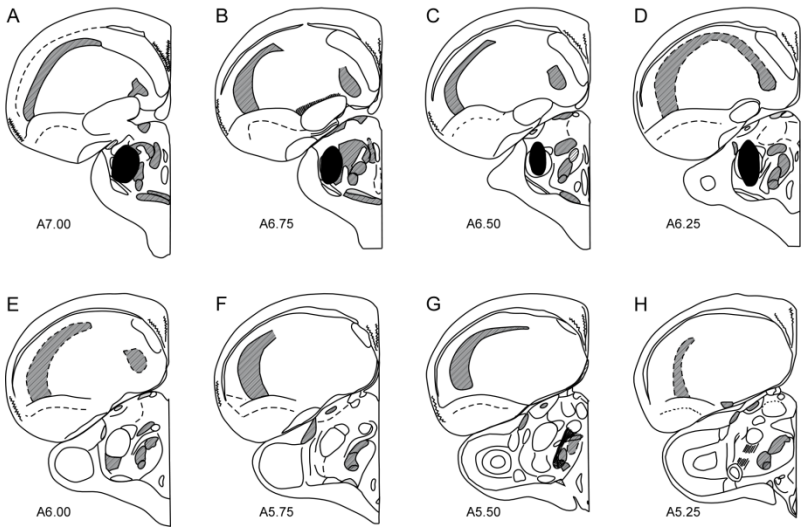

Figure 10. Rt damage reconstruction for subject PG239.

Figure 11 illustrates the degree of lesion damage for subject PG234. The damage overall was more substantial compared the previous two cases. The lesions included the entire rostral portion of Rt, leaving only a small portion of the caudal sections (Figure 11 G-H). Damage to other structures was restricted to some moderate damage in the adjacent T (Figure 11 C-F).

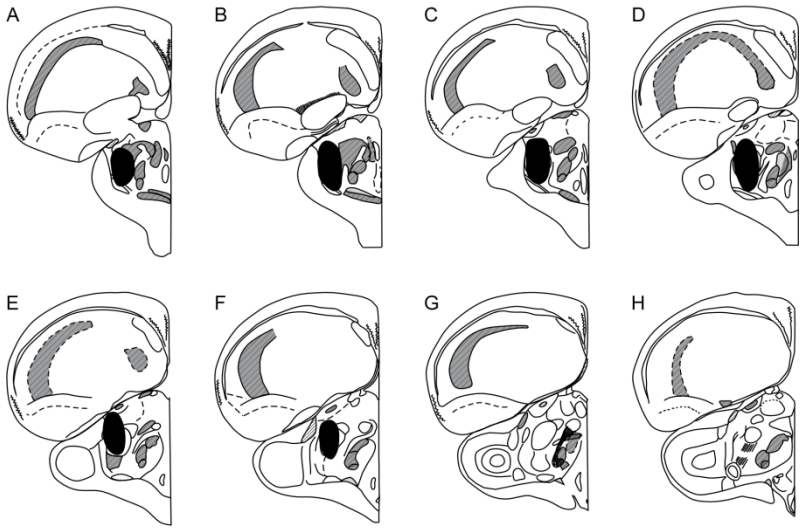

Figure 11. Rt damage reconstruction for subject PG234.

Figure 12 illustrates the degree of lesion damage for subject PG259. The damage overall was also substantial from A7.00 through A5.50. The lesions included the entire rostral portion of Rt, sparing the most caudal sections (Figure 12 G-H). Damage to other structures was restricted to some moderate damage in the adjacent T (Figure 12 C-F).

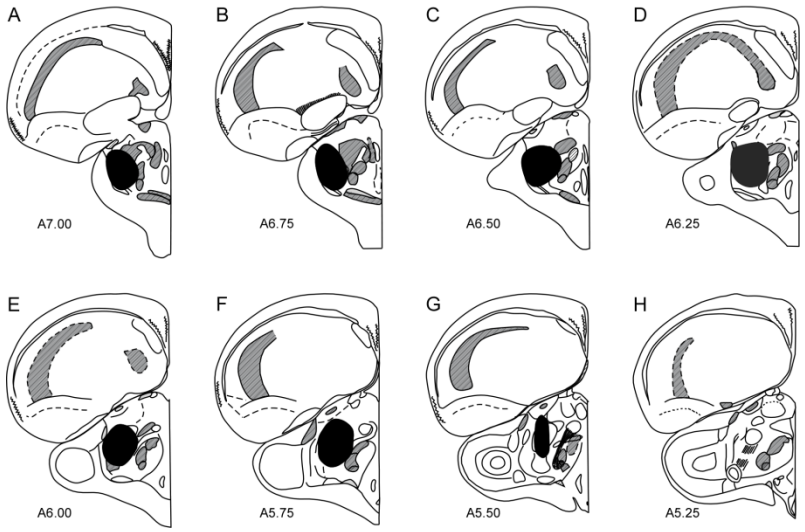

Figure 12. Rt damage reconstruction for subject PG259.

Figure 13 illustrates the size of the lesion for subject PG254. The damage overall was substantial extending the entire anterior-posterior axis of Rt. Damage to other structures was restricted to some moderate damage in the adjacent T (Figure 13 C-F).

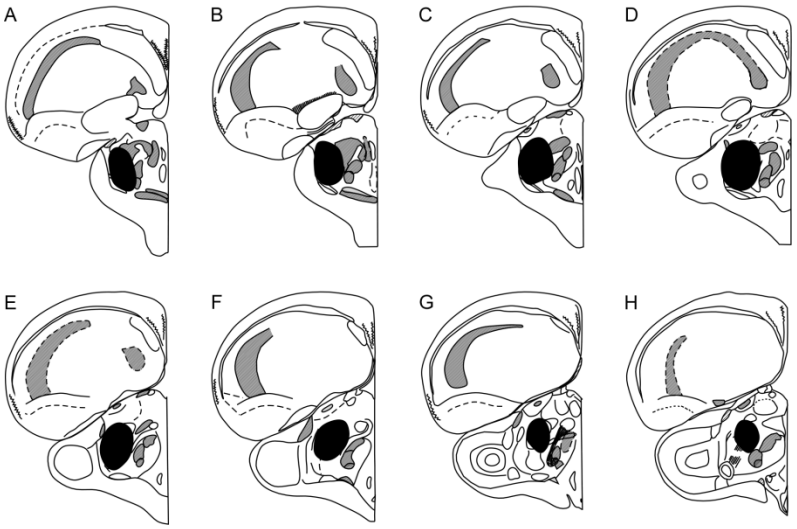

Figure 13. Rt damage reconstruction for subject PG254.

Figure 14 illustrates the degree of lesion damage for subject PG47. The damage overall was also substantial. It extended from anterior coordinate A7.00 through A5.25 and was centered in Rt.

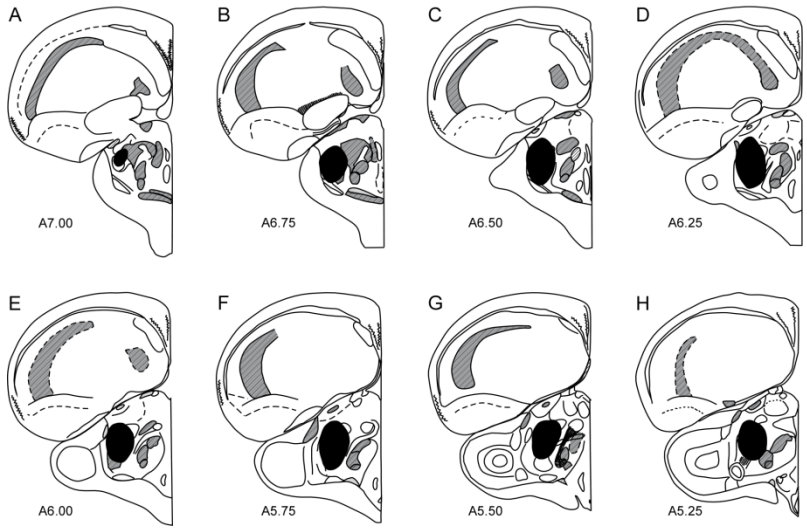

Figure 14. Rt damage reconstruction for subject PG47.

PV Immunohistochemistry

In total, the brain tissues of eight birds (four in the unilateral lesion condition and four in the monocular occlusion condition) were processed to detect PV-ir cell bodies and neuropil in E. Below are microphotographs showing E on the control and experimental hemispheres at each of the four different anterior-posterior locations for all of the birds.

Individual PV cases.

PG234 (Unilateral Lesion) PV expression in E (Figure 15).

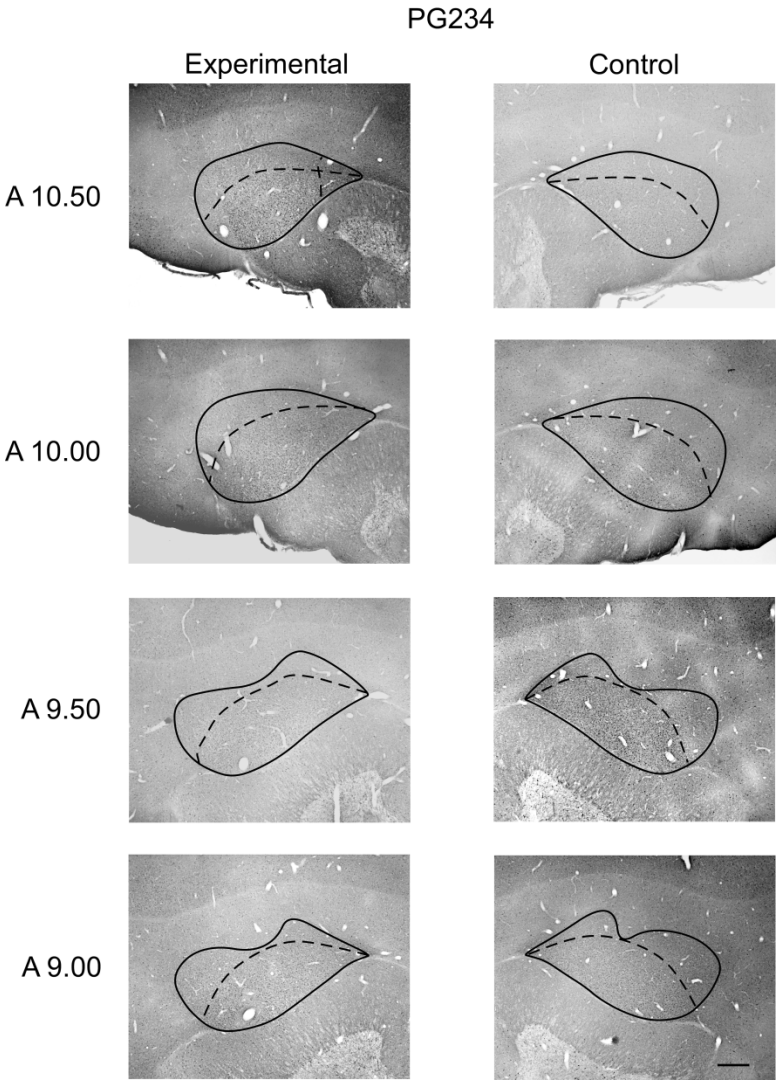

Figure 15. Microphotographs of PG234 showing the distribution pattern of PV in E after unilateral lesion. For this case, the left Rt was destroyed. Scale bar = 500 µm.

PG259 (Unilateral Lesion) PV expression in E (Figure 16).

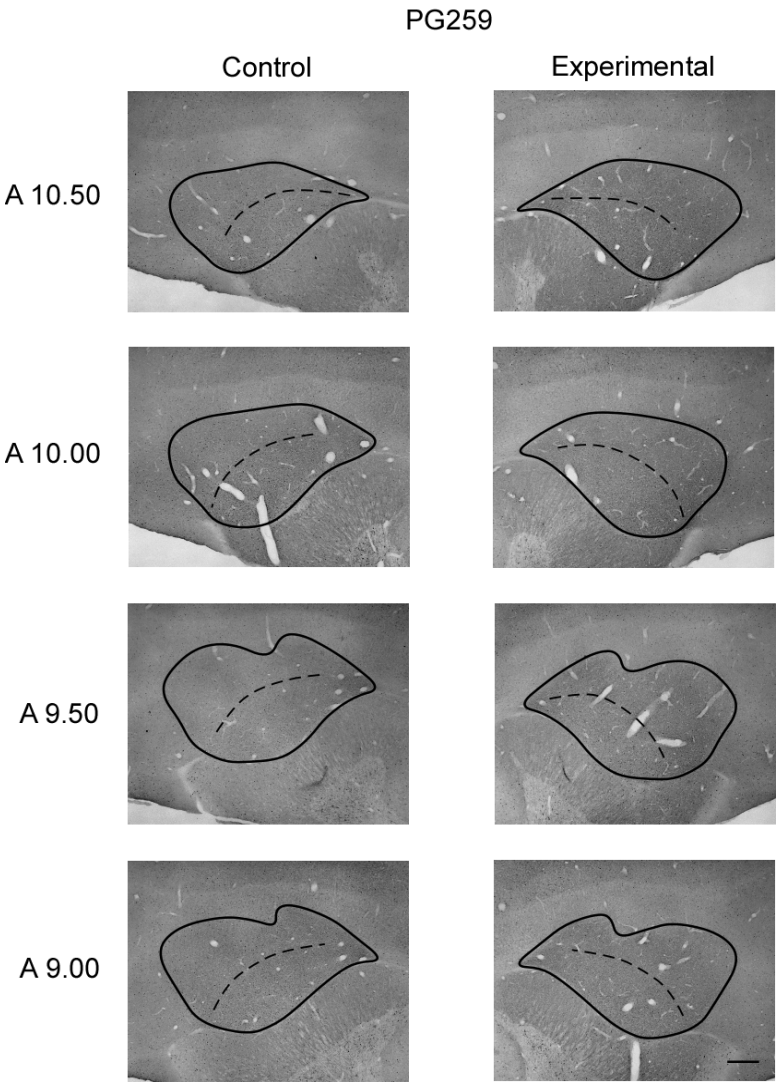

Figure 16. Microphotographs of PG259 showing the distribution pattern of PV in E after unilateral lesion. For this case, the right Rt was destroyed. Scale bar = 500 µm.

PG254 (Unilateral Lesion) PV expression in E (Figure 17).

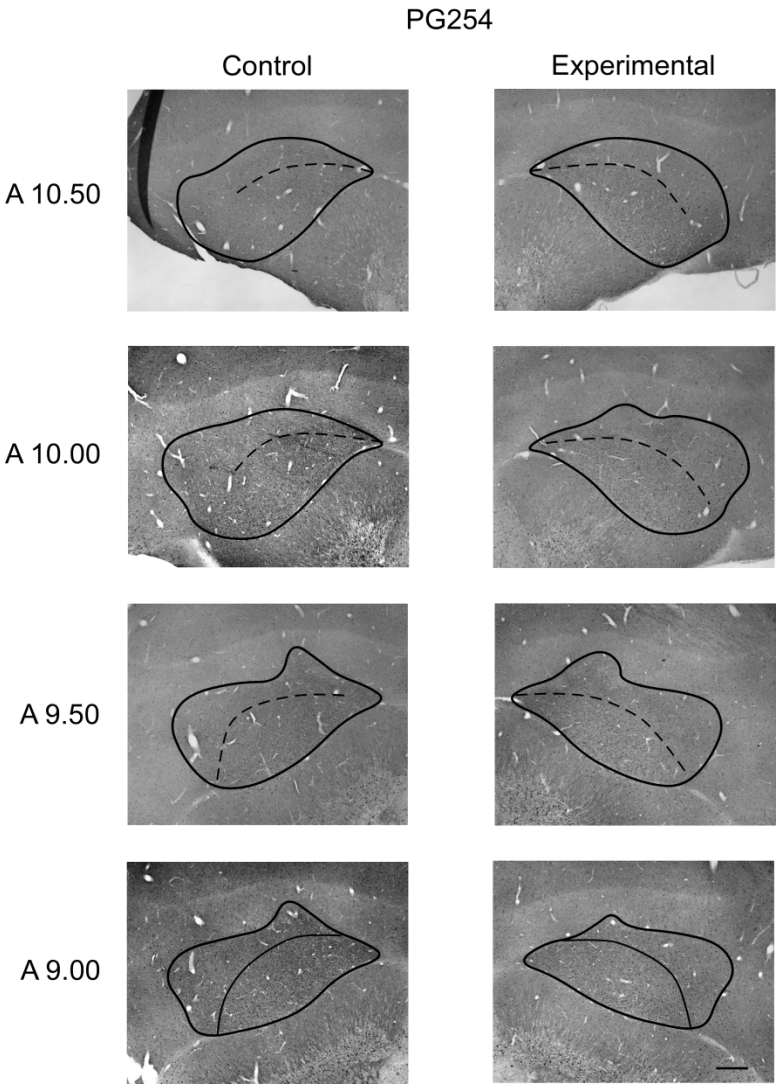

Figure 17. Microphotographs of PG254 showing the distribution pattern of PV in E after unilateral lesion. For this case, the right Rt was destroyed. Scale bar = 500 µm.

PG47 (Unilateral Lesion) PV expression in E (Figure 18).

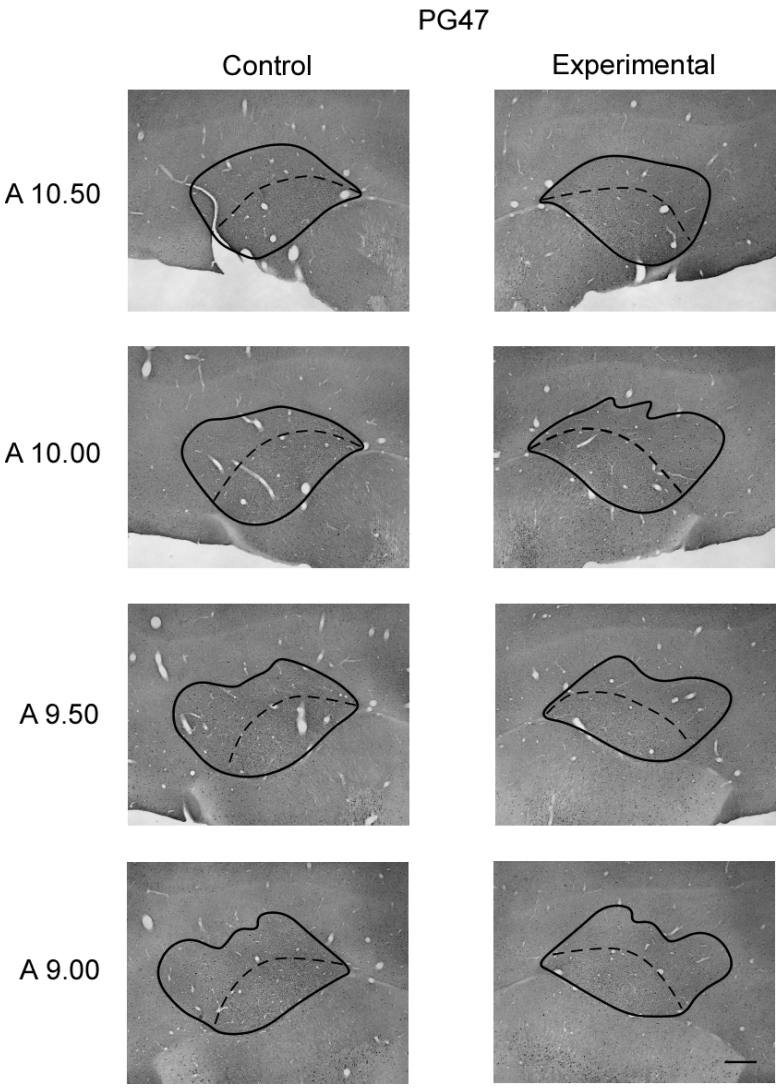

Figure 18. Microphotographs of PG47 showing the distribution pattern of PV in E after unilateral lesion. For this case, the right Rt was destroyed. Scale bar = 500 µm.

PG253 (Monocular Occlusion) PV expression in E (Figure 19).

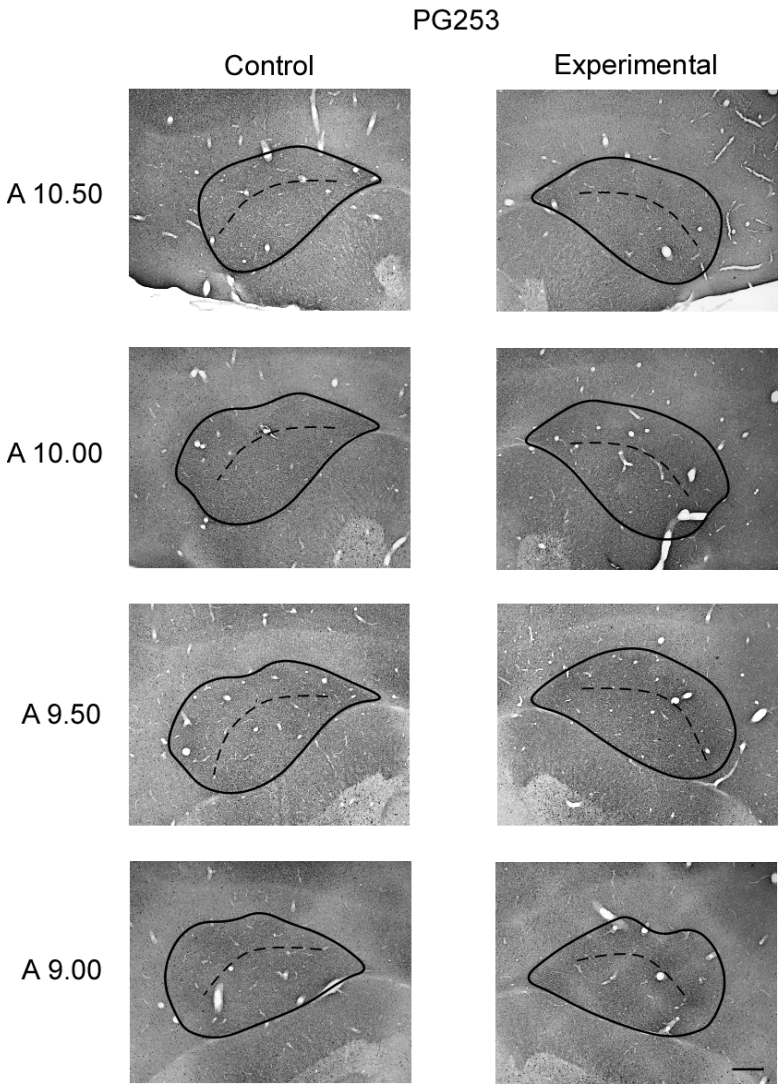

Figure 19. Microphotographs of PG253 showing the distribution pattern of PV in E after monocular occlusion. For this case, the left eye was occluded. Scale bar = 500 µm.

PG263 (Monocular Occlusion) PV expression in E (Figure 20).

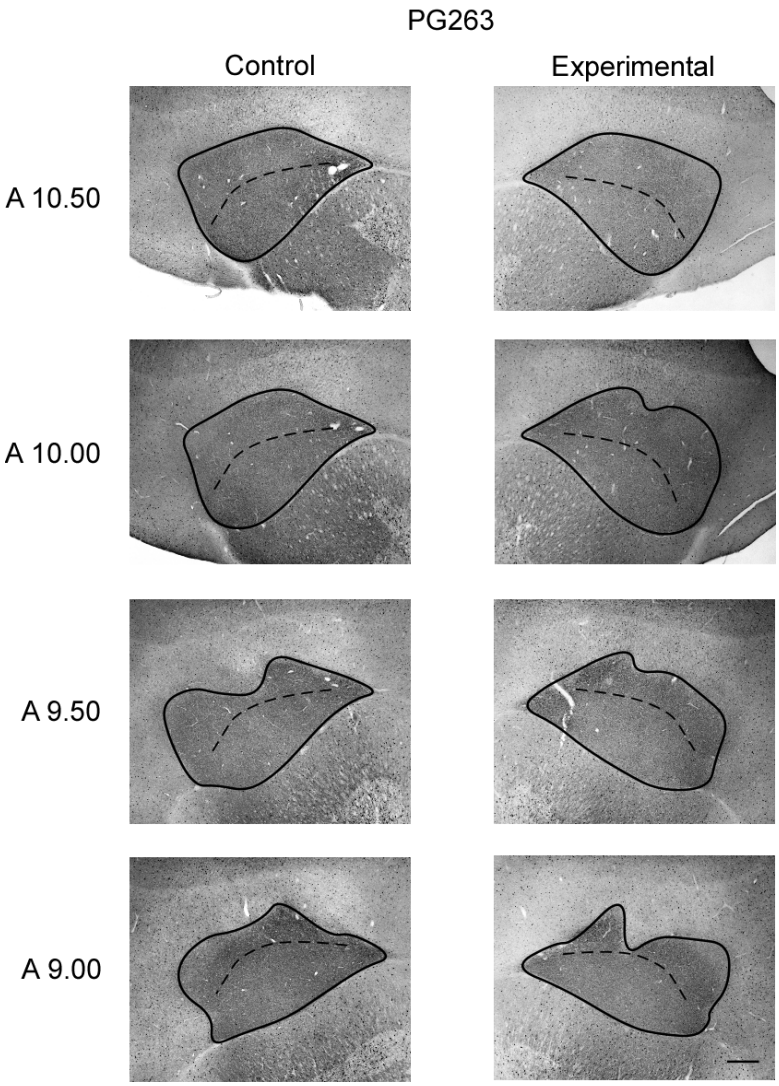

Figure 20. Microphotographs of PG263 showing the distribution pattern of PV in E after monocular occlusion. For this case, the left eye was occluded. Scale bar = 500 µm.

PG256 (Monocular Occlusion) PV expression in E (Figure 21).

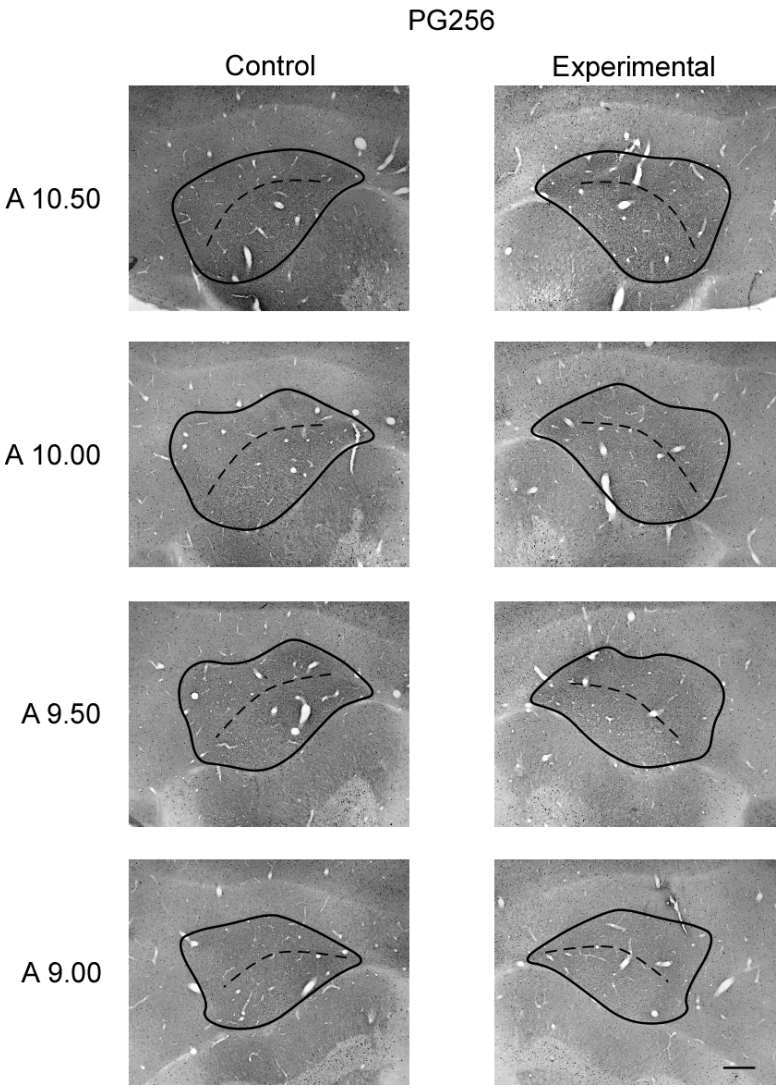

Figure 21. Microphotographs of PG256 showing the distribution pattern of PV in E after monocular occlusion. For this case, the left eye was occluded. Scale bar = 500 µm.

PG260 (Monocular Occlusion) PV expression in E (Figure 22).

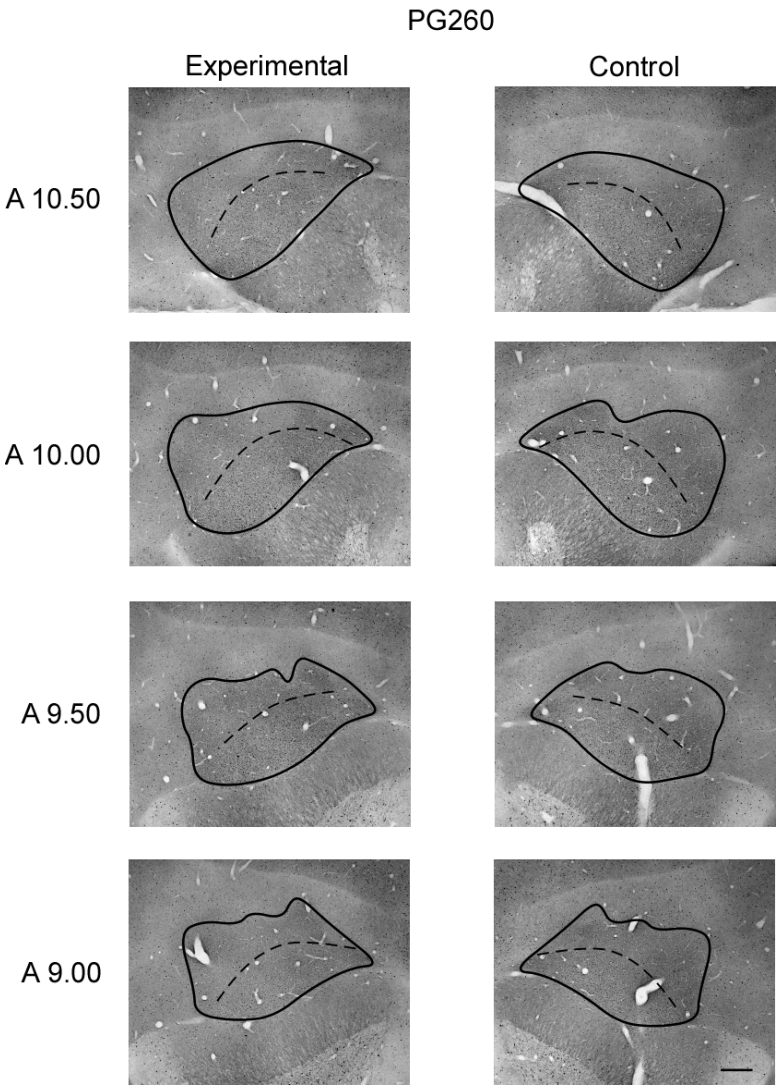

Figure 22. Microphotographs of PG260 showing the distribution pattern of PV in E after monocular occlusion. For this case, the left eye was occluded. Scale bar = 500 µm.

Number of PV-ir neurons in E.

Eight pigeons were used for Specific Aim One. Four birds received unilateral lesions to the thalamic nucleus, Rt (PG234, PG259, PG254, and PG47) and four birds received monocular occlusions (PG253, PG263, PG256, and PG260). A factorial mixed design ANOVA was conducted to determine whether or not there was a significant difference in the mean number of PV-ir cells in E based on: treatment (lesion versus occlusion), hemisphere (control versus experimental), region of E (inner versus outer), and location (anterior-posterior coordinates).

In terms of simple main effects, the results showed that there was a significant difference in the mean number of PV-ir cells depending on the region of E (inner versus outer) $F(1, 6) = 119.43$, $p < 0.001$. Specifically, the mean number of PV-ir cells was significantly higher for the inner region of E ($M = 38.00$) compared to the outer region of E ($M = 8.48$; see Figure 23).

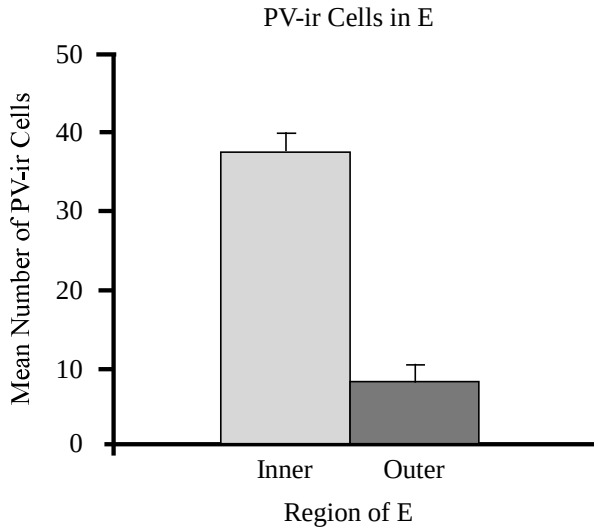

Figure 23. Graph showing the mean number of PV-ir cells counted in the inner and outer regions of E, across treatment (lesion versus occlusion), hemisphere (control versus experimental), and location (anterior-posterior coordinates). Mean values and standard error are shown.

No other simple main effects were significant. There was no significant main effect for treatment (lesion versus occlusion) $F(1, 6) = 0.01$, $p = 0.920$, hemisphere $F(1, 6) = 39.38$, $p = 0.160$, or location (anterior-posterior coordinates) $F(3, 8) = 2.31$, $p = 0.111$.

In terms of interaction effects, the Region of E x Location interaction was significant $F(3, 18) = 3.59$, $p = 0.034$; see Figure 24).

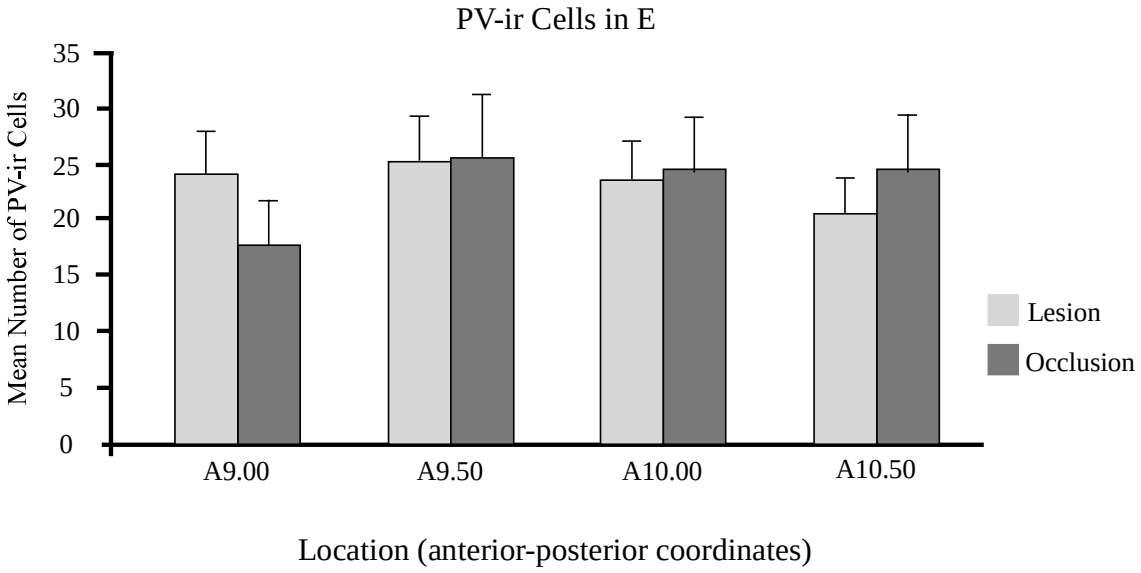

Figure 24. Graph showing the mean number of PV-ir cells in both regions of E (inner versus outer) at each of location (anterior-posterior coordinates). Mean values and standard error are shown.

No other two-way interaction effects were significant. Specifically, Region of E x Treatment $F(1, 6) = 3.98$, $p = 0.093$, Hemisphere x Treatment $F(1, 6) = 0.62$, $p = 0.460$, Region of E x Hemisphere $F(1, 6) = 0.87$, $p = 0.388$, and Location x Treatment $F(3, 18) = 3.07$, $p = 0.054$). Note, that this last interaction effect approached significance.

The following three-way interaction effects were significant, Region of E x Hemisphere x Treatment $F(1, 6) = 6.77$, $p = 0.041$, Region of E x Hemisphere x Location $F(3, 18) = 4.21$, $p = 0.020$, and Region of E x Treatment x Location $F(3, 18) = 3.38$, $p = 0.041$. Figure 25 graphically depicts the Region of E x Hemisphere x Treatment interaction. Specifically, note that the number of PV-ir cells in E differs as a function of treatment condition and region.

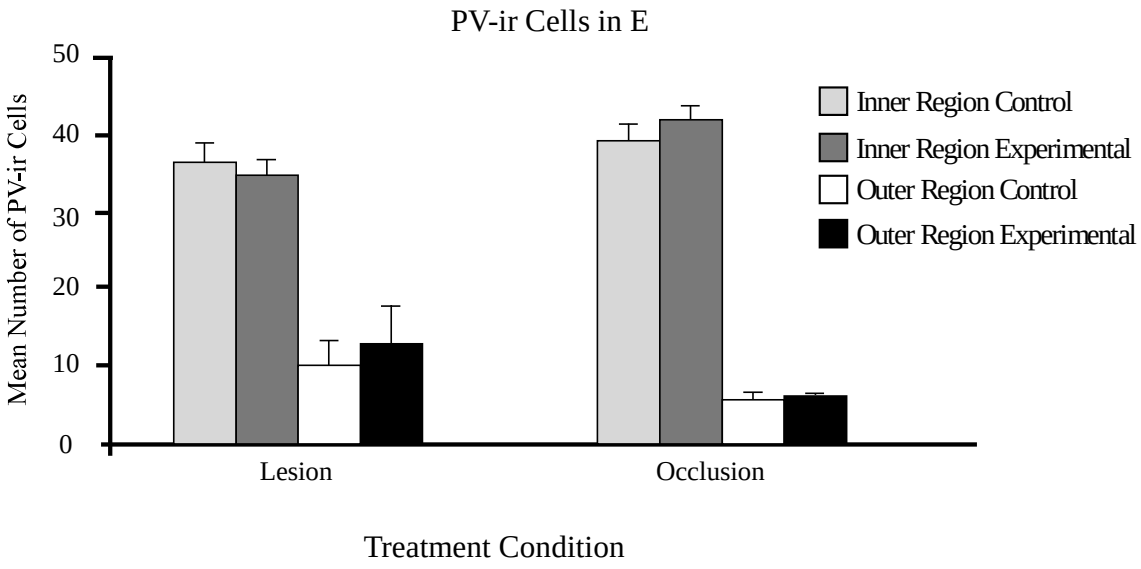

Figure 25. Graph showing the mean number of PV-ir cells in E for each treatment condition (lesion versus occlusion), hemisphere (control versus experimental), and region of E (inner versus outer) across location (anterior-posterior coordinates). Mean values and standard error are shown.

The Region of E x Hemisphere x Location interaction effect can be seen in Figure 26. Specifically, note that the number of PV-ir cells in E differs as a function of hemisphere and region.

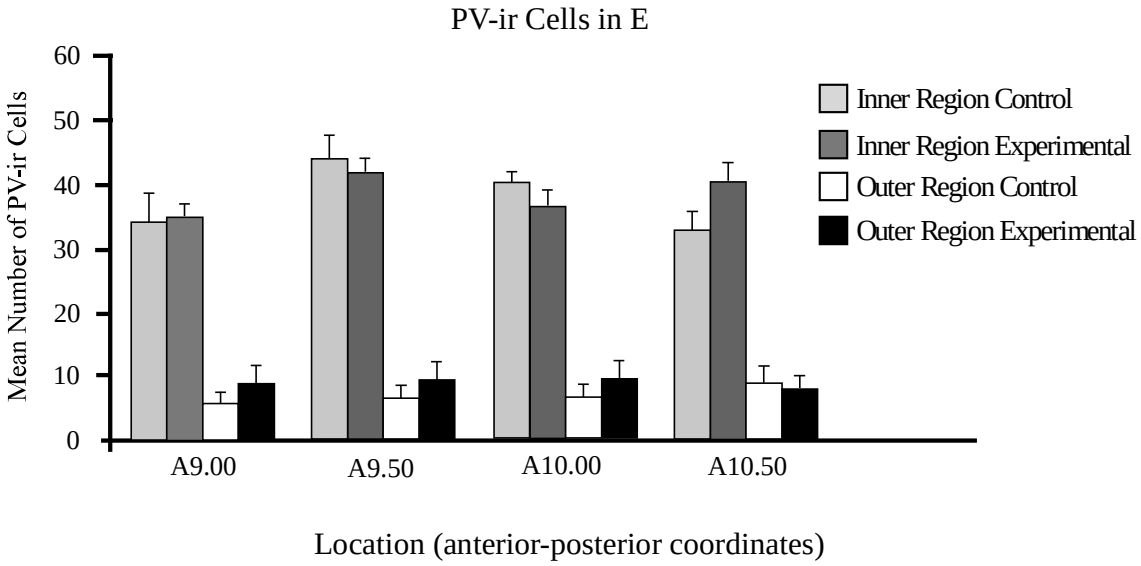

Figure 26. Graph showing the mean number of PV-ir cells by hemisphere (control versus experimental), region of E (inner versus outer), and location (anterior-posterior coordinates) across both treatment conditions (lesion versus occlusion). Mean values and standard error are shown.

The Region of E x Treatment x Location interaction effect can be seen in Figure 27.

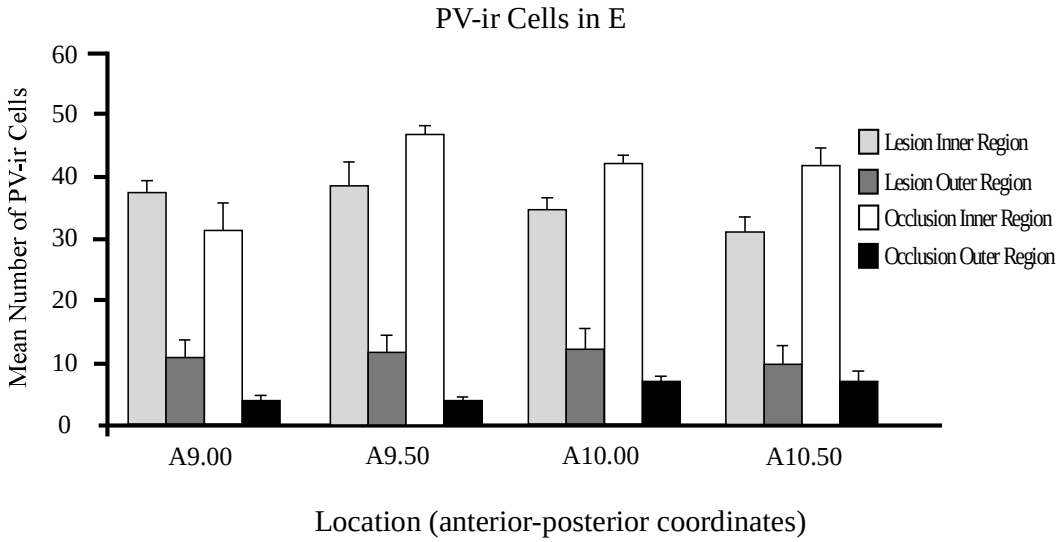

Figure 27. Graph showing the mean number of PV-ir cells by region of E (inner versus outer), treatment (lesion versus occlusion), and location (anterior-posterior coordinates) across both hemispheres. Mean values and standard error are shown.

The following interaction effects were not significant: Hemisphere x Location x Treatment $F(3, 18) = 0.13$, $p = 0.936$, Region of E x Hemisphere x Location x Treatment $F(3, 18) = 0.25$, $p = 0.856$.

Regarding cell morphology, a cursory glance showed that no obvious physical differences in cell size and shape were observed between the inner region of E and those the outer region. However, it was apparent that there were differences in the density of PV fiber connections (neuropil). Therefore, an optical density analysis procedure was used to measure the density level of several different regions within E.

Density of PV-ir neuropil in E.

In order to determine if the density of PV-ir neuropil in E varied as a function of treatment condition, hemisphere, regions within E, and anterior-posterior location, a factorial mixed design ANOVA was conducted. The between subjects variable was treatment condition (lesion versus occlusion) and the repeated measures were hemisphere (control versus experimental), region within E (sample areas *a* - *f*), and location (anterior-posterior coordinates: A10.50, 10.00, 9.50, 9.00),

There were two significant main effects. First, the main effect of region within E (*a* - *f*) $F(5, 30) = 12.32$, $p < 0.001$ was significant (Figure 28). Post hoc comparisons using the Fisher LSD test revealed that the mean PV-ir neuropil density values of specific regions within E were different from one another. Region *a* ($M = 0.63$, $SD = 0.11$) had significantly more PV-ir neuropil than that found in region *e* (M = 0.53, SD = 0.11; $t(30) = 2.614$, p = .014, two-tailed). Also, region *d* (M = 0.65, SD = 0.14) had significantly more PV-ir neuropil than that found in region *b* (M = 0.56, SD = 0.11; $t(30) = 2.567$, p

= .015, two-tailed), region *e* (M = 0.53, SD = 0.11; *t*(30) = 3.217, p = .003, two-tailed), and region *f* (M = 0.56, SD = 0.11; *t*(30) = 2.565, p = .015, two-tailed). A summary of these comparisons can be found in Table 1. In addition, the main effect of treatment (lesion versus occlusion) was significant $F(1, 6) = 11.08$, $p = 0.016$; see Figure 29).

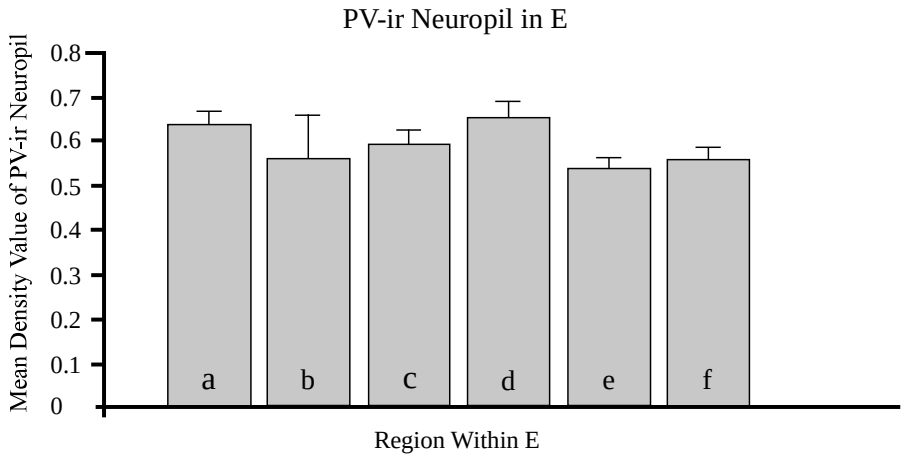

Figure 28. Graph showing the mean density value of PV-ir neuropil in the six target regions within E across treatment condition, hemisphere, and location. Mean values and standard error are shown.

Table 1
Pairwise Comparisons of Regions Within E

Region Within E	*M*	*SD*
a	0.63^{A}	0.11
b	0.56^{A}	0.11
c	0.59^{A}	0.12
d	0.65^{A}	0.14
e	0.53^{B}	0.11
f	0.56^{B}	0.11

Table 1. Means with the same letter in their superscripts do not differ significantly from one another according to a Fisher's LSD test.

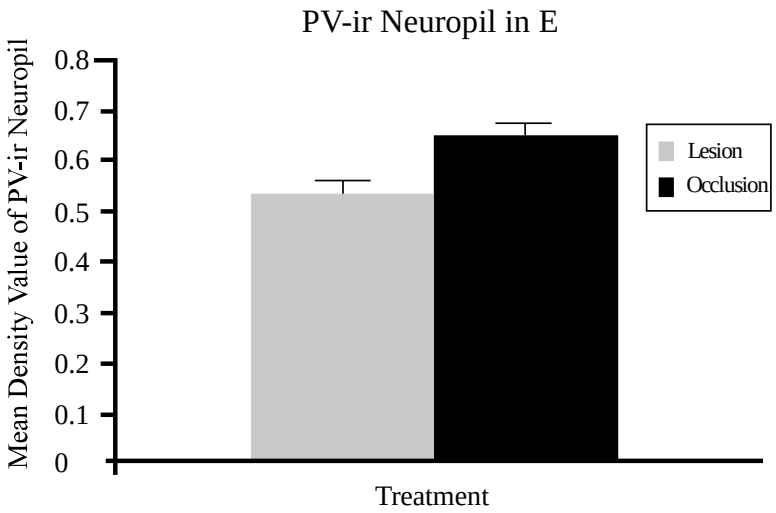

Figure 29. Graph showing the mean density value of PV-ir neuropil for both treatment conditions (lesion versus occlusion) across hemisphere, region within E, and location.

There was not a significant effect for hemisphere (control versus experimental) $F(1, 6) = 4.19$, $p = 0.087$ or location (anterior-posterior coordinates) $F(3, 18) = 0.08$, $p = 0.967$.

However, there were significant interaction effects for Treatment x Hemisphere $F(1, 6) = 16.25$, $p = 0.007$. Specifically, the mean density value of PV-ir neuropil was greater for the control hemisphere than the experimental hemisphere for the lesion treatment condition. There was not a difference between the control and experimental hemispheres for the monocular occlusions (see Figure 30).

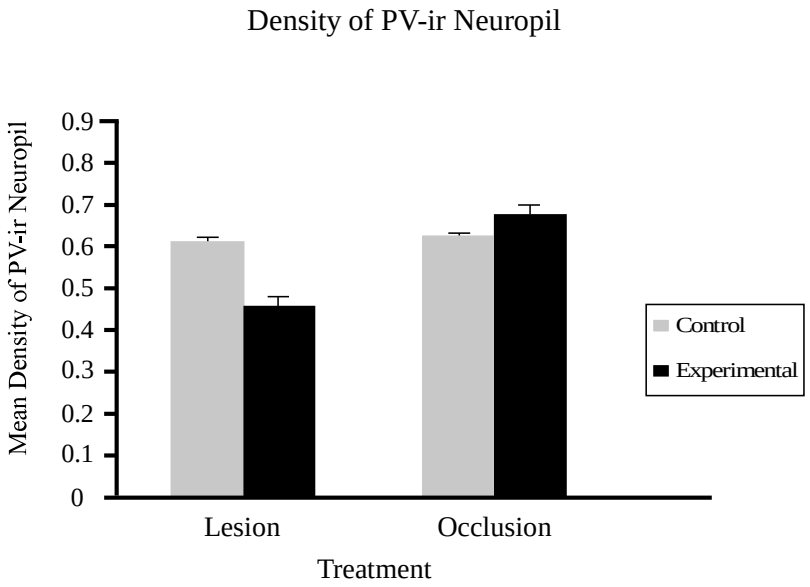

Figure 30. Graph showing the mean density value of PV-ir neuropil after unilateral lesion and monocular occlusion across the different regions within E and all locations (anterior-posterior coordinates). Mean values and standard error are shown.

Figure 31. further shows the density differences of six regions within E.

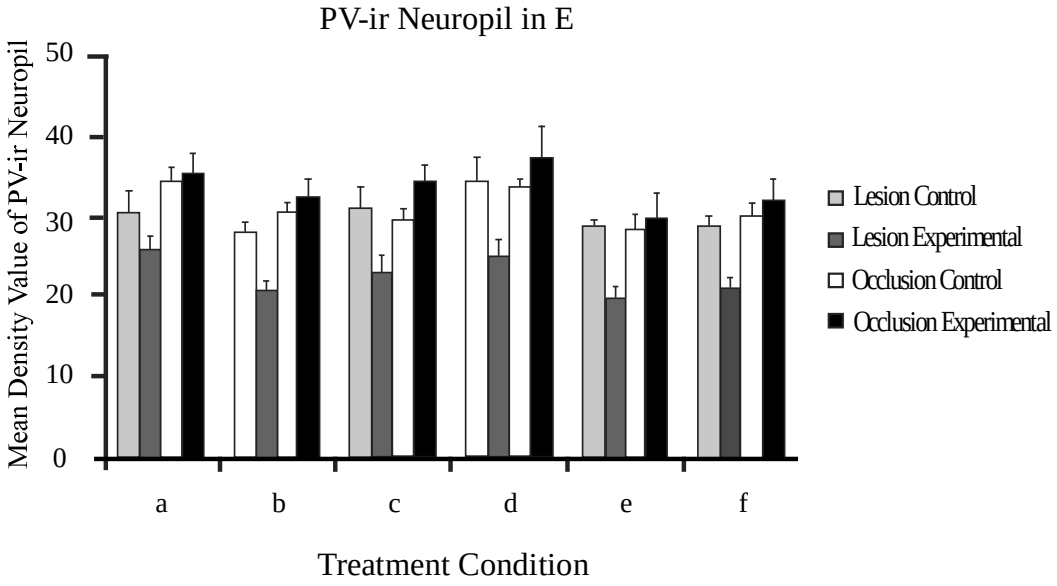

Figure 31. Graph showing the mean density value of PV-ir neuropil after unilateral lesion and monocular occlusion for each hemisphere at each of the different regions within E. Mean values and standard error are shown.

In addition, the Location x Region within *E* interaction effect was significant $F(15, 90) = 2.25$, $p = 0.010$; see Figure 32).

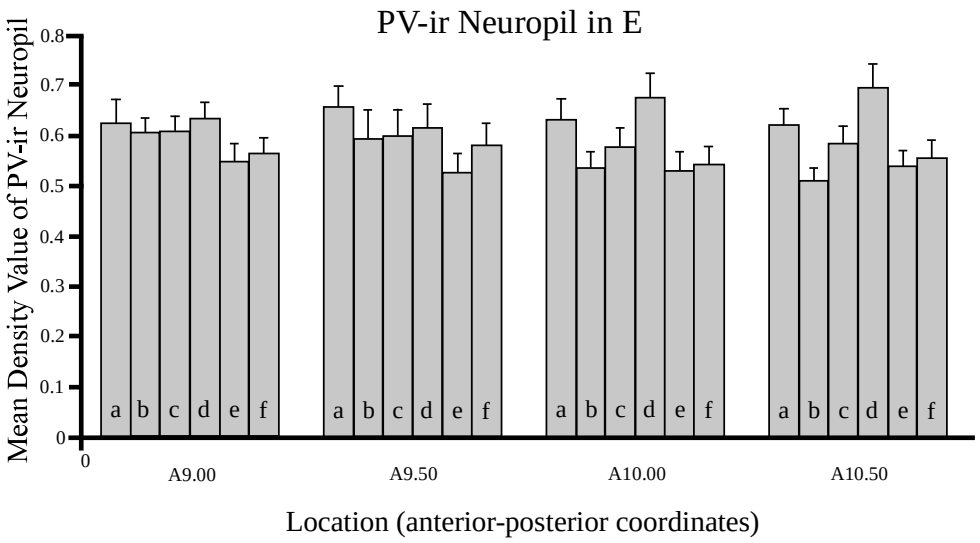

Figure 32. Graph showing the mean density value of PV-ir neuropil at each of the regions within E and all four locations (anterior-posterior coordinates) across treatment condition and hemisphere. Mean values and standard error are shown.

The following interactions were not significant: Location x Treatment $F(3, 18) = 0.63$, $p = 0.605$, Region within E x Treatment $F(5, 30) = 0.46$, $p = 0.801$, Hemisphere x location $F(3, 18) = 0.19$, $p = 0.900$, Hemisphere x Location x Treatment $F(3, 18) = 0.49$, $p = 0.693$, Hemisphere x Region within E $F(5, 30) = 0.17$, $p = 0.971$, Hemisphere x Region within E x Treatment $F(5, 30) = 0.62$, $p = 0.682$, Location x Region within E x Treatment $F(15, 90) = 0.99$, $p = 0.471$, Hemisphere x Location x Region within E $F(15, 90) = 0.52$, $p = 0.922$, and Hemisphere x Location x Region within E x Treatment $F(15, 90) = 1.38$, $p = 0.174$.

CO Histochemistry

In total, ten cases were processed for CO. However, the tissue in some of these cases was not suitable for analysis. Therefore, the brain tissues of seven birds (three in the unilateral lesion condition and four in the monocular occlusion condition) were processed to detect CO staining in E. Below are microphotographs showing E on the control and experimental hemispheres at each of the four different locations (anterior-posterior coordinates) for all of the birds.

Individual CO cases.

PG234 (Unilateral Lesion) CO density (Figure 33).

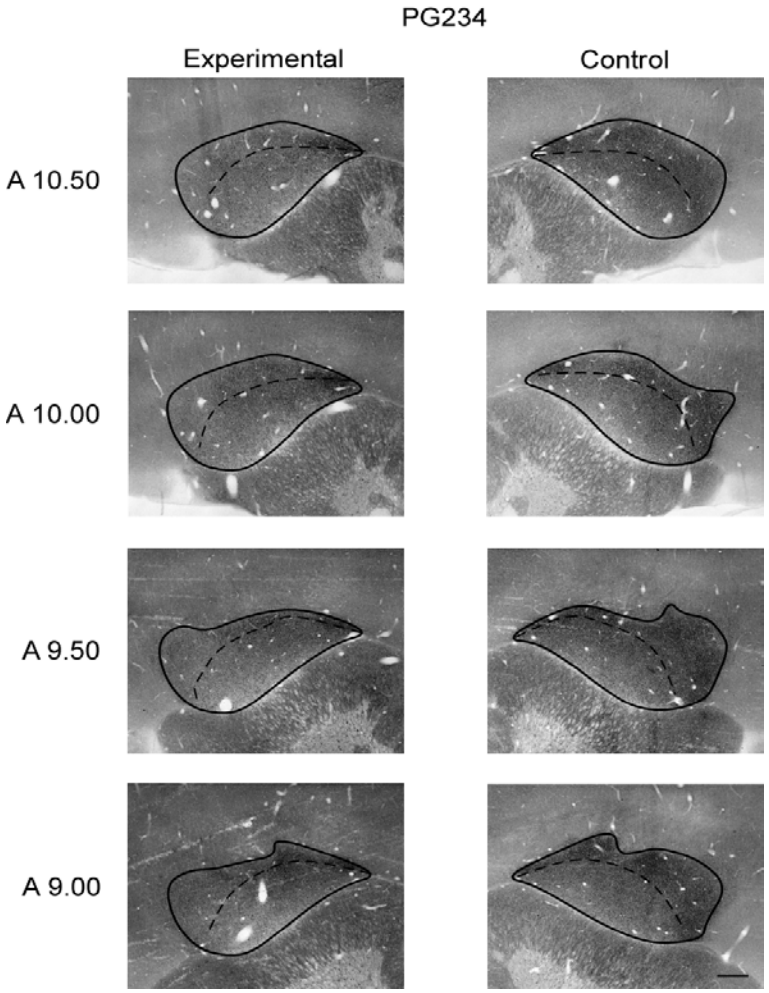

Figure 33. Microphotographs of PG234 showing the distribution pattern of CO in E after unilateral lesion. For this case, the left Rt was destroyed. Scale bar = 500 µm.

PG259 (Unilateral Lesion) CO density (Figure 34).

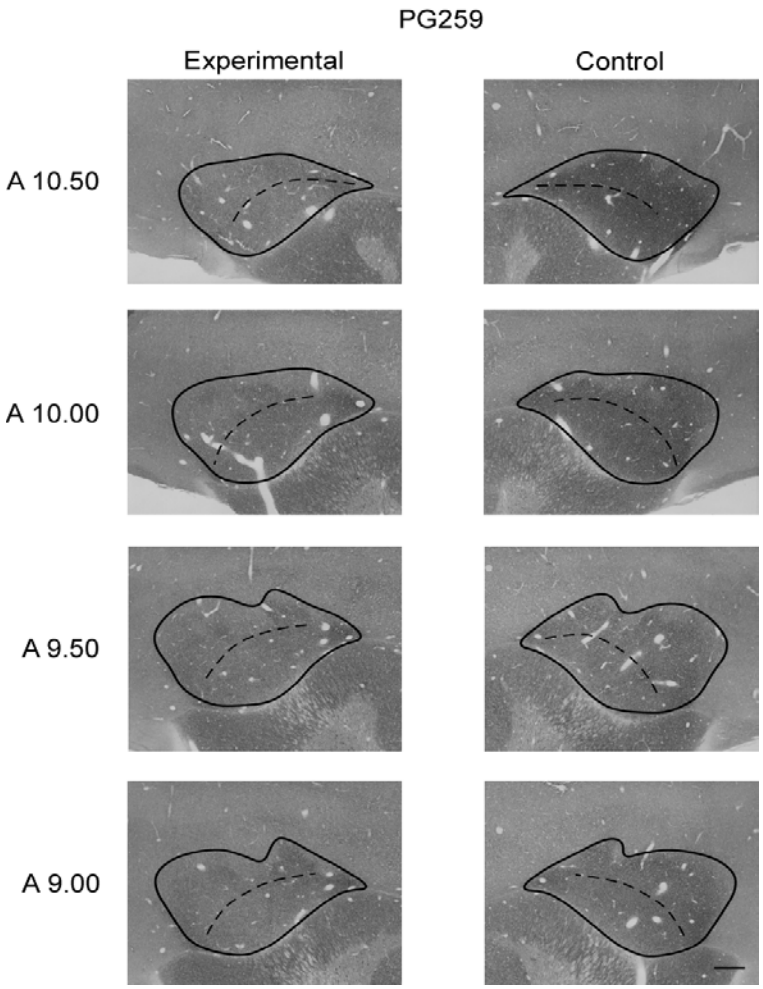

Figure 34. Microphotographs of PG259 showing the distribution pattern of CO in E after unilateral lesion. For this case, the left Rt was destroyed. Scale bar = 500 µm.

PG254 (Unilateral Lesion) CO density (Figure 35).

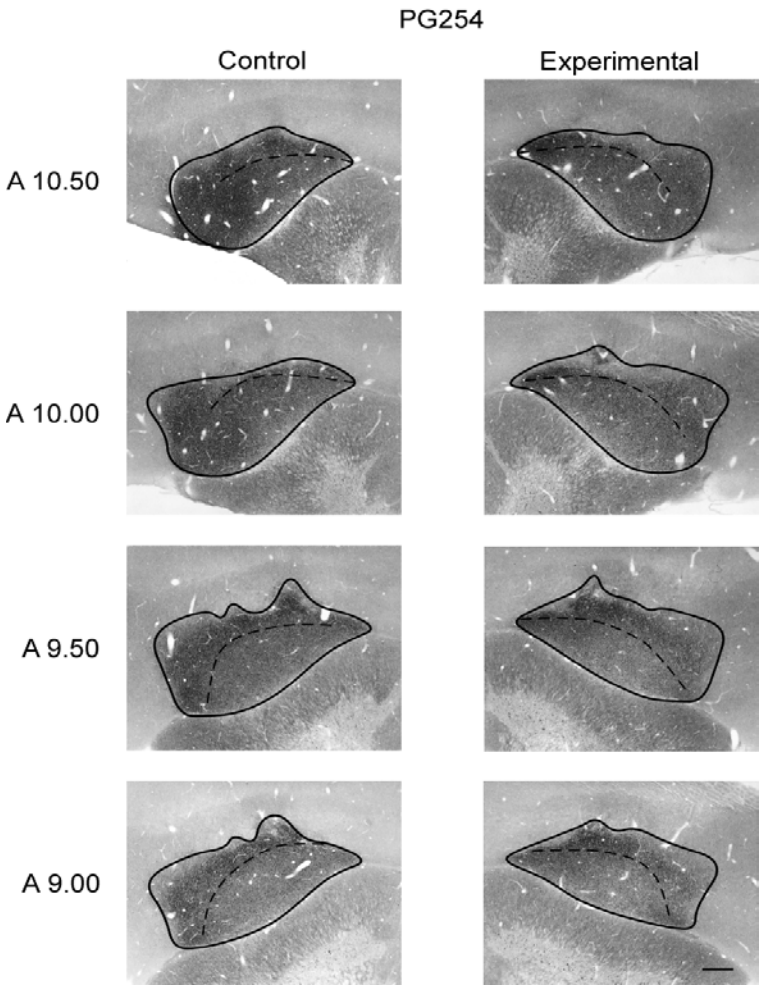

Figure 35. Microphotographs of PG254 showing the distribution pattern of CO in E after unilateral lesion. For this case, the right Rt was destroyed. Scale bar = 500 µm.

PG264 (Monocular Occlusion) CO (Figure 36).

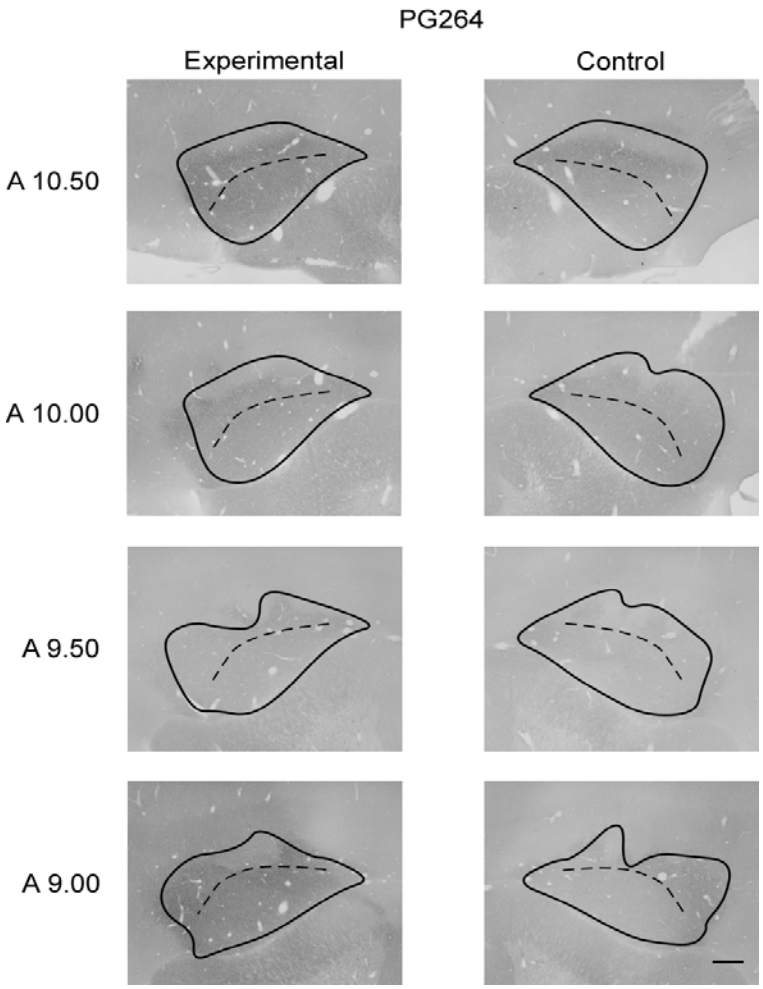

Figure 36. Microphotographs of PG264 showing the distribution pattern of CO in E after monocular occlusion. For this case, the right eye was occluded. Scale bar = 500 µm.

PG263 (Monocular Occlusion) CO (Figure 37).

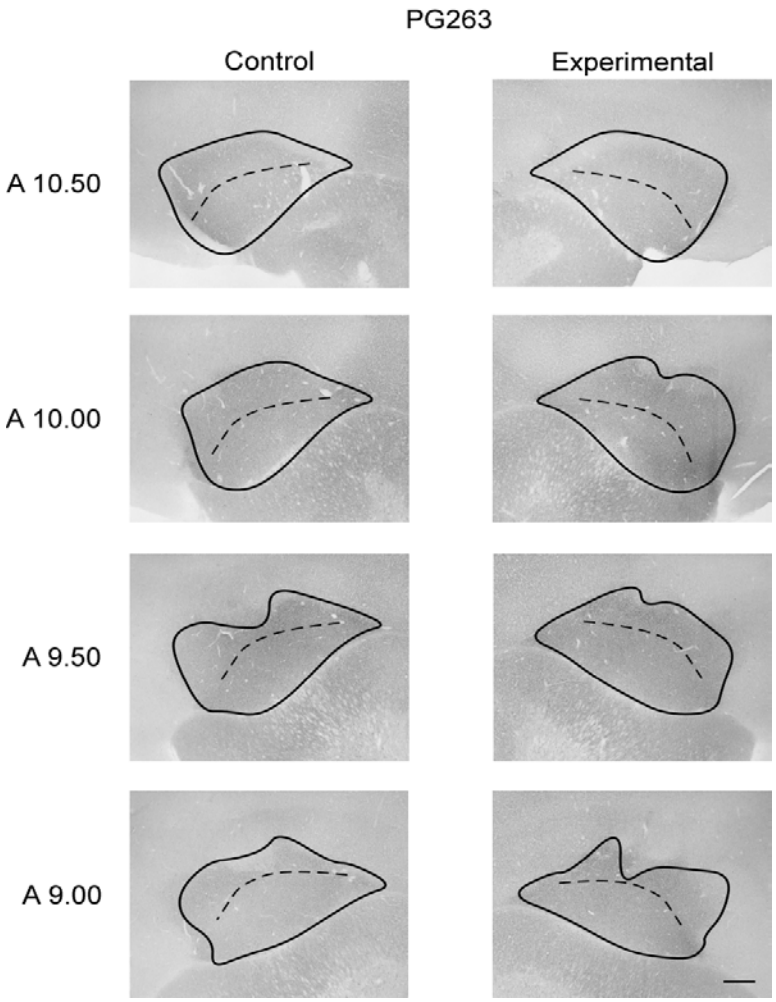

Figure 37. Microphotographs of PG263 showing the distribution pattern of CO in E after monocular occlusion. For this case, the left eye was occluded. Scale bar = 500 µm.

PG256 (Monocular Occlusion) CO (Figure 38).

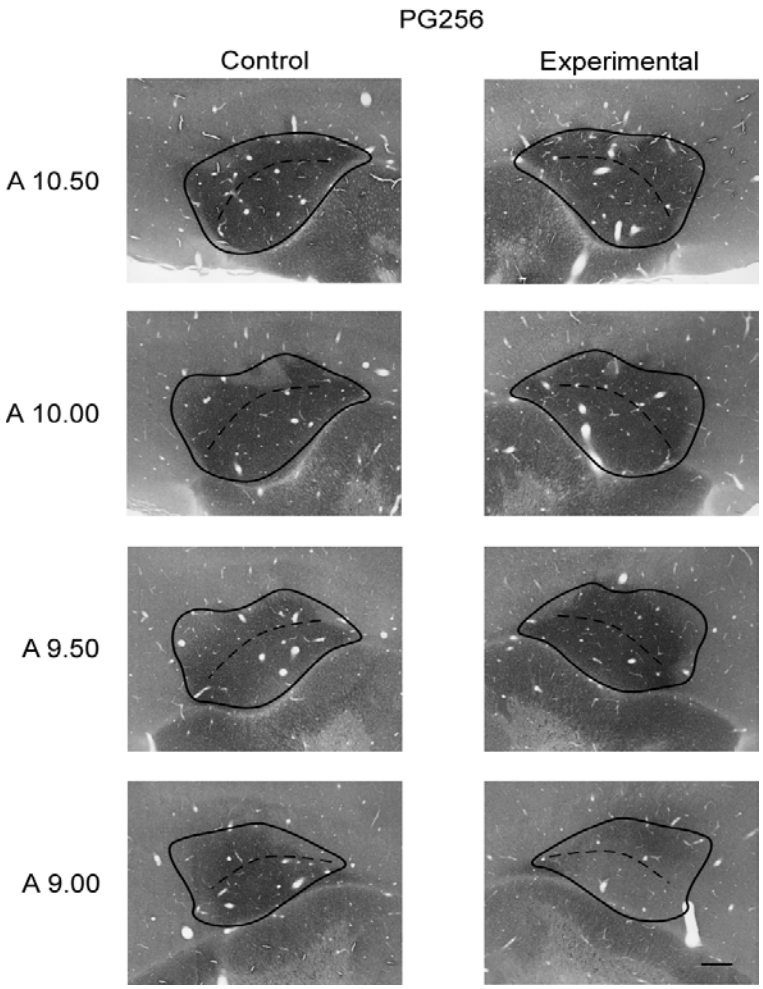

Figure 38. Microphotographs of PG256 showing the distribution pattern of CO in E after monocular occlusion. For this case, the left eye was occluded. Scale bar = 500 µm.

PG260 (Monocular Occlusion) CO (Figure 39).

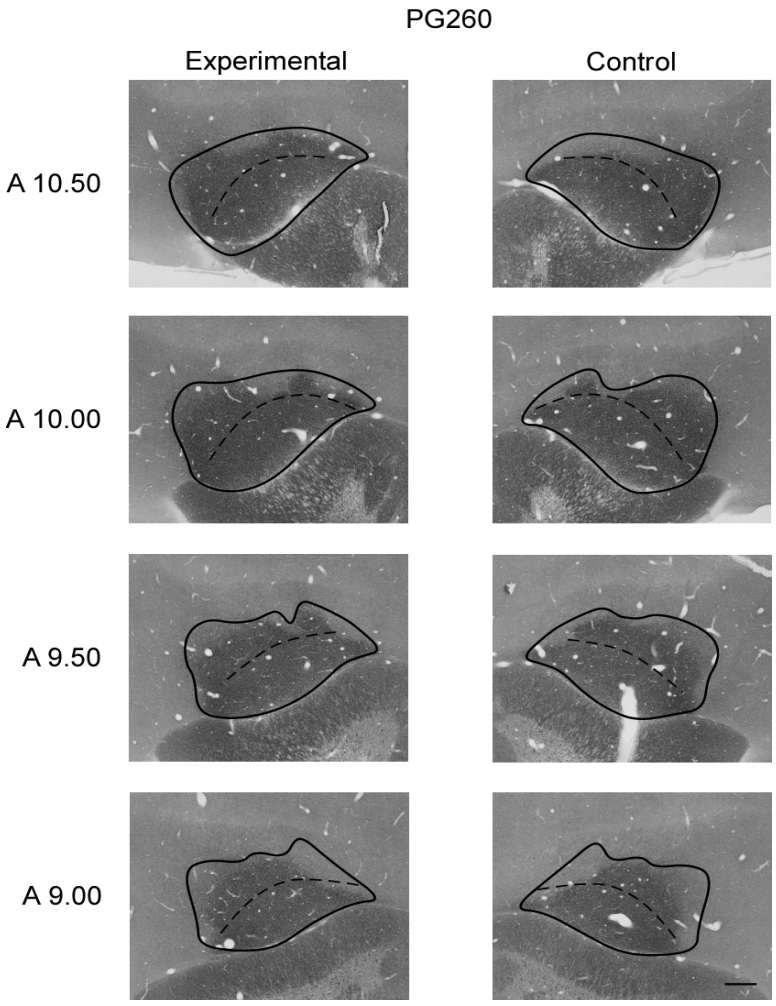

Figure 39. Microphotographs of PG260 showing the distribution pattern of CO in E after monocular occlusion. For this case, the right eye was occluded. Scale bar = 500 µm.

Density of CO staining in E.

In order to determine if the density of CO activity normally present in E varied as a function of treatment condition, hemisphere, region within E, and location (anterior-posterior coordinates), a factorial mixed design ANOVA was conducted. The between subjects variable was treatment condition (lesion versus occlusion) and the repeated

measures were hemisphere (control versus experimental), region within E (*a* - *f*), and location (anterior-posterior coordinates: A10.50, 10.00, 9.50, 9.00).

There was a significant main effect for region within *E* (*a* - *f*) $F(5, 25) = 6.51$, $p = 0.001$ indicating that there are differences in the mean density value of CO staining in the six different target regions within E across treatment condition, hemisphere, and location (anterior-posterior coordinates; see Figure 40). Post hoc comparisons using the Fisher LSD test revealed that the mean CO staining density value of specific regions within E were different from one another. Region *a* ($M = 0.88$, $SD = 0.20$) had significantly more CO staining than that found in region *e* ($M = 0.62$, $SD = 0.22$; $t(25) = 2.432$, p = .022, two-tailed). Also, region *e* ($M = 0.62$, $SD = 0.22$) had significantly less CO staining than that found in region *c* ($M = 0.85$, $SD = 0.23$; $t(25) = .188$, p = .038, two-tailed) and region f ($M = 0.84$, $SD = 0.27$; $t(25) = 2.094$, p = .046, two-tailed). A summary of these comparisons can be found in Table 2.

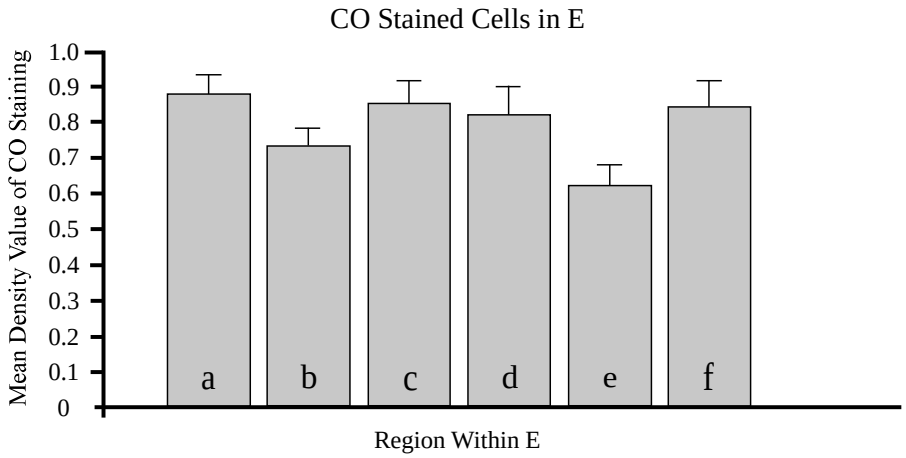

Figure 40. Graph showing the mean density value of CO activity in the six target regions within E across treatment condition, hemisphere, and location (anterior-posterior coordinates). Mean values and standard error are shown.

Table 2

Pairwise Comparisons of Regions Within E

Region Within E	*M*	*SD*
a	0.88^{A}	0.20
b	0.74^{A}	0.18
c	0.85^{A}	0.23
d	0.82^{B}	0.29
e	0.62^{B}	0.22
f	0.84^{A}	0.27

Table 2. Means with the same letter in their superscripts do not differ significantly from one another according to a Fisher's LSD test.

The following main effects were not significant: treatment (lesion versus occlusion) $F(1, 5) = 0.14$, $p = 0.726$, hemisphere (control versus experimental) $F(1, 5) = 1.60$, $p = 0.262$, and location $F(3, 15) = 0.96$, $p = 0.437$.

However, there was a significant Hemisphere x Treatment interaction effect $F(1, 5) = 11.14$, $p = 0.021$), meaning that the difference in CO activity between hemispheres was dependent on the treatment condition (see Figure 41).

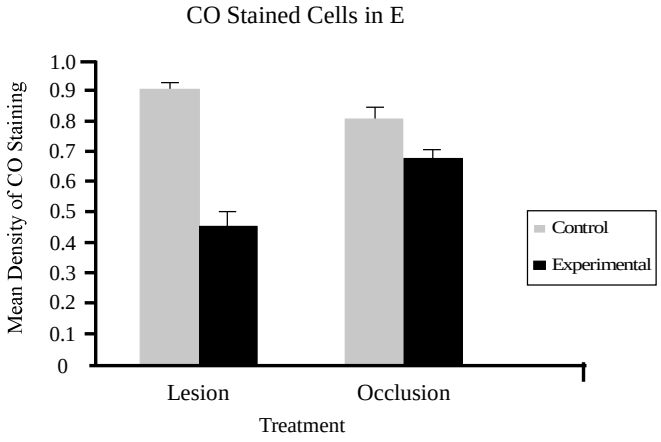

Figure 41. Graph showing mean density value of CO activity after unilateral lesion and monocular occlusion across all six regions within E and across all four locations (anterior-posterior coordinates). Mean values and standard error are shown.

Furthermore, the Hemisphere x Treatment x Region within E interaction effect was significant $F(5, 25) = 7.84$, $p < 0.001$). Figure 42 shows the density differences of CO in six different regions.

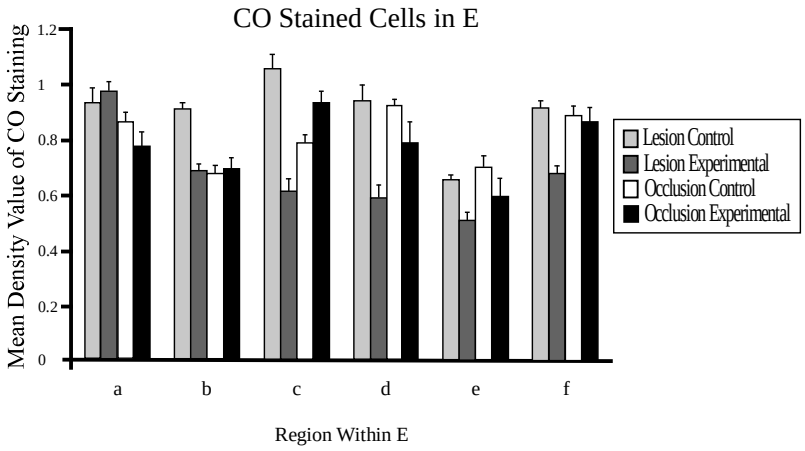

Figure 42. Graph showing the mean density value of CO activity for each hemisphere, treatment condition, and the six target regions within E across location (anterior-posterior coordinates). Mean values and standard error are shown.

The following interaction effects were also significant: location had an interaction effect with region within E $F(15, 75) = 2.34$, $p = 0.008$) (see Figure 43), and hemisphere interacted with region within E $F(15, 25) = 3.165$, $p = 0.024$) (see Figure 44). No other interactions were significant.

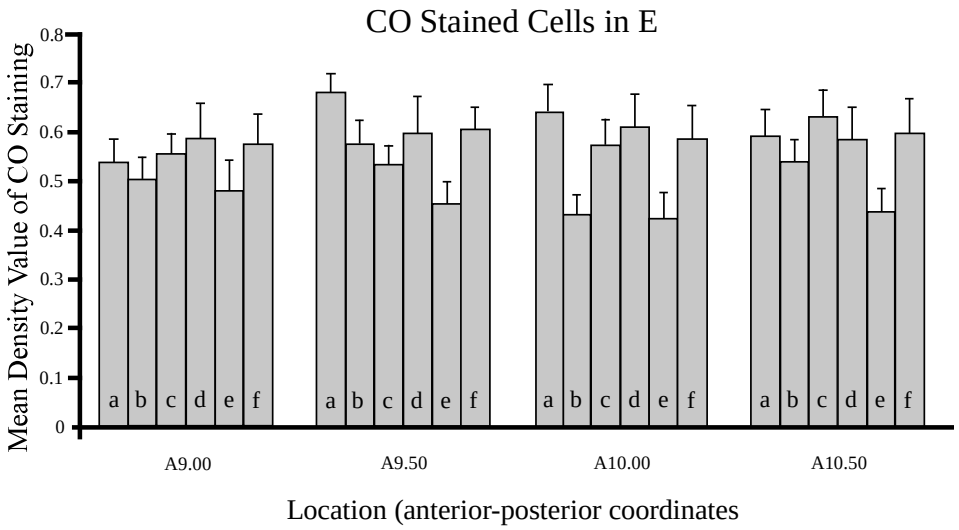

Figure 43. Graph showing the mean density value of CO activity at each of the six regions within E and at all locations (anterior-posterior coordinates) across treatment condition and hemisphere. Mean values and standard error are shown.

Below, is a graph showing the mean density values of CO and PV together. Notice that the staining pattern is more differential for CO than for PV.

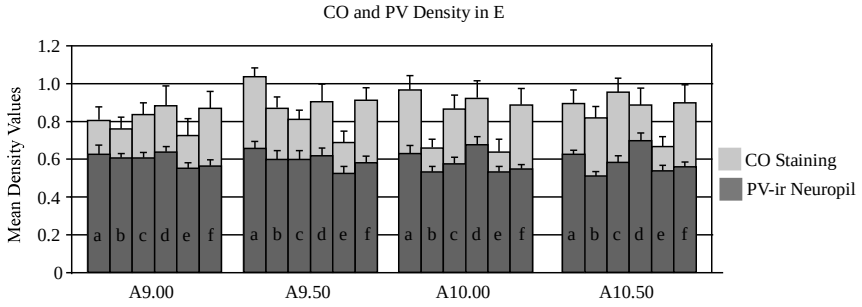

Figure 44. Graph showing the mean density value of CO and PV activity at each of the six regions within E and at all locations (anterior-posterior coordinates) across treatment condition and hemisphere. Mean values and standard error are shown.

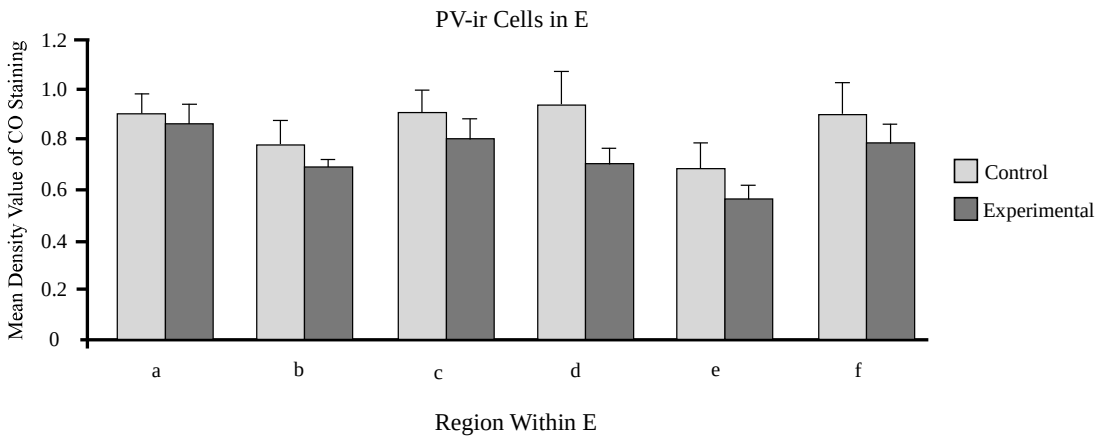

Figure 45. Graph showing the mean density value of CO activity at each of the six regions within E for both hemispheres across treatment condition (lesion versus occlusion) and location (anterior-posterior coordinates). Mean values and standard error are shown.

ZENK Immunohistochemistry

Eleven pigeons (five in the unilateral lesion condition and six in the monocular occlusion condition) were used to visualize ZENK-ir cells of NIL. Below, composite microphotographs (consisting 42 original photos) of ZENK-ir for each hemisphere are presented for individual cases. They are accompanied by corresponding images showing ZENK-ir distribution patterns visualized by the Maxima transformation method. Based on these digitized images, the putative NIL is specified as the region surrounded by DA and the caudal end of E, which extended from A 7.00 to A6.00.

Individual ZENK cases.

PG234 (Unilateral Lesion) ZENK-ir cells in NIL (Figure 46).

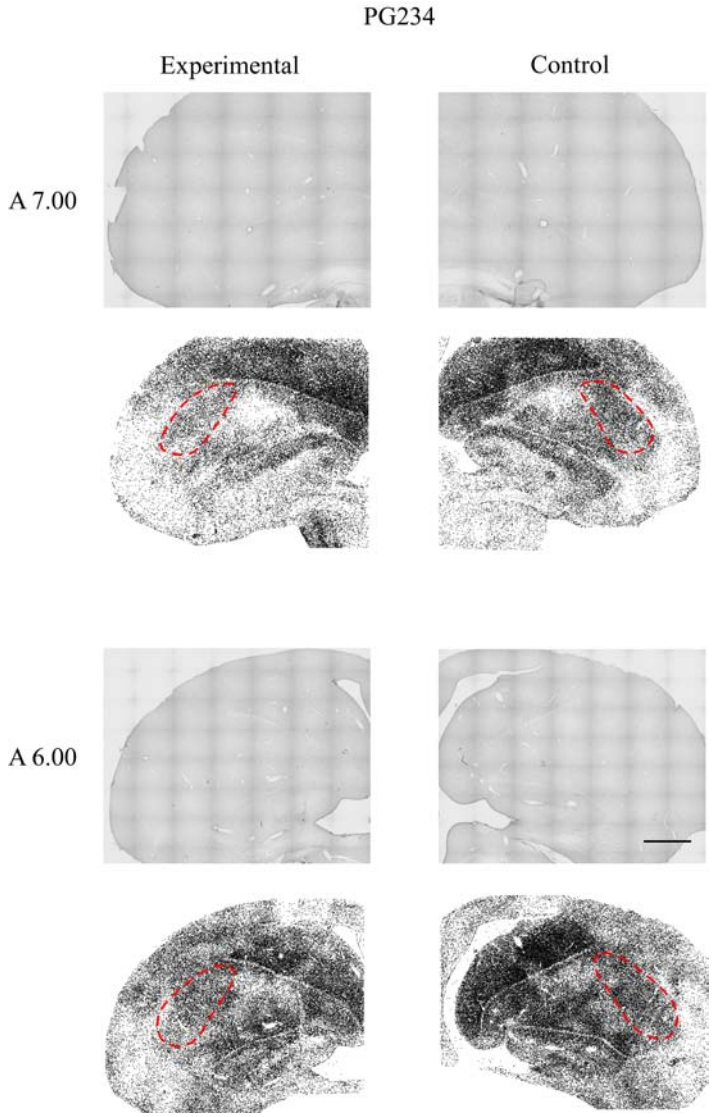

Figure 46. Microphotographs and corresponding transformed images of PG234 showing the distribution pattern of ZENK in the telencephalon after unilateral lesion. The putative NIL is specified by dotted lines in the digitized images. For this case, the left Rt was destroyed. Scale bar = 1 mm.

PG236 (Unilateral Lesion) ZENK-ir cells in NIL (Figure 47).

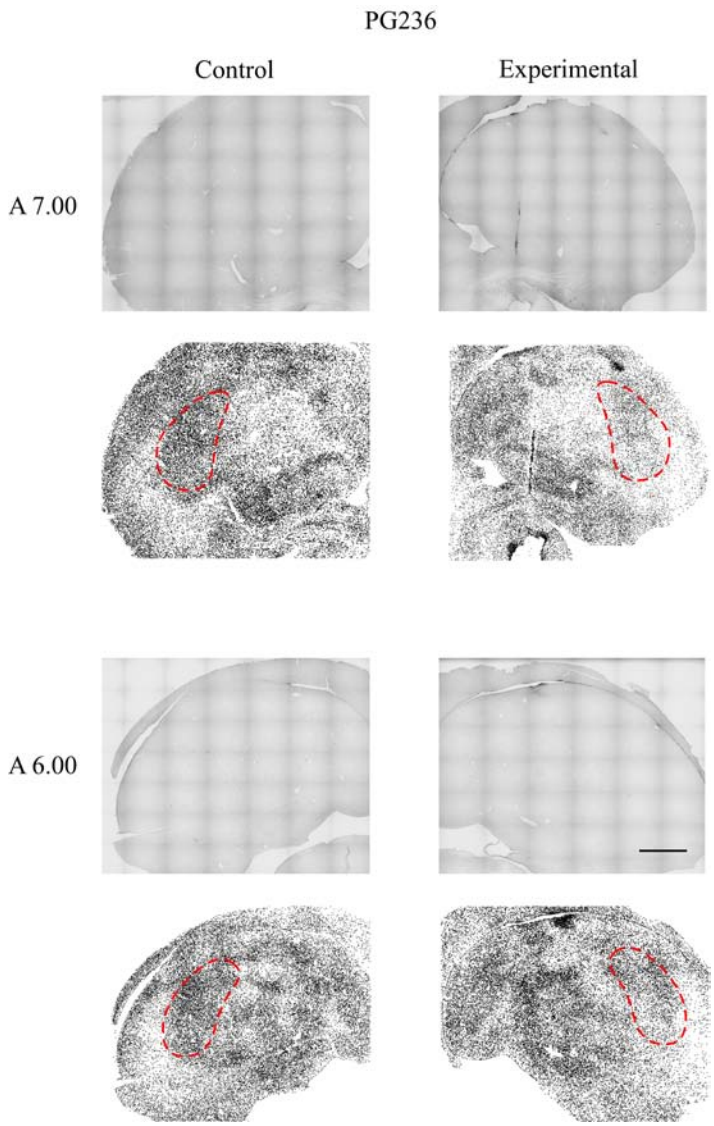

Figure 47. Microphotographs of PG236 showing the distribution pattern of ZENK in the telencephalon after unilateral lesion. The putative NIL is specified by dotted lines in the digitized images. For this case, the right Rt was destroyed. Scale bar = 1 mm.

PG239 (Unilateral Lesion) ZENK-ir cells in NIL (Figure 48).

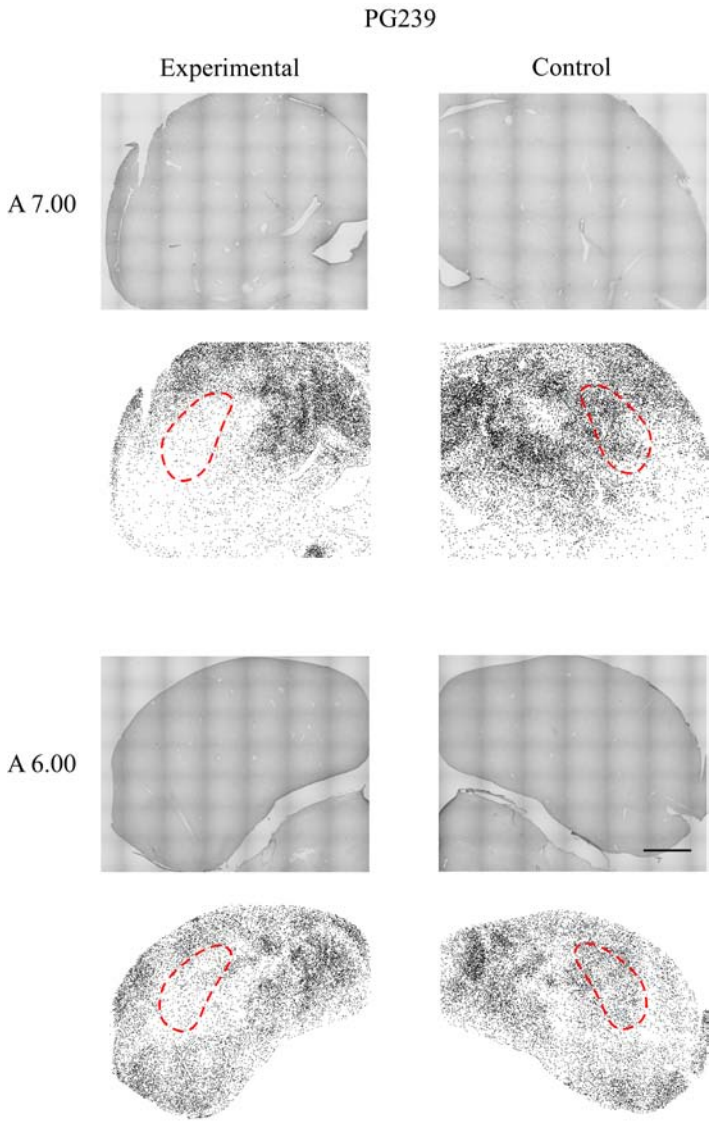

Figure 48. Microphotographs of PG239 showing the distribution pattern of ZENK in the telencephalon after unilateral lesion. The putative NIL is specified by dotted lines in the digitized images. For this case, the left Rt was destroyed. Scale bar = 1 mm.

PG254 (Unilateral Lesion) ZENK-ir cells in NIL (Figure 49).

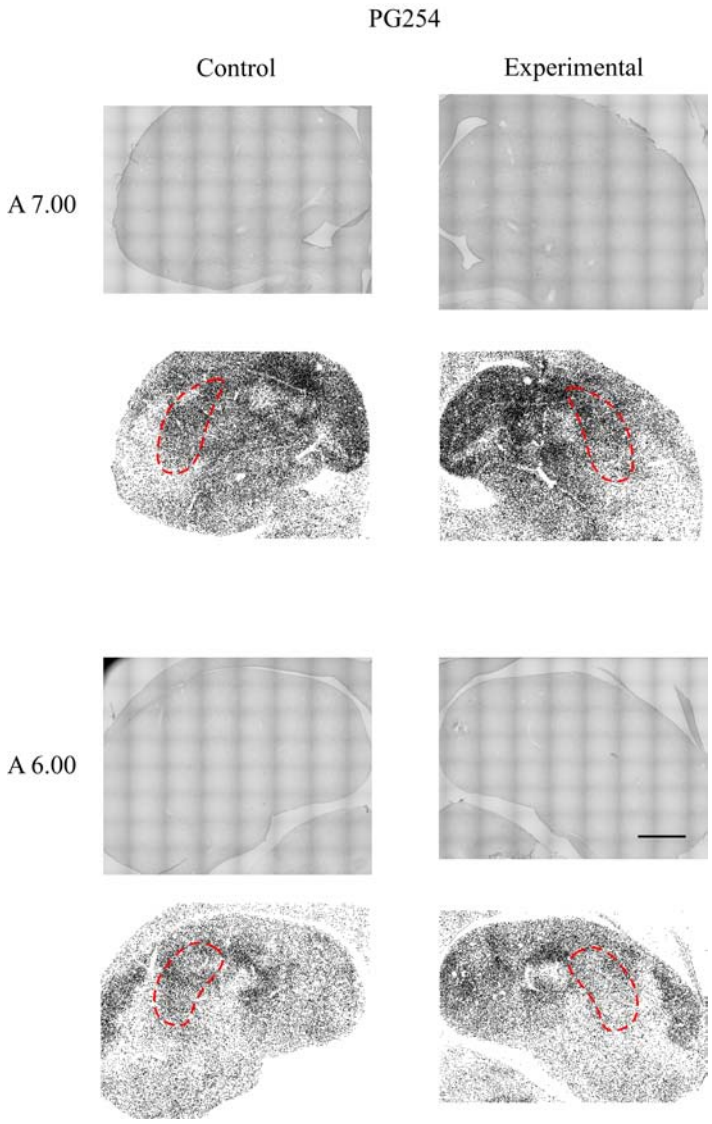

Figure 49. Microphotographs of PG254 showing the distribution pattern of ZENK in the telencephalon after unilateral lesion. The putative NIL is specified by dotted lines in the digitized images. For this case, the right Rt was destroyed. Scale bar = 1 mm.

PG259 (Unilateral Lesion) ZENK-ir cells in NIL (Figure 50).

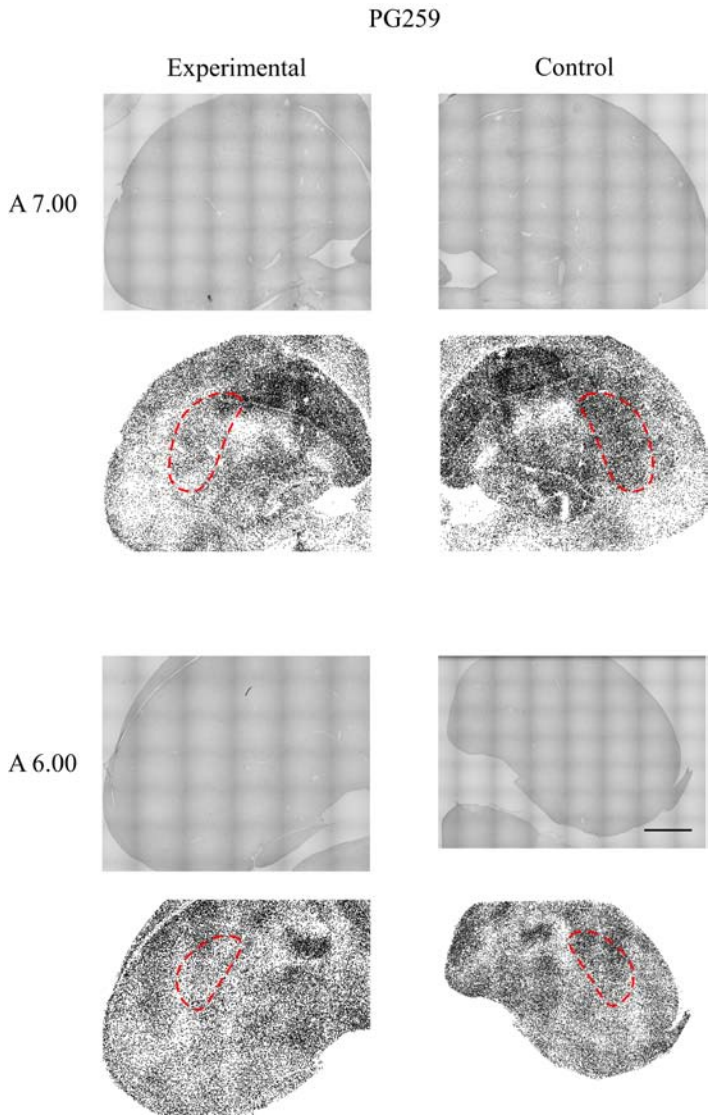

Figure 50. Microphotographs of PG259 showing the distribution pattern of ZENK in the telencephalon after unilateral lesion. The putative NIL is specified by dotted lines in the digitized images. For this case, the left Rt was destroyed. Scale bar = 1 mm.

PG253 (Monocular Occlusion) ZENK-ir cells in NIL (Figure 51).

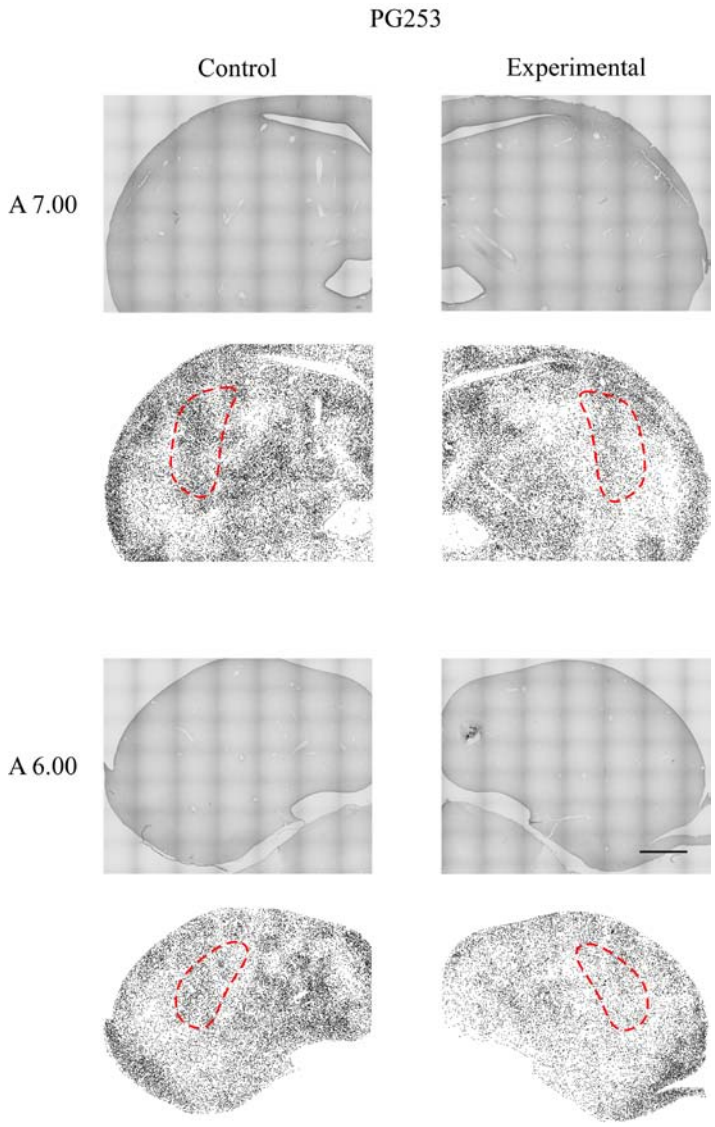

Figure 51. Microphotographs of PG253 showing the distribution pattern of ZENK in the telencephalon after monocular occlusion. The putative NIL is specified by dotted lines in the digitized images. For this case, the left eye was occluded. Scale bar = 1 mm.

PG264 (Monocular Occlusion) ZENK-ir cells in NIL (Figure 52).

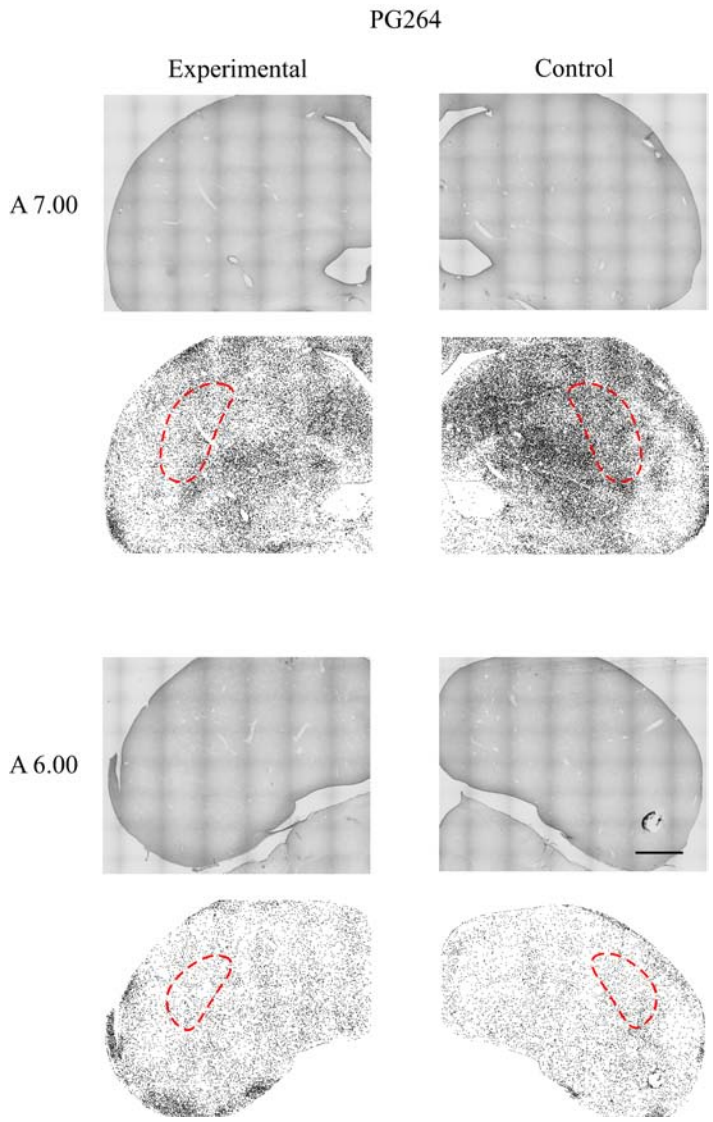

Figure 52. Microphotographs of PG264 showing the distribution pattern of ZENK in the telencephalon after monocular occlusion. The putative NIL is specified by dotted lines in the digitized images. For this case, the right eye was occluded. Scale bar = 1 mm.

PG170 (Monocular Occlusion) ZENK-ir cells in NIL (Figure 53).

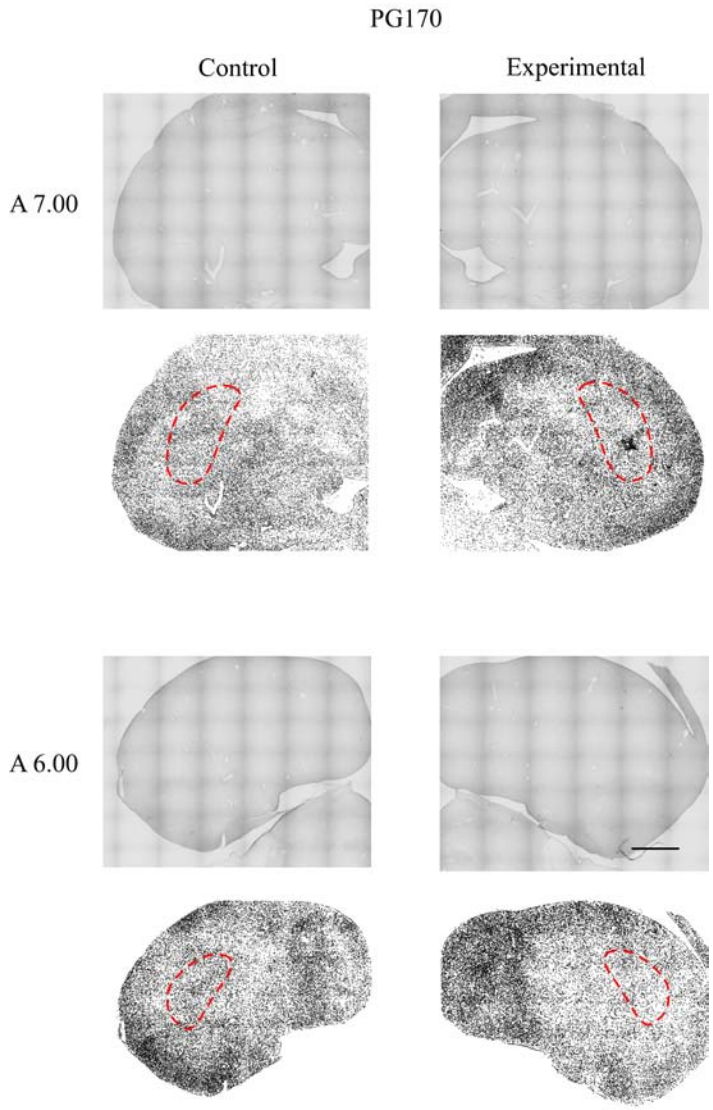

Figure 53. Microphotographs of PG170 showing the distribution pattern of ZENK in the telencephalon after monocular occlusion. The putative NIL is specified by dotted lines in the digitized images. For this case, the left eye was occluded. Scale bar = 1 mm.

PG263 (Monocular Occlusion) ZENK-ir cells in NIL (Figure 54).

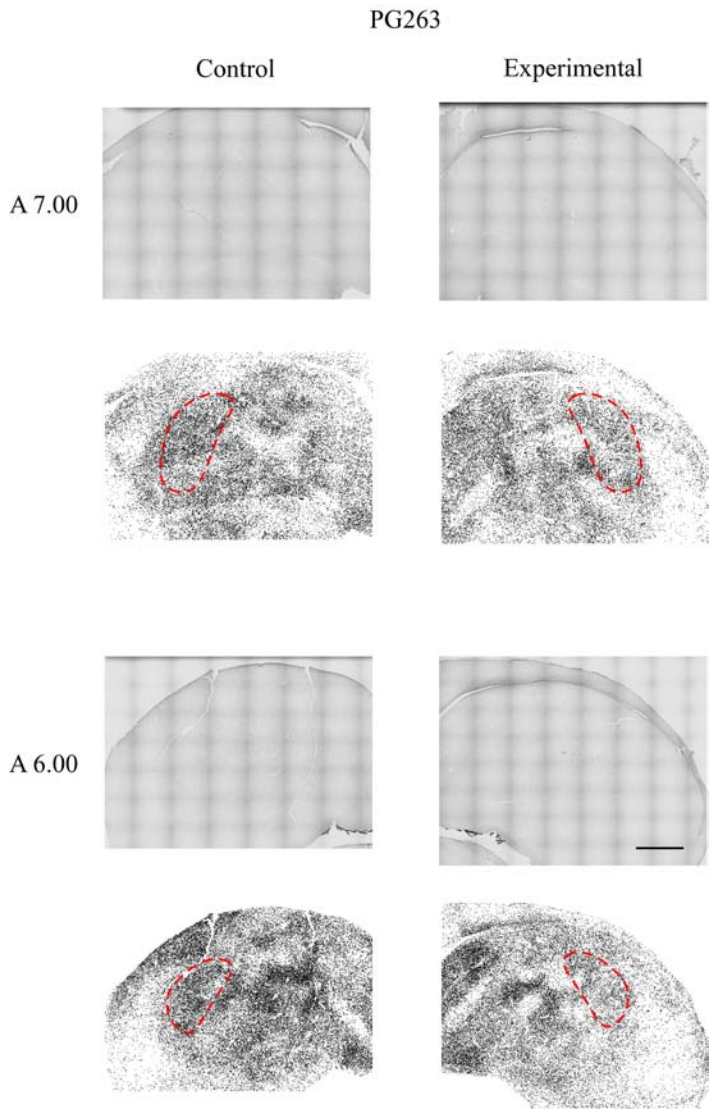

Figure 54. Microphotographs of PG263 showing the distribution pattern of ZENK in the telencephalon after monocular occlusion. The putative NIL is specified by dotted lines in the digitized images. For this case, the left eye was occluded. Scale bar = 1 mm.

PG256 (Monocular Occlusion) ZENK-ir cells in NIL (Figure 55).

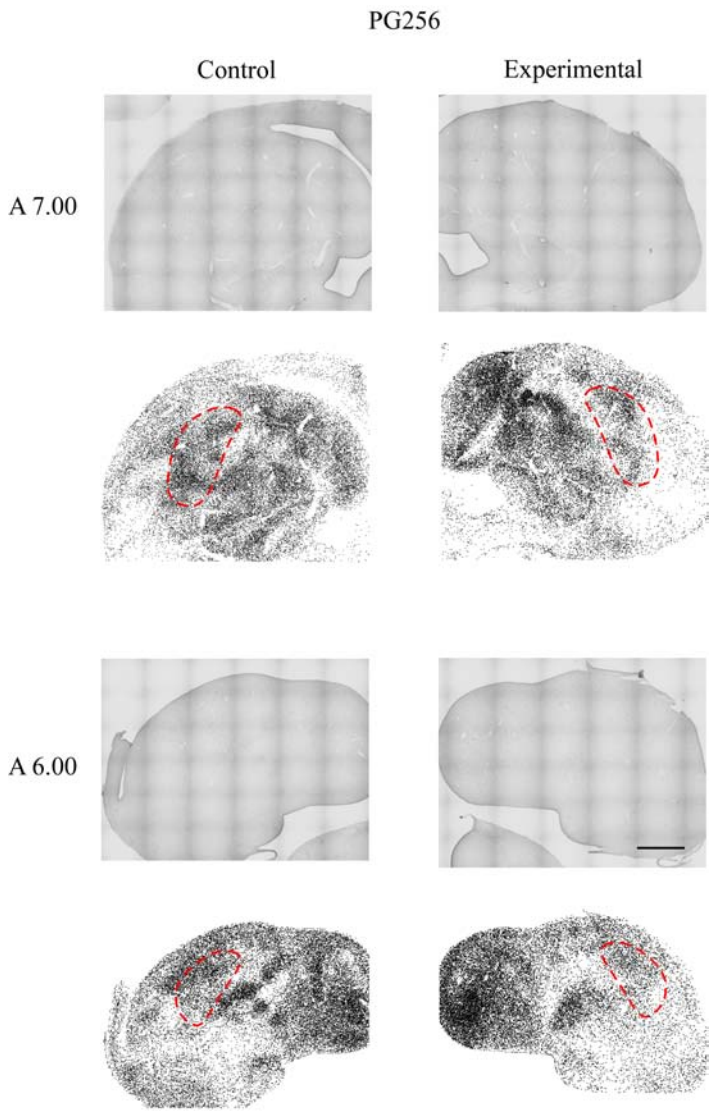

Figure 55. Microphotographs of PG256 showing the distribution pattern of ZENK in the telencephalon after monocular occlusion. The putative NIL is specified by dotted lines in the digitized images. For this case, the left eye was occluded. Scale bar = 1 mm.

PG260 (Monocular Occlusion) ZENK-ir cells in NIL (Figure 56).

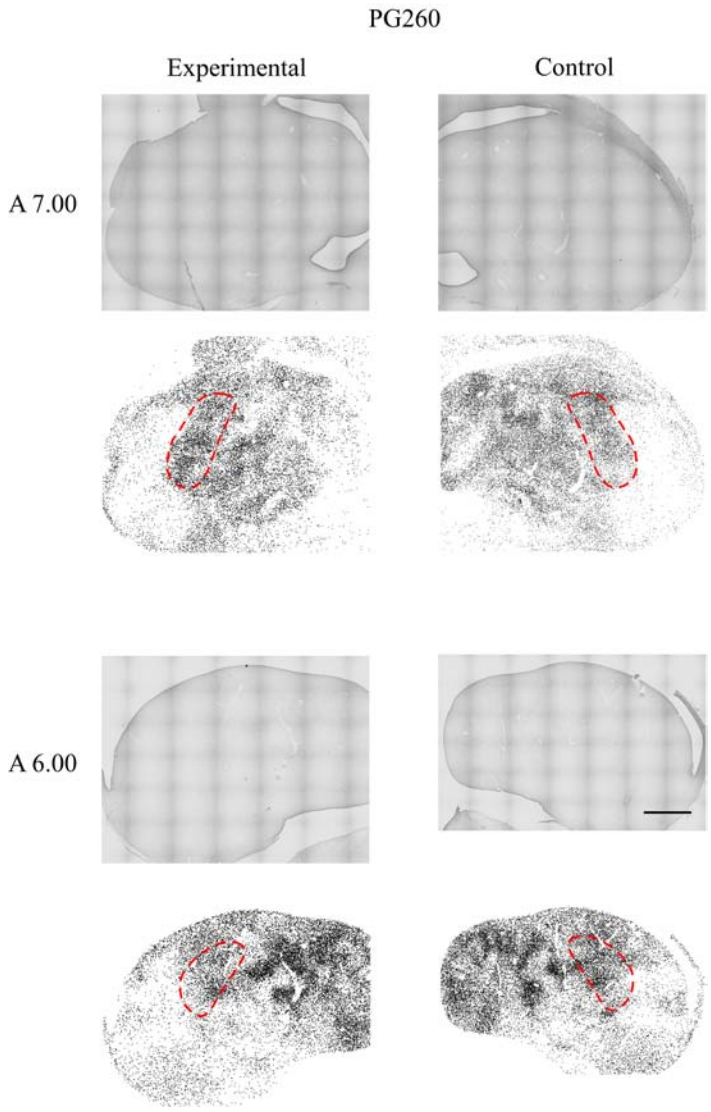

Figure 56. Microphotographs of PG260 showing the distribution pattern of ZENK in the telencephalon after monocular occlusion. The putative NIL is specified by dotted lines in the digitized images. For this case, the right eye was occluded. Scale bar = 1 mm.

Number of ZENK-ir neurons in NIL.

In order to determine if the number of ZENK-ir neurons in NIL varied as a function of treatment condition and hemisphere, a 2 x 2 mixed groups factorial ANOVA was conducted. The between subjects variable was the treatment with two levels (lesion and occlusion) and the within subject measure was hemisphere (control and experimental). Data from two anterior-posterior locations (A7.00 and A6.00) were combined for the analysis since ZENK distribution patterns were similar between them. Figure 57 shows the mean number of ZENK-ir neurons found in the NIL target regions after unilateral lesion and monocular occlusion. The results showed that there was a main effect for hemisphere $F(1, 9) = 94.14$, $p < 0.001$) meaning that regardless of the treatment (lesion or occlusion), there was a difference between the mean number of ZENK-ir cells in the control NIL versus the experimental NIL. There was not a significant effect for treatment $F(1, 9) = 0.50$, $p = 0.498$). The Hemisphere x Treatment interaction effect was not significant either $F(1, 9) = 1.30$, $p = 0.283$)

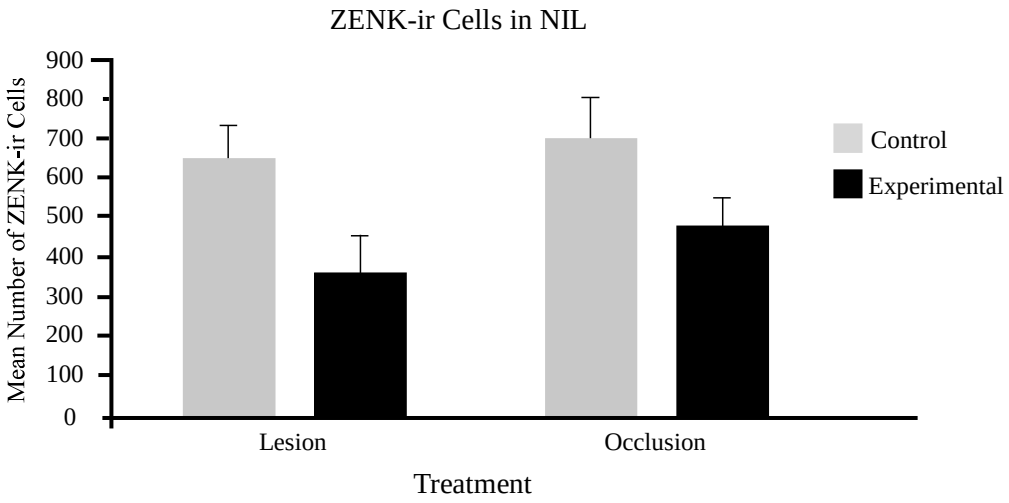

Figure 57. Graph showing the mean number of ZENK-ir cells counted in the control and experimental hemispheres for both treatment groups (lesion and occlusion). Mean values and standard error are shown.

Discussion

The specific aims of this study were to: 1) identify distinct anatomical subregions within the primary visual structure (E) in the telencephalon, 2) define the size and extent of another telencephalic structure NIL, and 3) determine the extent to which activity in these two telencephalic structures is dependent on neural input and visual signal.

Each of these specific aims was addressed by analyzing the distribution patterns of various cellular activity markers. Overall, these activity patterns showed that visual cell groups in the telencephalon were differentially affected not only between the various treatment conditions (lesions versus occlusions), but also within these conditions. In particular, PV and CO facilitated the identification of specific subregions in E (Aim One). Furthermore, mapping the cellular activity of ZENK in the telencephalon made it possible to determine the size and shape of NIL (Aim Two). Lesion and occlusion procedures had differential effects on the expression of PV-ir and CO staining in E, but not the ZENK expression in NIL (Aim Three). These results provided new information about the anatomical definitions, and suggest possible functional segregations of the telencephalic visual areas.

For Specific Aim One, there were significantly more PV-ir cell bodies in the inner region of E compared to the outer region. These results are congruent with the findings by Krützfeldt and Wild (2005), who showed that E can be separated based on the levels of PV-ir expression. While their conclusion was based on non-quantitative visual observations, the present study confirmed their observation based on quantitative analysis.

The statistical results showed that the interaction effect between Region within E and Location was significant, suggesting that the inner vs. outer regional differentiation varied by the location along the anterior-posterior axis. Furthermore, the three-way interaction analyses showed that Region variables interacted with 1) Hemisphere and Treatment, 2) Hemisphere and Location, and 3) Treatment and Location variables. These results suggest that the regional differences of PV-ir cells were more or less affected by different variables, including the anterior vs. posterior locations, lesion vs. occlusion conditions, and targeted vs. control hemispheres. However, in all experimental conditions analyzed in the study, the inner region had consistently more PV-ir cells than the outer region. Therefore, the PV-ir expression difference between the inner and outer regions is consistent regardless of these variables. The present results found that cells in the inner and outer regions were not obviously different in cell size and type. Thus, the difference of PV-ir cells between inner and outer regions is primarily in density, not in morphology.

In terms of the PV-ir neuropil, the results were slightly different from the cell body pattern. When the PV-ir neuropil density was compared between the outer regions (b and c; mean = 0.576) and inner regions (*e* and *f*; *M* = 0.55), no clear differences were observed, unlike the PV-ir cell bodies. The results showed that the expression patterns of PV-ir cell bodies and neuropil in E are not identical, suggesting that they were controlled by different mechanisms.

The regional differences among the six areas within E were significant as well as the Region within E x Location (anterior-posterior coordinates) interaction. In particular, the ventrolateral E (region *d*) tended to have a higher density of PV-ir neuropil than other regions except the most ventromedial area (region *a*) which was also high in PV-ir

(Figure 28). This difference between regions was more obvious in the anterior locations than in the posterior locations (Figure 32). It is possible that the intensity difference among areas is related to a topographical organization of the Rt-E projection pattern. For instance, the region *d* may receive distinct projections from a specific part of Rt. However, further studies are necessary to understand the significance of the specific subregion since little is known about the internal organization of E, including this region. Region *a* appeared to be distinct in terms of PV-ir neuropil, in that it did not appear to be as affected by either treatment condition compared to the other five regions (Figure 28). It is likely that this region receives input from some location other than Rt. A study by Gamlin and Cohen (1986) used anterograde autoradiographic and retrograde pathway tracing techniques to show an additional projection from the optic tectum to the nucleus dorsolateralis posterior of the thalamus (DLP). One of the main findings of this study showed that anterograde tracers injected into the caudal portion of DLP (DLPc) project to a discrete region of the ipsilateral telencephalon. This cytoarchitecturally distinct cell group matches with region *a* in the current study. Thus, it is likely that the lesion to Rt had little effect on region a due to the likelihood that this region is receiving DLP terminations.

As for CO staining, the overall pattern of the current study agrees with the results of Hellmann et al. (1995). The six different regions of E examined in Hellmann et al. (1995) roughly corresponded to the six regions that were analyzed in the present study. The current findings are similar to theirs in the respect that many of these areas showed similarly intense staining patterns. Furthermore, both studies found that the ventro-intermedial area (region e) showed a low level of CO staining compared to the other

areas. It is possible that the low CO intensity in this region is associated with the fact that massive thalamo-telencephalic projection fibers are passing through this region. Thus, CO activity may not be expressed much in these passing fibers in the region e.

Hellmann et al. (1995) found that the dorsolateral area (region *c*) also had low CO staining intensity whereas the present study did not show such a pattern. A closer look at this region suggests that the dorsolateral border of E in the present study was defined more conservatively than the previous study, which encroached into a further dorsal area including dense efferent fiber passages of E. In the Hellmann et al. (1995) study, the CO activity in this region was low because this dorsolateral region included passing fibers whereas the present study did not. As in the PV-ir neuropil, no clear difference was found for CO staining patterns to separate between the inner and outer regions.

The results of CO staining patterns, together with those of PV-ir cell and neuropil patterns, suggest that E consists of multiple distinct subregions. Specifically, the present study concludes that the density of PV-ir cell bodies can be used to clearly distinguish the inner and outer subregions within E. The PV-ir neuropil and CO activity patterns show that further subregions exists within the inner and outer regions, indicating a complex heterogeneity within E. The current findings will be used to further refine the identity of E subdivisions, providing a map of these subregions that may, in turn, reflect physiologically and functionally distinct cell groups within E.

For Specific Aim Two, the expression of protein product of *zenk* was examined in the nidopallium by comparing the hemispheres in both treatment conditions (lesions and occlusions). There was a significant reduction of ZENK-ir cell bodies on NIL in the

experimental hemisphere compared to control side. Based on the differential expression of ZENK, it was possible for the first time to visualize the location of NIL.

To accomplish the visualization, the newly developed image analysis was used (Mahmud, 2008), and, the distribution patterns of ZENK positive cells were more accurately identified in low-power images than any previous analysis. Based on these images, the present study showed that the nidopallial area dorsocaudal to E, ventromedial to DA, in the control hemisphere had a significantly high density of ZENK positive cells (Figures 46 - 56) compared to the corresponding area in the control side (Figure 57). The putative NIL is 3 - 4 mm in the anterior-posterior axis, 2 - 2.5 mm in the dorsal ventral axis, and 1 - 1.5 mm along the lateral-medial axis. This definition is rather conservative because the borders with the surrounding regions are difficult to differentiate cytoarchitectonically. The ZENK expression might also be more heterogeneous within NIL than assumed in the present study. Thus, the real NIL may even larger than the putative NIL discussed in the study.

Although the exact functional significance of NIL remains unclear, the fact that ZENK expression in NIL was significantly influenced by disrupting visual input suggests that this structure is important for higher-order visual processing. The expression of *zenk* gene and its protein product have been used for identifying higher-order auditory and vocal brain areas in songbirds. For example, the level of the mRNA transcribed from *zenk* is expressed strongly in certain structures within the specific auditory areas in the telencephalon during song acquisition by juvenile birds (Jin & Clayton, 1997) and the perception of song by adults (Mello et al., 1992; Mello & Clayton, 1995; Jarvis et al., 1995). Z*enk* genes are also known to play a major role in the consolidation of long-term

auditory memories in these higher auditory regions (Tischmeyer & Grimm, 1999; Davis, Bozon, & Laroche, 2003). Based on the similarities with the higher auditory areas in songbirds in terms of the connection and ZENK expression patterns, it is possible that NIL is similarly involved in the higher-order visual learning and memory of biologically relevant events such as encounters with potential mates. If so, the results suggest that biologically relevant auditory and visual information is processed in a similar manner in the avian telencephalon. The finding will be of importance for understanding the general neural principles of sensory information processing.

Using the new digital imaging protocol for signal detection and distribution analysis (Mahmud 2008), the results showed that ZENK immunoreactivity was only found in the nucleus region of each positive cell and thus characterized by a morphologically highly uniform appearance from cell to cell. The new protocol took advantage of this uniformity and succeeded in accurately generating a low-power graphical representation of signal density patterns. This method proved to be extremely useful for the present study, and should be valuable for analyses in similar quantitative studies, especially when the target signals are relatively uniform in terms of size and morphology.

In contrast to NIL, much fewer ZENK positive cells were observed in E, as well as other primary sensory areas such as Field L and n. basolateralis. The lack of ZENK expression in the primary sensory areas is consistent with previous studies (Ruscio & Adkins-Regan, 2004; Thode, Bock, Braun, & Darlison, 2005).

Regarding specific Aim Three, the results showed that Treatment (lesions vs. occlusions) had significant effects for PV-ir neuropil and CO staining in E, but no differential effects were found for ZENK-ir in NIL.

As for PV-ir, the numbers of cell bodies were not affected by either lesion or occlusion treatment (Figure 25). However, lesions caused a significant reduction of PV-ir neuropil density in the experimental hemisphere, but not in the control hemisphere. This effect was not observed after occlusions.

As for the CO patterns, the results also showed that lesions caused a significant reduction of CO staining in the experimental hemisphere, but not in the control hemisphere. This effect was not observed after occlusions. In addition, there were differential staining patterns for CO at each of the six different regions of E. These regional differences were significant and were dependent on the location along the anterior-posterior axis and hemisphere.

Why did occlusions not have a significant effect compared to lesions in the PV-ir neuropil and CO staining? In the lesion condition, visual processing of E in the experimental hemisphere was disrupted by destroying the unilateral Rt and thus destroying the entire thalamic input to E. In the occlusion condition, visual processing of E in the experimental side was interrupted by occluding the contralateral eye, but the thalamic connection from Rt to E remained physically intact. Thus, E could still receive visual input from the ipsilateral eye via the inter-hemispheric connections. It is most likely that the ipsilateral input played a role to maintain the PV expression in E for the occlusion condition, whereas no such input existed in the lesion condition.

However, there are at least two other possible explanations for the results. It is possible that PV in E was transported from cell bodies of Rt to terminals in E, and thus Rt lesions, but not monocular occlusions, caused the reduction effect. However this possibility is unlikely because no PV was observed in cell bodies of Rt although there were abundant PV-ir neuropil. In terms of CO activity in E, they might be present mainly in terminals of Rt fibers, but not intrinsic fibers in E. Thus, lesions of the thalamic fibers caused more significant effects in the CO activity than occlusions.

Another possibility is that lesions had more acute and quick impacts than occlusions in the PV-ir and CO in E. It is possible that the difference in the effect of treatment condition might be similar if the occlusion period was longer than one week. That is, perhaps the visual information must be blocked for a longer period of time in order to significantly alter the levels of PV and CO.

Could the size of the lesion affect the pattern of PV immunoreactivity and CO staining in E? It is possible, but not likely, due to the fact that the four cases analyzed for this specific aim (PG234, PG254, PG259, PG47) received extensive lesions covering most, if not all, of Rt (see Figures 11-14).

As for ZENK-ir in NIL, both the lesion and occlusion treatments resulted in significant reductions of ZENK expression in NIL. The results are similar to a previous study (Hara, Kubikova, Hessler, & Jarvis, 2009), in which monocular occlusions had been performed to investigate visual telencephalic brain structures. The present study is the first to use thalamic lesions as well as monocular occlusions to show similar results in ZENK-ir in the visual telencephalon. Because there were no clear treatment effects, the results provide three important insights about the high visual telencephalic structures in

birds. First, the similar findings in both treatment conditions suggest that visual input to NIL from the ipsilateral thalamus through E is essential for the expression of ZENK-ir cells in NIL. Under the assumption that ZENK is involved in the long-term memory formation, this indicates that the possible learning and memory function of NIL is dependent upon the ipsilateral thalamic input. Second, the presence of interhemispheric connections in the occlusion treatment did not contribute to the maintenance of a high level of ZENK-ir in NIL. The fact that occlusions caused the same pattern of ZENK-ir as lesions suggests that information via any interhemispheric connections did not trigger sufficiently the ZENK expression in NIL. Finally, the results suggest that ZENK expression is more sensitively affected by the event that occurred just prior to the treatment compared to PV-ir or CO-staining, which were not significantly influenced by the occlusion procedure. It is also important to note that the occlusion procedure in the most peripheral organ affected the protein expression in one of the highest visual areas in the avian visual system. In this sense, the analysis of ZENK distribution is one of the most powerful techniques to study molecular consequences of real-time events on different brain regions, even in the higher telencephalic regions as reported here.

In conclusion, the present study revealed the complex heterogeneity of the avian visual telencephalon, which had been considered to be a rather homogenous entity. This anatomical finding provides new information about how visual processing is carried out in the non-mammalian cerebrum, and will be the foundation for future anatomical, physiological, and functional studies. In particular, the present study suggests that subdivisions of E are organized in a topographic manner, and a more detailed topographical map of E, as well as NIL, will be useful in order to delineate the whole

picture of the avian visual telencephalon. The significance of visual information exchange between the left and right hemispheres needs to be further explored as well. In the avian brain, there are multiple inter-hemispheric connections in the tectofugal visual route, including the tectal commissure, supraoptic decussation, and extra-telencephalic descending routes (see Figure 1). The role of these visual connections must be studied individually and compared with the mammalian counterparts. These studies will eventually reveal the general and specific neural rules associated with visual processing in vertebrates.

References

Abramoff, M.D., Magelhaes, P.J., & Ram, S.J. (2004). Image processing with ImageJ. *Biophotonics International, 11*, 36–42.

Baimbridge, K.G., Miller, J.J., & Parkes, C.O. (1982). Calcium-binding protein distribution in the rat brain. *Brain Research, 239*, 519-525.

Ball, G.F. & Balthazart, J. (2001). Ethological concepts revisited: Immediate early gene induction in response to sexual stimuli in birds. *Brain, Behavior, and Evolution, 57*, 252-270.

Benowitz, L.I. & Karten, H.J. (1976). Organization of the tectofugal pathway in the pigeon: A retrograde transport study. *Journal of Comparative Neurology, 167*, 503-520.

Bessette, B.B. & Hodos, W. (1989). Intensity, color, and pattern discrimination deficits after lesions of the core and belt regions of the ectostriatum. *Visual Neuroscience, 2*, 27-34.

Braun, K., Scheich, H., Braun, S., Rogers, J.H., & Heizmann, C.W. (1991). Parvalbumin-, calretinin- and calbindin-D28k-immunoreactivity and GABA in a forebrain region involved in auditory filial imprinting. *Brain Research, 539*, 31-44.

Braun, K., Scheich, H., Schachner, M., & Heizmann, C.W. (1985). Distribution of parvalbumin, cytochrome oxidase activity and [14] C-2-deoxyglucose uptake in the brain of the zebra finch. I. Auditory and vocal motor systems. *Cell Tissue Research, 240*, 101-115.

Braun, K., Scheich, H., Schachner, M., & Heizmann, C.W. (1985). Distribution of parvalbumin, cytochrome oxidase activity and [14] C-2-deoxyglucose uptake in the brain of the zebra finch. II. Visual system. *Cell Tissue Research, 240*, 117-127.

Brown, S.D. & Dooling, R.J. (1992). Perception of conspecific faces by budgerigars (*Melopsittacus undulatus*): I. natural faces. *Journal of Comparative Psychology, 106*, 203-216.

Brown, S.D. & Dooling, R.J. (1993). Perception of conspecific faces by budgerigars (*Melopsittacus undulatus*): II. Synthetic models. *Journal of Comparative Psychology, 107*, 48-60.

Butler, A.B. & Hodos, W. (1996). Comparative vertebrate neuroanatomy: Evolution and Adaptation. New York: Wiley-Liss.

Can, A., Domjan, M., & Delville, Y. (2007). Sexual experience modulates neuronal activity in male Japanese quail. *Hormones and Behavior*, *52*, 590-599.

Celio, M.R. (1990). Calbindin D-28k and parvalbumin in the rat nervous system. *Neuroscience*, *35*, 375-475.

Celio, M.R. & Heizmann, C.W. (1981). Calcium-binding protein parvalbumin as a neuronal marker. *Nature*, *293*, 300-302.

Chaudhuri, A. (1997). Neural activity mapping with inducible transcription factors. *Neuroreport*, *8*, iii-vii.

Clayton, D.F. (2000). The genomic action potential. *Neurobiology of Learning and Memory*, *74*, 185-216.

Cook, R.G., Cavoto, K.K., & Cavoto, B.R. (1995). Same/different texture discrimination and concept learning in pigeons. *Journal of Experimental Psychology: Animal Behavior Processes*, *21*, 253-260.

Cook, R., Levision, D.G., Gillet, S.R., & Blaisdell, A.P. (2005). Capacity and limits of associative memory in pigeons. *Psychonomic Bulletin & Review*, *12*, 350-358.

Davies, M.N.O. & Green, P.R. (1990). Optic flow-field variables trigger landing in hawk but not in pigeons. *Naturwissenschaften*, *77*, 142-144.

Davis, S., Bozon, B., & Laroche, S. (2003). How necessary is the activation of the immediate early gene *zif268* in synaptic plasticity and learning? *Behavioural Brain Research*, *142*, 17-30.

DeYoe, E.A. & Van Essen, D.C. (1988). Concurrent processing streams in monkey visual cortex. *Trends in Neurosciences*, *11*, 219-226.

Engelage, J, Bischof H-J (1993). The Organization of the tectofugal pathway in birds: A comparative review. In H.P. Zeigler & H-J. Bischof (Eds.), *Vision, brain, and behavior in birds* (pp 137-158). Cambridge, MA: MIT.

Ehrlich, D. & Saleh, C.N. (1982). Composition of the tectal and posterior commissures of the chick. *Neuroscience Letters*, *33*, 115-121.

Farroni, T., Massaccesi, S., Menon, E., & Johnson, M.H. (2006). Direct gaze modulates face recognition in young infants. *Cognition*, *102*, 396-404.

Frost, B.J. & Nakayama, K. (1983). Single visual neurons code opposing motion independent of direction. *Science*, *220*, 744-745.

Frost, B.J. & Sun, H. (1997). Visual motion processing for figure/ground segregation, collision avoidance, and optic flow analysis in the pigeon. In M.V. Srinivasan, & S. Venkatesh (Eds.), *From living eyes to seeing machines* (pp. 80-103). New York: Oxford University Press.

Gamlin, P.D.R. & Cohen, D.H. (1986). A second ascending visual pathway from the optic tectum to the telencephalon in the pigeon (C*olumba livia*). *The Journal of Comparative Neurology, 250,* 296-310.

Gauthier, I. & Logothetis, N.K. (2000). Is face recognition not so unique after all? *Cognitive Neuropsychology, 17,* 125-142.

Goelet, P., Castellucci, V.F., Schacher, S., & Kandel, E.R. (1986). The long and the short of long-term memory—a molecular framework. *Nature, 322,* 419-422.

Goodale, M.A. & Milner, A.D. (1992). Separate visual pathways for perception and action. *Trends in Neurosciences, 15,* 20-25.

Granda, A.M. & Yazulla, S. (1971). The spectral sensitivity of single units in the nucleus rotundus of pigeon, Columbia livia. *Journal of General Physiology, 57,* 363-384.

Güntürkün, O. (2000). Sensory physiology: vision. In: G.C. Whittow (Ed.), *Sturkie's avian physiology 5th edn* (pp. 1-19). New York: Academic.

Güntürkün, O, Miceli D, Watanabe M (1993) Anatomy of the avian thalamofugal pathway. In H.P. Zeigler & H-J. Bischoff (Eds.), *Vision, brain, and behavior in birds* (pp. 115-136). Cambridge, MA: MIT.

Hara, E., Kubikova, L., Hessler, N.A., & Jarvis, E.D. (2009). Assessing visual requirements for social context-dependent activation of the songbird song system. *Proceedings of the Royal Society B, 276,* 279-289.

Hellmann, B. & Güntürkün, O. (1999). Visual-field specific heterogeneity within the tecto-rotundal projection of the pigeon. *European Journal of Neuroscience, 11,* 2635-2650.

Hellmann, B., Waldmann, C., & Güntürkün, O. (1995). Cytochrome oxidase activity reveals parcellations of the pigeon's ectostriatum. *Neuroreport, 6,* 881-885.

Herdegen, T. & Leah, J.D. (1998). Inducible and constitutive transcription factors in the mammalian nervous system: control of gene expression by Jun, Fos and Krox, and CREB/ATF proteins. *Brain Research. Brain Research Reviews, 28,* 370-490.

Herrnstein, R.J., & Loveland, D.H. (1964). Complex visual concept in the pigeon. *Science 146,* 549-551.

Herrnstein, R.J., Loveland, D.H., & Cable, C. (1976). Natural concepts in pigeons. *Journal of Experimental Psychology: Animal Behavior Processes, 2*, 285-302.

Hodos, W. (1993). The visual capabilities of birds. In H.P. Zeigler & H.-J. Bischof (Eds.), *Vision, brain, and behavior in birds* (pp. 77-98). Cambridge, MA: MIT Press.

Hodos, W. & Bonbright, J.C., Jr. (1974). Intensity difference thresholds in pigeons after lesions of the tectofugal and thalamofugal visual pathways to the telencephalon. *Journal of Comparative Physiology and Psychology*, *87*, 1013-1031.

Hodos, W. Macko, K.A., & Bissette, B.B. (1984). Near-field acuity changes after visual system lesions in pigeons, II. Telencephalon. *Behavioral Brain Research*, *13*, 15-30.

Hodos, W., Weiss, S.R.B., & Bessette, B.B. (1986). Size-threshold changes after lesions of the visual telencephalon in pigeons. *Behavioral Brain Research, 28*, 203-214.

Hodos, W., Weiss, S.R.B., & Bessette, B.B. (1988). Intensity difference thresholds after lesions of ectostriatum in pigeons. *Behavioral Brain Research, 30*, 43-53.

Huber, L. (2001). Visual categorization in pigeons. In: R.G. Cook (Ed.), *Avian Visual Cognition*. Retrieved from Tufts University, Psychology Department Web Site: www.pigeon.psy.tufts.edu/avc/huber/.

Huchzermeyer, C., Husemann, P., Lieshoff, C., & Bischof, H.J. (2006). ZENK expression in a restricted forebrain area correlates negatively with preference for an imprinted stimulus. *Behavioural Brain Research*, *171*, 154-161.

Husband, S.A. & Shimizu, T. (1999). Efferent projections of the ectostriatum in the pigeon (*Columba livia*). *The Journal of Comparative Neurology*, *406*, 329-345.

Jarvis, C.D. (1974). Visual discrimination and spatial localization deficits after lesions of the tectofugal pathway in pigeons. *Brain, Behavior, and Evolution, 9*, 195-212.

Jarvis, E.D., Mello, C.V., & Nottebohm, F. (1995). Associative learning and stimulus novelty influence the song-induced expression of an immediate early gene in the canary forebrain. *Learning & Memory, 2*, 62-80.

Jarvis, E.D., Gunturkun, O., Bruce, L., Csillag, A. Karten, H., Kuenzel, W., Medina, L., Paxinos, G., Perkel, D.J., Shimizu, T. Streidter, G., Wild, J.M., Ball, G.F., Dugas-Ford, J., Durand, S.E., Hough, G.E., Husband, S. Kubikova, L. Lee, D.W., Mello, C.V., Powers, A., Siang, C., Smulders, T.V., Wada, K., White, S.A., Yamamoto, K., Yu, J., Reiner, A., & Butler, A. (2005). Avian brains and a new understanding of vertebrate brain evolution. *Nature Reviews Neuroscience, 6,* 151-159.

Jin, H. & Clayton, D.F. (1997). Localized changes in immediate early gene regulation during sensory and motor learning in zebra finches. *Neuron, 19,* 1049-1059.

Karten, H.J., Cox, K., & Mpdozis, J. (1997). Two distinct populations of tectal neurons have unique connections within the retinotectorotundal pathway of the pigeon (*Columba livia*). *Journal of Comparative Neurology, 26,* 449-465.

Karten, H.J. & Hodos, W. (1967). *A Stereotaxic Atlas of the Brain of the Pigeon (Columba livia).* Baltimore: Johns Hopkins Press.

Karten, H.J. & Hodos, W. (1970). Telencephalic projections of the nucleus rotundus in the pigeon (Columba livia). *Journal of Comparative Neurology, 140,* 35-51.

Kertzman, C. & Hodos, W. (1988). Size difference thresholds after lesions of thalamic visual nuclei in pigeons. *Visual Neuroscience, 1,* 83-92.

Krützfeldt, N.O.E. & Wild, J.M. (2004). Definition of novel connections of the entopallium in the zebra finch (*Taeniopygia guttata*). *The Journal of Comparative Neurology, 468,* 452-465.

Krützfeldt, N.O.E. & Wild, J.M. (2005). Definition of novel connections of the entopallium in the pigeon (*Columba livia*). *The Journal of Comparative Neurology, 490,* 40-56.

Kimberly, R.P., Holden, A.L., & Bamborough, P. (1971). Response characteristics of pigeon forebrain cells to visual stimulation. *Vision Research, 11,* 475-478.

Laverghetta, A.V. & Shimizu, T. (2003). Organization of the ectostriatum based on afferent connections in the zebra finch (*Taeniopygia guttata*). *Brain Research, 963,* 101-112.

Lieshoff, C., Grosse-Ophoff, J. & Bischof, H.J. (2004). Sexual imprinting leads to lateralized and non-lateralized expression of the immediate early gene zenk in the zebra finch brain. *Behavioural Brain Research, 148,* 145-155.

Lubow, R.E. (1974). High-order concept formation in the pigeon. *Journal of the Experimental Analysis of Behavior, 21,* 475-483.

Macko, K.A., & Hodos, W. (1984). Near-field acuity after visual system lesions in pigeons: I. Thalamus. *Behavioural Brain Research*, *13*, 1-14.

Mahmud, A. (2008). *A new digital imaging protocol for signal detection and distribution analysis in histological samples*. (Unpublished honors thesis) University of South Florida, Tampa, FL.

Maxwell, J.H. & Granda, A.M. (1979). Receptive fields of movement-sensitive cells in the pigeon thalamus. In A.M. Granda and J.H. Maxwell (Eds.), *Neural Mechanisms of Behavior in the Pigeon* (pp. 177-197). New York :Plenum Press.

Mello, C.V. & Clayton, D.F. (1995). Diffeprential induction of the ZENK gene in the avian forebrain and song control circuit after metrazole-induced depolarization. *Journal of Neurobiology*, *26*, 145-161.

Mello, C.V. & Ribeiro, S. (1998). ZENK protein regulation by song in the brain of songbirds. *Journal of Comparative Neurology*, *393*, 426-438.

Mello, C.V., Vicario, D.S., & Clayton, D.F. (1992). Song presentation induces gene expression in the songbird forebrain. *Neurobiology*, *89*, 6818-6822.

Morgan, J. I. & Curran, T. (1989). Stimulus-transcription coupling in neurons: Role of cellular immediate-early genes. *Trends in Neurosciences*, *12*, 459-462.

Nastiuk, K.L., Mello, C.V., George, J.M., & Clayton, D.F. (1994). Immediate-early gene responses in the avian song control system: cloning and expression analysis of the canary c-jun cDNA. *Brain Research. Molecular Brain Research*, *27*, 299-309.

Nguyen, A.P., Spetch, M.L., Crowder, N.A., Winship, I.R., Hurd, P.L., & Wylie, D.R. (2004). A dissociation of motion and spatial-pattern vision in the avian telencephalon: Implications for the evolution of "visual streams". *Journal of Neuroscience*, *24*, 4962-4970.

Nixdorf, B.E. & Bischof, H.J. (1982). Afferent connections of the ectostriatum and visual wulst in the zebra finch (*Taeniopygia guttata castanotis Gould*) – an HRP study. *Brain Research*, *248*, 9-17.

Pasternak, T. & Hodos, W. (1977). Intensity difference thresholds after lesions of the visual wulst in pigeons. *Journal of Comparative Physiology and Psychology*, *91*, 485-497.

Patton, T.B., Husband, S.A., & Shimizu, T. (2009). Female stimuli trigger gene expression in male pigeons. *Social Neuroscience*, *4*, 28-39.

Patton, T.B., Szafranski, G., & Shimizu, T. (2010). Male pigeons react differentially to altered facial features of female pigeons. *Behaviour*, *147*, 757-773.

Rasband, W.S. (1997-2009). *ImageJ* [Internet] US National Institutes of Health, Bethesda. *Optical Density Calibration*. Retrieved from: http://rsb.info.nih.gov/ij/docs/examples/calibration/

Revzin, A.M. (1970). Some characteristics of wide-field-units in the brain of the pigeon. *Brain Behavior and Evolution*, *3*, 195-204.

Revzin, A.M. (1979).Functional localization in the nucleus rotundus. In A.M. Granda and J.H. Maxwell (Eds.), *Neural Mechanisms of Behavior in the Pigeon* (pp. 165-175). New York:Plenum Press.

Ritchie, T.C. & Cohen, D.H. (1977). The avian tectofugal visual pathway: Projections of its telencephalic target the ectostriatal complex. *Social Neuroscience Abstracts*, *3*, 94.

Ruscio, M.G. & Adkins-Regan, E. (2004). Immediate early gene expression associated with induction of brooding behavior in Japanese quail. *Hormones and Behavior*, *46*, 19-29.

Sheng, M. & Greenberg, M. E. (1990). The regulation and function of c-fos and other immediate early genes in the nervous system. *Neuron*, *4*, 477-485.

Sherry, D.F. (1984). Food storage by black-capped chickadees: Memory for the location and contents of caches. *Animal Behaviour*, *32*, 451-464.

Sherry, D.F., Krebs, J.R., & Cowie, R.J. (1981). Memory for the location of stored food in marsh tits. *Animal Behaviour*, *29*, 1260-1266.

Shettleworth, S.J. (1983). Memory in food hoarding birds. *Scientific American*, *248*, 102-110.

Shettleworth, S.J. & Krebs, J.R. (1986). Stored and encountered seeds: A comparison of two spatial memory tasks in marsh tits and chickadees. Journal of Experimental Psychology: *Animal Behavior Processes*, *12*, 248-257.

Shimizu, T. (1998). Conspecific recognition in pigeons (*Columba livia*) using dynamic video images. *Behaviour*, *133*, 43-53.

Shimizu T (2001) Evolution of the forebrain in tetrapods. In: G. Roth & M.F. Wulliman (Eds.), *Brain Evolution and Cognition* (pp. 135-184). New York :Wiley/Spektrum.

Shimizu, T. & Bowers, A.N. (1999). Visual circuits of the avian telencephalon: Evolutionary implications. *Behavioural Brain Research, 98*, 183-191.

Shimizu, T., Bowers, A.N., Budzynski, C.A., Kahn, M.C., & Bingman, V.P. (2004). What does a pigeon (*Columba livia*) brain look like during homing? Selective examination of ZENK expression. *Behavioral Neuroscience, 118*, 845-851.

Shimizu, T. & Karten, H.J. (1991). Central visual pathways in reptiles and birds: Evolution of the visual system. In J.R. Cronly-Dillon & R.L. Gregory (Eds.), *Evolution of the Eye and Visual System, Volume 2* (pp. 421-441). Boca Raton: CRC Press.

Shimizu, T, Karten, H.J. (1993) The avian visual system and the evolution of the neocortex. In H.P. Zeigler & H-J. Bischof (Eds.), *Vision, brain, and behavior in birds* (pp 137-158). Cambridge, MA: MIT.

Shimizu, T., Patton, T.B., & Szafranski, G. (2008) Evolution of the visual system in birds. In M. D. Binder, N. Hirokawa, U. Windhorst, & M. C. Hirsch (Eds.), *Encyclopedic Reference of Neuroscience*. Heidelberg, Germany: Springer.

Thode, C., Bock, J., Braun, K. & Darlson, M.G. (2005). The chicken immediate early gene *zenk* is expressed in the medo-rostral neostriatum/hyperstriatum ventrale, a brain region involved in acoustic imprinting, and is up-regulated after exposure to an auditory stimulus. *Neuroscience, 130*, 611-617.

Tigges, M. & Tigges, J. (1991). Parvalbumin immunoreactivity of the lateral geniculate nucleus in adult rhesus monkeys after monocular eye enucleation. *Visual Neuroscience, 6*, 375-382.

Tigges, M. & Tigges, J. (1993). Parvalbumin immunoreactivity in the lateral geniculate nucleus of rhesus monkeys raised under monocular and binocular deprivation conditions. Visual *Neuroscience, 10*, 1043-1053.

Timmermans, S., Lefebvre, L., Boire, D., & Basu, P. (2000). Relative size of the hyperstriatum ventrale is the best predictor of feeding innovation rate in birds. Brain, Behavior and Evolution, *56*, 196-203.

Tischmeyer, W. & Grimm, R. (1999). Activation of immediate early genes and memory formation. *Cellular and Molecular Life Sciences, 4*, 564-574.

Vander Wall, S.B. & Balda, R.P. (1977). Coadaptation of the Clark's nutcracker and the pinyon pine for efficient seed harvest and dispersal. *Ecological Monographs, 47*, 89-111.

Vates, G.E., Broome, B.M., Mello, C.V., & Nottebohm, F. (1996). Auditory pathways of caudal telencephalon and their relation to the song system of adult male zebra finches (*Taenopygia guttata*). *Journal of Comparative Neurology, 366*, 613-642.

Vaughan, W. & Greene, S.L. (1984). Pigeon visual memory capacity. *Journal of Experimental Psychology: Animal Behavior Processes, 10*, 256-271.

Wang, Y. & Frost, B.J. (1992). Time to collision is signaled by neurons in the nucleus rotundus of the pigeon. Nature (London), *356*, 236-238.

Wang, Y.C., Jiang, S. & Frost, B.J. (1993). Visual processing in pigeon nucleus rotundus: luminance, color, motion, and looming subdivisions. *Visual Neuroscience, 10*, 21-30.

Watanabe, S. (1992). Effect of lesions in the ectostriatum and Wulst on species and individual discrimination in pigeons. *Behavioural Brain Research, 49*, 197-203.

Watanabe, S. (1996). Effects of ectostriatal lesions on discriminations of conspecific, species and familiar objects in pigeons. *Behavioural Brain Research, 81*, 183-188.

Watanabe, M., Ito, H., Ikushima, M. (1985). Cytoarchitecture and ultrastructure of the avian ectostriatum: afferent terminals from the dorsal telencephalon and some nuclei in the thalamus. *The Journal of Comparative Neurology, 236*, 241-257.

Watanabe, S., Lea, S.E.G., & Dittrich W.H. (1993). What can we learn from experiments on pigeon concept discrimination? In H.P. Zeigler & H-J. Bischof (Eds.), *Vision, brain, and behavior in birds* (pp 351-376). Cambridge, MA: MIT.

Watanabe, S., Sakamoto, J., Masumi, W. (1995). Pigeons' discrimination of painting by Monet and Picasso. *Journal of Experimental Analysis of Behavior, 63*, 165-174.

Wong-Riley, M.T.T. (1989). Cytochrome oxidase: An endogenous metabolic marker for neuronal activity. *Trends In Neurosciences, 12*, 94-101.

Xiao, Q., Li, D.P., & Wang, S.R. (2006). Looming-sensitive responses and receptive field organization of the telencephalic neurons in the pigeon. *Brain Research Bulletin, 68*, 322-328.

Appendices

Appendix A

A protocol for conducting optical density analysis.

Photographs

All photographs were taken using Wild Makroscope.
Apo lens Magnification: 25
Aperture: half
Light source: 9 V

Protocol 1 – No-Normalization Method

-Open macrophoto of section in ImageJ
-In "Image" menu, change "Type" to "8-bit"
-In "Analyze" menu, select "Calibrate"
-In "Calibrate" window, select "Open"
-In file menu, select "OD calibration" file (I/Willottlab/NIAD/CO/OD analysis/OD calibration); change "Function" to "Rodbard", and for "Unit" type "O.D."
-Use "Rectangular selections" tool to make a 250 X 250 µm (0.0625 mm^2) for measuring the different regions within E
-In "Analyze" menu, select "Measure"
-The measurement "Results" window data can be saved in Excel format (.xls)

Appendix B

A New Digital Imaging Protocol for Signal Detection and Distribution Analysis

Protocol Instructions:

1. Open ImageJ
2. Open Digital Photograph of Stained Slide
3. If Noise Tolerance Calibration is necessary follow Step 4 – if not go to step 12
4. Zoom in on picture until signals are visible
5. Using the "Rectangle Select Tool" select a segment within the image
6. Manually count and make note of every signal
7. Select *Find Maxima* under *Binary* sub-menu within *Process* menu
8. Select "Preview Point Selection"
9. Enter various numbers within the "Noise Tolerance" field until every signal manually counted is correctly labeled (with no extras or none missing) – make note of the value
10. Close Maxima Window
11. Deselect Selection (single-click any part of picture)
12. Select *Find Maxima* under *Binary* sub-menu within *Process* menu
13. Enter value in "Noise Tolerance" based on the previous calibration step
14. Select "Light Background" if slide has a lighter background compared to the signals
15. Select "Single Points" under the "Output Type" drop-down menu
16. Click "OK"
17. Select *Dilate* under *Binary* sub-menu within *Process* menu
18. Repeat step 17 until dots are the same size as a typical signal
19. Save the Maxima image as either TIFF or JPEG

A New Digital Imaging Protocol 22

20. Open GIMP
21. Open Maxima image from step 19
22. Select *Mosaic* under *Distorts* sub-menu within *Filters* menu
23. Set and Select following parameters: Square tiling, 0 tile height, 1.0 tile spacing, 1.0 tile neatness, 0 light direction, 0 color variation, checked antialiasing, checked color averaging, unchecked tile splitting, unchecked pitted surfaces and checked FG/BG lighting (make sure foreground and background colors are black and white respectively).
24. Set "Tile Size"
25. Click "OK"
26. Select *RGB* under *Mode* sub-menu within *Image* menu
27. Select gradient in gradient menu of toolbox
28. Select *Gradient Map* under *Map* sub-menu within *Color* menu

About the Author

Tadd Patton earned his bachelor's degree of Psychology from the University of South Florida in 1994. After taking some graduate level coursework at Georgia State University and working in private industry, he made the decision to further his education of the brain. This decision led Tadd Patton back to his Alma mater to complete his doctoral degree in Psychology with a special emphasis in neuroscience.

Throughout his graduate training, Tadd has taught several courses, including Psychology of Learning and Physiology of Behavior. During this period he also conducted scholarly research and presented his findings at international conferences, including the Society for Neuroscience and the Conference on Comparative Cognition. In addition he traveled to Keio University in Tokyo, Japan to conduct research under the direction of Dr. Shigeru Watanabe. Several of Tadd's research efforts during his graduate training have been published, including one based on his Master's Thesis work in which he investigated the face features important for conspecific recognition and mate selection in male pigeons.